CREWES

Research Report 2012
Volume 24

In this volume…

Report Summaries

On the memory stick…

Complete Reports
Student Theses

UNIVERSITY OF CALGARY

CREWES Project faculty, staff and students, October 2012

Left to Right:
Fourth Row: Joe Wong, Dave Henley, Kevin Hall, Laura Baird, Andrew Nicol, Kris Innanen, Todor Todorov, Hormoz Izadi
Third Row: Peng Cheng, Danping Cao , Eric Gallant, Helen Isaac, Hassan Khaniani, Davood Nowroozi, Heather Lloyd, Mohammed Alarfaj, Roohollah Askari, Raúl Cova, Melissa Hernández, Adrian Smith, Larry Lines
Second Row: Jean Cui, Penny Pan, Wenyong Pan, Dawson Holloway, Glen Young, Shahin Moradi, Jessie Arthur, Steve Kim, Rob Ferguson, Marcus Wilson, Chris Harrison, Byron Kelly, Kevin Bertram
First Row: Mahdi Al-Mutlaq, Don Lawton, Nasser Yousefzadeh, Thais Guirigay, John Bancroft, Shahin Jabbari, Gary Margrave (Director), Faranak Mahmoudian, Roy Lindseth, Chris Petten, Ben Wards, Michael Lamoureux, Vladimir Zubov

CREWES in 2012

In 2012, CREWES is one year shy of its 25 year anniversary. Our productivity this year, and the technical relevance and difficulty of our research, compare very strongly to our past efforts. While we are proud of our project and our work, we also recognize that we are completely reliant on the continued support of our Sponsors and NSERC. The current research volume represents the collective effort of our project to return value to our Sponsors and contribute meaningfully to the knowledge and experience base of elastic-wave seismology. We hope that you will find it valuable.

At this time CREWES has 11 faculty (including several not resident at the UofC), 10 full-time staff, 3 PDFs (post-doctoral fellows), and 34 graduate students (including 6 new students who joined us in September). We also had 10 students defend during the year, and are expecting 4 more new students in January 2013. A very welcome addition to our technical expertise (included in the 11 faculty) is Roy Lindseth, who has agreed to act as a technical advisor.

Ideally, our sponsorship would grow monotonically, but the truth is that our support has always fluctuated. New this year are sponsors Hewlett-Packard, DownUnder GeoSolutions, PTTEP (Thailand), NWGI (a division of PetroChina), Arcis (through current sponsor TGS-NOPEC), and Global Geophysical (through current sponsor Sensor). Unfortunately, these entries were offset by a nearly equal number of departures, so that our sponsor number remains unchanged at 28. However, we have several other companies who are currently considering sponsorship. Among these are Acceleware, Fugro, and Sinopec all of whom are attending this year's meeting as Observers.

As in recent years, we conducted a major field experiment in 2012. This time we worked on the University's land at the Rothney Astrophysical Observatory at Priddis (80km SW of the University), and laid out several dense spreads of various types of receivers. Additionally, we made another attempt at what we call the Pulse-Probe experiment. For this experiment, we recorded a line twice, once with a single vibe with a conventional sweep, and again with two vibes, where the second vibe emitted a monochromatic 25Hz sweep while the first used the original conventional sweep. The hope is that the difference between these two surveys will reveal a nonlinear effect with possible value to exploration. With data recorded by the dense receiver spread, we hope to study receiver performance and array formation.

In the coming year, we plan to drill a new 150m borehole at Priddis and instrument it with a permanently emplaced 40 level 3C geophone string. This will enable an experiment in the mid-year to study the evolution of the seismic waveform in the upper part of the near-surface layer. We welcome any suggestions regarding this experiment or other possible fieldwork.

Our project objective continues to be the advancement of all aspects of the seismic method, from acquisition through inversion, but with a special focus on the evolution from migration to full inversion. Since inversion is limited by the quality of the data, we continue acquisition, data processing, and algorithm development efforts. Additionally, final seismic images, whether migrations or inversions, must be understood by humans and so we cannot neglect interpretation either.

So, enjoy our meeting and give us your feedback on the quality and effectiveness of our research. Please feel free to make suggestions or offer guidance as you see fit. If the opportunity arises, we always welcome your direct involvement in our ongoing research.

Thank you all for your continued and generous support, and thank you for attending our annual meeting.

Calgary, Alberta
November, 2012

Gary Margrave
CREWES Director

Table of Contents

2012 CREWES Sponsors

BHP Billiton Petroleum

CGGVeritas

Chevron Corporation

ConocoPhillips

Devon Canada Corporation

DownUnder GeoSolutions Pty Ltd.

Encana Corporation

Eni S.p.A.

Exxon Mobil Corporation

Geokinetics Inc.

Geophysical Exploration & Development Corporation (GEDCO)

Hewlett-Packard

Husky Energy Inc.

INOVA Geophysical Equipment Limited

Landmark Graphics Corporation

Nexen Inc.

Northwest Geology Institute, CNCP

PennWest Exploration

Petrobras

PTTEP Exploration and Production Public Company Limited

Saudi Aramco

Sensor Geophysical Ltd.

Shell Canada

Statoil ASA

Talisman Energy Inc.

TGS-NOPEC

Tullow Oil p.l.c.

WesternGeco

Natural Sciences and Engineering Research Council of Canada (NSERC)
- Collaborative Research and Development Grant

CREWES Personnel

DIRECTOR

Gary F. Margrave
Professor, Department of Geoscience, University of Calgary

B.Sc. Physics, 1975, University of Utah
M.Sc. Physics, 1977, University of Utah
Ph.D. Geophysics, 1981, University of Alberta

- Work Experience: Chevron Canada Resources, Chevron Geoscience Company

ASSOCIATE DIRECTORS

Don C. Lawton
Professor, Department of Geoscience, University of Calgary

B.Sc. (Hons. Class I) Geology, 1973, University of Auckland
Ph.D. Geophysics, 1979, University of Auckland

- Work Experience: New Zealand Steel Mining Ltd., Amoco Minerals (N.Z.) Ltd.

Kristopher A. Innanen
Associate Professor, Department of Geoscience, University of Calgary

B.Sc. Physics and Earth Science, 1996, York University
M.Sc. Physics, 1998, York University
Ph.D. Geophysics, 2003, University of British Columbia

- Work Experience: University of Houston

ADJUNCT DIRECTORS

Laurence R. Lines
Professor, Department of Geoscience, University of Calgary

B.Sc. Physics, 1971, University of Alberta
M.Sc. Geophysics, 1973, University of Alberta
Ph.D. Geophysics, 1976, University of B.C.

- Work Experience: Amoco Production Research, Tulsa University, Memorial University of Newfoundland

Robert R. Stewart
Cullen Chair in Exploration Geophysics, University of Houston
Adjunct Professor, Department of Geoscience, University of Calgary

B.Sc. Physics and Mathematics, 1978, University of Toronto
Ph.D. Geophysics, 1983, Massachusetts Institute of Technology

- Work Experience: Arco Exploration and Production Research Centre, Chevron Geoscience Company, Veritas Software Ltd., Gennix Technology Corp., University of Calgary.

ASSOCIATED FACULTY AND SCIENTISTS

John C. Bancroft
Adjunct Professor, Department of Geoscience, University of Calgary

B.Sc. Electrical Engineering, 1970, University of Calgary
M.Sc. Electrical Engineering, 1972, University of Calgary
Ph.D. Electrical Engineering, 1975, Brigham Young University

- Work Experience: Geo-X Systems Ltd., Veritas Software Ltd., Ulterra Geoscience Ltd.

Robert J. Ferguson
Associate Professor, Department of Geoscience, University of Calgary

B.Sc. Geophysics, 1989, University of British Columbia
M.Sc. Geophysics, 1996, University of Calgary
Ph.D. Geophysics, 1999, University of Calgary

- Work Experience: Chevron Research, University of Texas at Austin

Michael P. Lamoureux
Professor and Department Head, Department of Mathematics and Statistics, University of Calgary
Adjunct Professor, Department of Geoscience, University of Calgary

B.Sc. Mathematics, 1982, University of Alberta
M.Sc. Mathematics, 1983, Stanford University
Ph.D. Mathematics, 1988, University of California, Berkeley

- Work Experience: Farallon Computing, NSERC Canada

Roy O. Lindseth MC., FRSC
Technical Advisor, CREWES, University of Calgary

Doctor of Laws, Honoris Causa, 1978, University of Calgary

- Work Experience: Chevron; NSERC, Teknica Corporation; TCPL

Brian H. Russell
Adjunct Professor, Department of Geoscience, University of Calgary

B.Sc. Physics, 1972, University of Saskatchewan
Honours Certificate in Geophysics, 1975, University of Saskatchewan
M.Sc., Geophysics, 1978, University of Durham
Ph.D., Geophysics, 2004, University of Calgary

- Work Experience: Chevron Geoscience Company, Teknica Resource Development, Veritas Software Ltd., Hampson-Russell Software Ltd.

Matt Yedlin
Associate Professor, Department of Electrical and Computer Engineering, University of British Columbia

B.Sc. Honors Physics, 1971, University of Alberta
M.Sc. Physiology, 1973, University of Toronto
Ph.D. Geophysics, 1978, University of British Columbia

- Work Experience: Conoco

RESEARCH AND ADMINISTRATION STAFF

Laura A. Baird
BA, History, 1992, University of Calgary
- Work Experience: Department of Geoscience, University of Calgary

Kevin L. Bertram
Electronics Technician Certificate, 2005, Southern Alberta Institute of Technology
- Work Experience: Aram Systems Ltd.

Malcolm B. Bertram
B.Sc. Geology, Auckland, New Zealand
- Work Experience: Allied Minerals NL (Western Australia), GSI (Western Australia), Western Geophysics (Western Australia), Auckland University, University of Calgary.

Patrick F. Daley
B.Sc. Mathematics, 1974, University of Alberta
M.Sc. Physics 1976, University of Alberta
Ph.D. Geophysics, 1979, University of Alberta
- Work Experience: Independent contractor associated with research centres of major oil companies

Eric V. Gallant
Journeyman Interprovincial Ticket in Electrical Construction, 1976, Cape Breton Institute of Technology
- Work Experience: IBEW, University of Calgary

Kevin W. Hall
B.Sc. Geophysics, 1992, University of Calgary
M.Sc. Geophysics, 1996, University of Calgary
- Work Experience: Lithoprobe Seismic Processing Facility, University of Calgary

Christopher B. Harrison
B.Sc. Physics, 1999, University of Calgary
B.Sc. Geophysics, 2001, University of Calgary
PhD. Geophysics, 2009, Curtin University of Technology, Perth, Western Australia
- Work Experience: University of Calgary, Total Depth Pty, Australia,

David C. Henley
B.Sc. Physics, 1967, Colorado State University
M.Sc. Physics, 1968, University of Michigan
- Work Experience: Shell Oil Co., Shell Canada Ltd

Helen Isaac
B.Sc. Mathematics, 1973, Imperial College, London
M.Sc. Geophysics, 1974, Imperial College, London
Ph.D. Geophysics, 1996, University of Calgary
- Work Experience: Phillips Petroleum, Hudson's Bay Oil and Gas, Canterra Energy, Husky, Fold-Fault Research Project

Rolf Maier
B.Sc. Chemical Engineering, 1978, Technikum Winterthur, ZH, Switzerland
M.Sc. Physical Chemistry, 1984, University of Calgary
Ph.D. Physical Chemistry, 1988, University of Calgary
- Work Experience: Lithoprobe Seismic Processing Facility, University of Calgary

Peter M. Manning
B.Sc. Mathematics, 1961, University of British Columbia
Ph.D. Geophysics, 2007, University of Calgary
- Work Experience: Mobil Oil Canada

Joe Wong
B.Sc. Physics/Mathematics, 1971, Queen's University
M.Sc. Applied Geophysics, 1973, University of Toronto
Ph.D. Applied Geophysics, 1979, University of Toronto
- Work Experience: Ontario Ministry of the Environment, University of Toronto, JODEX Applied Geoscience Limited

Vladimir Zubov
B.Sc. Mathematics, 2004, Rostov State University, Russia
M.Sc. Mathematics, 2006, Rostov State University, Russia
Ph.D. Mathematics, 2009, Southern Federal University, Russia
- Work experience: Computing Center of Southern Federal University, Russia

GRADUATE STUDENTS

Mahdi Almutlaq
B.Sc. Exploration Geophysics, 1998, Boise State University
M.Sc. Geophysics, 2007, King Fahd University of Petroleum and Minerals
- Work Experience: Saudi Aramco, South Rub Al-Khali Co.

Mohammed Alarfaj
B.Sc. Geophysics, 2007, Boise State University
- Work Experience: Saudi Aramco

Jessie Arthur
B.Sc., Geophysics, 2003, University of Alberta.
- Work Experience: Hampson-Russell Reservoir Characterization Services, ConocoPhillips

Roohollah Askari
B.Sc. Applied Physics, 2002, University of Hormozgan
M.Sc. Geophysics, 2005, University of Tehran
- Work Experience: Institute for Advanced Studies in Basic Sciences, Zanjan, Iran, CGGVeritas, Calgary

Peng Cheng
B.Sc. Applied Geophysics, 2001, Jilin University, China
M.Sc. Electrical Engineering, 2005, Peking University
- Work Experience: VIA Technologies (China) Inc.

David Cho
B.Sc. Physics and Geophysics, 2007, University of Calgary
- Work experience: Vermilion Energy, Apache Canada

Raúl Cova
B.Sc. Geophysical Engineering, 2004. Simon Bolivar University, Venezuela.
Graduate Diploma in Petroleum Studies, 2011. IFP School. Venezuela
- Work experience: PDVSA Intevep. Venezuela

Jean Cui
B.Sc. Geophysics, 1998, Petroleum University
M.Sc. Geophysics, 2005, China University of Mining & Technology
- Work experience: CGGveritas Canada

Peter Gagliardi
B.Sc. Geophysics, 2010, University of Calgary
M.Sc. Geophysics, 2012, University of Calgary
- Work Experience: Talisman Energy, Shell Canada

Patricia Gavotti
B.Sc. Geophysical Engineering, 2006. Simon Bolivar University, Venezuela
- Work Experience: Hampson-Russell Reservoir Characterization Services Caracas, Venezuela, Encana Corporation

Saul Guevara
B.Eng. Civil Engineering, 1984, National University of Colombia
M.Sc. Geophysics, 2001, University of Calgary
- Work Experience: Ecopetrol ICP

Thais Guirigay
B.Sc. Geophysics, 1994, Universidad Simon Bolivar
M.Sc. Geology, 2001, Colorado School of Mines
M.Sc. Geophysics, 2012, University of Calgary
- Work Experience: Geotrace (Houston), WesternGeco (Calgary)

Melissa Hernández
B.Sc. Geophysical Engineering, 2006, Simon Bolivar University, Venezuela
- Work Experience: BP, Calgary

Dawson Holloway
B.Sc. Geophysics, 2012, University of Saskatchewan
- Work Experience: Shell Canada

Hormoz Izadi
B.Sc. Applied Mathematics, 2010, University of Calgary

Shahin Jabbari
B.Sc. Mathematics applied in Physics, 1992, University of Tehran, Iran
M.Sc. Medical Physics, 1997, Tabriz University of Medical Sciences, Iran
M.Sc. Medical Physics, 2010, University of Calgary
- Work Experience: Encana Corporation

Zaiming Jiang
B. Eng. Geology, 1992, Northeast Institute of Technology
M. Eng. Communications & Electronics, 1998, Northeastern University
Ph.D. Geophysics, 2012, University of Calgary
- Work Experience: Key Seismic Solution Ltd.

Byron Kelly
B.Sc. Geophysics, 2010, Memorial University of Newfoundland
- Carnegie Institution of Washington, Devon Canada

Hassan Khaniani
B.Sc. Petroleum Exploration Engineering, 2003, Petroleum University of Technology
M.Sc. Petroleum Exploration Engineering, 2006, University of Calgary & Petroleum University of Technology
- Work Experience: Terras Persia Seismic Company (TPS), Nexen Inc.

Steve Kim
B.Sc. Geophysics, 2010, University of Calgary

Oliver Lahr
B.Sc. Pure and Applied Mathematics, 1988, University of Calgary
- Work Experience: Hampson-Russell Software Ltd.

Heather Lloyd
Diploma in Fashion Design and Technology, 2004, Kwantlen Polytechnic University
B.Sc. Geology, 2010, University of Calgary
B.Sc. Geophysics, 2010, University of Calgary

Li Lu
BSc., Geophysics, 1989, Daqing Petroleum University, China
- Work experience: CGGVeritas, Canada

Faranak Mahmoudian
B.Sc. Applied Physics, 2000, Khage Nassir Toosi University
M.Sc. Geophysics, 2006, University of Calgary
- Work Experience: Shell Canada

Matt McDonald
B.Sc. Hons. Applied Mathematics, 2010, University of Calgary
M.Sc. Mathematics, 2012, University of Calgary
- MMC Construction, Fotech Solutions

Shahin Moradi
B.Sc. Applied Physics, 2006, University of Razi, Iran
M.Sc. Geophysics, 2010, University of Tehran, Iran

E. Andrew Nicol
B.Sc. Hons. Geophysics, 2010, University of Western Ontario
- Work Experience: Sander Geophysics Limited, Devon Canada

Pan (Penny) Pan
B.Sc. Geophysics, 2012, Xi'an Shiyou University, China

Wenyong Pan
B.Sc. Computer and Software Engineering, 2009, China University of Geosciences (Beijing)
M.Sc. Geophysics, 2012, China University of Geosciences (Beijing)

Chris Petten
BSc. Physics, 2011, University of Calgary
BSc. Geophysics, 2011, University of Calgary
- Work Experience: University of Calgary Research Assistant - Stable Isotopes

A.-Nassir Saeed
B.Sc. Geology, 1991, University of Salahaddin
M.Sc. Geophysics, 1998, University of Science Malaysia
- Work Experience: University of Sciences and National University of Malaysia, Divestco Company

Adrian Smith
B.Sc. Honours Geophysics 2012, University of Western Ontario
- Work Experience: Husky Energy Inc.

Todor Todorov
B.Sc. Exploration Geophysics, 1994, University of Mining and Geology, Bulgaria
M.Sc. Geophysics, 2000, University of Calgary
- Work Experience: Hampson-Russell Software, Suncor Energy

Ben Wards
B.Sc. Hons. Applied and Pure Mathematics, 2003, University of Calgary
M.Sc. Applied and Pure Mathematics, 2005, University of Alberta

Marcus Wilson
B.Sc. Hons. Pure and Applied Mathematics, 2006, University of Calgary

Glen Young
B.Sc. Physics and Astrophysics, 1988, University of Calgary
B.Sc. Hons. Geophysics, 2011, University of Calgary
- Work Experience: PanCanadian/EnCana Corp., Nexen Inc.

Abdolnaser Yousefzadeh
B.Sc. 1997, Shahid Bahonar University of Kerman, Iran
M.Sc. Geophysics, 2001, Institute of Geophysics, University of Tehran, Iran
M.Sc. Geophysics, University of Alberta
- Work Experience: National Iranian Oil Company

Student Theses

The following theses are included with the CREWES 2012 Research Report:

M.Sc.	Christopher Bird	Amplitude-variation-with frequency (AVF) analysis of seismic data over anelastic targets
M.Sc.	Pietro (Peter) Gagliardi	Orientation Azimuth Calibration of Borehole Geophones
M.Sc.	Thais Guirigay	Estimation of Shear wave velocities from P-P and P-S seismic data using Equivalent Offset Migration
Ph.D.	Zaiming Jiang	Elastic wave modelling and reverse-time migration by a staggered-grid finite-difference method
M.Sc.	Diane Jael Lespinasse Fung	Evaluation of the seismic reflection method as a monitoring tool during primary and enhanced coalbed methane production
M.Sc.	Matt McDonald	Numerical Methods in Seismic Wave Propagation
Ph.D.	Agnieszka Pawlak	Crustal Structure beneath Hudson Bay from Ambient-Noise Tomography
M.Sc.	Virginia Cecilia Vera	Seismic modelling of CO2 in a sandstone aquifer, Priddis, Alberta
M.Sc.	Vanja Vracar	Fluid flow modelling and its seismic differencing in time-lapse
M.Sc.	Liliana M. Zuleta Tobon	Near-surface characterization and Vp/Vs analysis of a shale gas basin

Interpreting fault-related gas leakage

Mohammed Alarfaj and Don C. Lawton

ABSTRACT

Faults in extensional regimes can act as gas migration pathways when in contact with a hydrocarbon source. Gas presence associated with the leaking faults may be detected in seismic surveys. We observed the presence of gas associated with faults in a 3D seismic survey. The survey was acquired in an active tectonic zone in southern Taranaki basin, New Zealand. Interpreted faults appeared to be created at a later geologic time due to extension. The leaking faults seemed to be charged by being in contact with hydrocarbon reservoirs or by encountering other leaking faults. Seismic responses of waves traveling through low velocity intervals within the leakage zones show incoherent reflections. This is caused by scattering, attenuation, and a decrease in P-wave velocity. The interpretation of gas presence is supported by observations of amplitude anomalies and incoherent reflections within the leakage zone. We found seismic attributes such as semblance and curvature extracted from the survey to be effective in identifying the leaking faults. We filtered these attributes to show values at these identifiable gas reflections. When overlain on amplitude sections, the filtered attributes assist in identifying the distribution of gas-leakage zones (Fig. 1). Since different attributes are computed with different algorithms, the combination of multi-attributes can lead to better estimates of these gas zones.

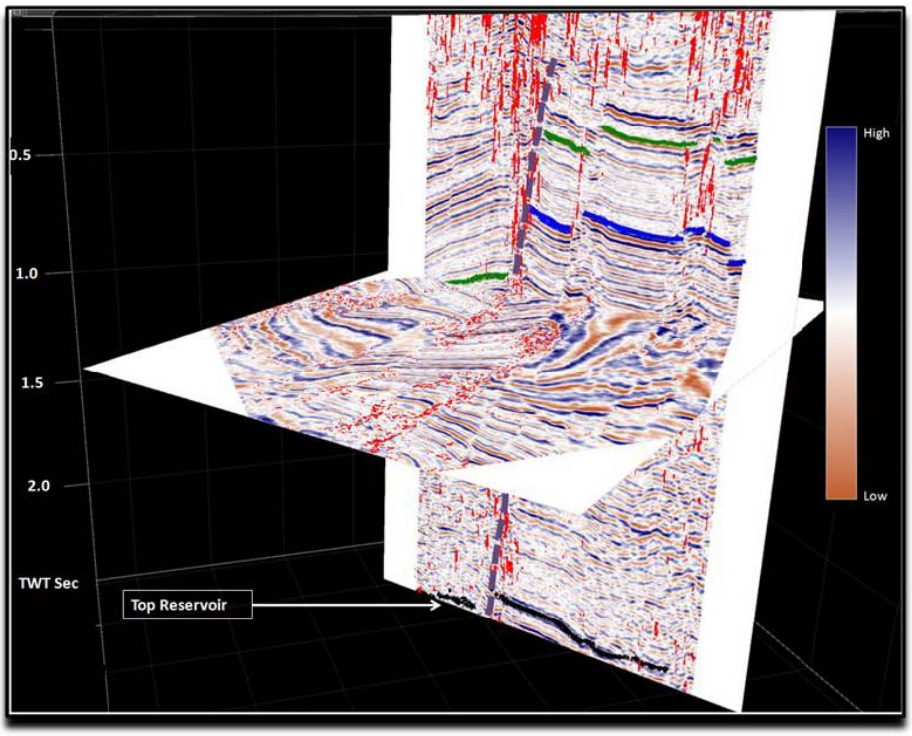

FIG. 1. Most positive curvature filtered and superimposed on amplitude sections. Curvature (red) appears to highlight the gas leaking through a non-sealing fault (purple) cutting through the top reservoir (black).

Surface-consistent matching filters for time-lapse seismic processing

Mahdi Almutlaq and Gary Margrave

ABSTRACT

We introduce the concept of surface-consistent matching filters for processing time-lapse seismic data, where matching filters are convolutional filters that minimize the sum-squared error between two signals. Since in the Fourier domain, a matching filter is the spectral ratio of the two signals, we extend the well known surface-consistent hypothesis such that the data term is a trace-by-trace spectral ratio of two data sets instead of only one (i.e. surface-consistent deconvolution). To avoid unstable division of spectra, we compute the spectral ratios in the time domain by first designing trace-sequential, least-squares matching filters, then Fourier transforming them. A subsequent least-squares solution then factors the trace-sequential matching filters into four operators: two surface-consistent (source and receiver), and two subsurface-consistent (offset and midpoint).

We present a time-lapse synthetic data set with nonrepeatable acquisition parameters, complex near surface geology, and a variable subsurface reservoir layer. We compute the four-operator surface-consistent matching filters from two surveys, baseline and monitor, then apply these matching filters to the monitor survey to match it to the baseline survey over a temporal window where changes are not expected. This algorithm significantly reduces the effect of most of the nonrepeatable parameters, such as differences in source strength, receiver coupling, wavelet bandwidth and phase, and static shifts. We compute the NRMS (normalized root mean square difference) on raw stacked data (baseline and monitor) and obtained a mean value of 70%. This value was significantly reduced after applying the four-component surface-consistent matching filters to about 15% (Figure 1).

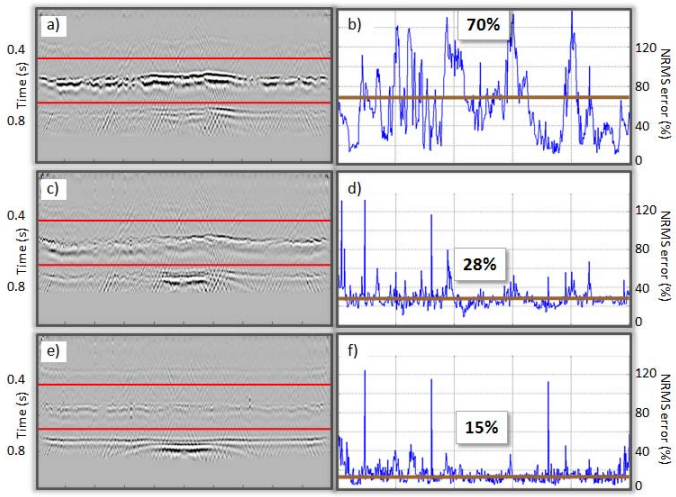

FIG.1. Difference stacks between baseline survey and monitor survey before applying matching filters (a), after applying matching filters (c), and final stage after NMOC. The computed NRMS are shown in (b), (d) and (f) for each of the stacks.

Violet Grove time-lapse data revisited: a surface-consistent matching filters application

Mahdi Almutlaq and Gary Margrave

ABSTRACT

We apply the surface-consistent matching filters to a real data set from the Violet Grove area in central Alberta. Detecting time-lapse difference on this data has proved to be difficult due the small impedance contrast at the Cardium reservoir where CO_2 is injected. However, we decided to examine the matching filters algorithm on this data for two main reasons: 1) to test the algorithm on a real data set and 2) to compare our results with previous processing on the same data. For this purpose, we evaluate two zones: a shallow one above the reservoir centered on the Ardley Coal Zone, and a deeper one below the reservoir.

After applying the surface-consistent matching filters to the monitor survey, we reduce most of the mismatch caused by acquisition differences and near surface variations (Figure 1). Differences caused by nonrepeatable noise in the data are difficult to remove since they are nonstationary. The shallow window above the reservoir is dominated by the near-surface noise compared to the deeper window of analysis. Despite this issue, we notice an improvement in the pre-stack and the post-stack image after applying the surface-consistent matching filters.

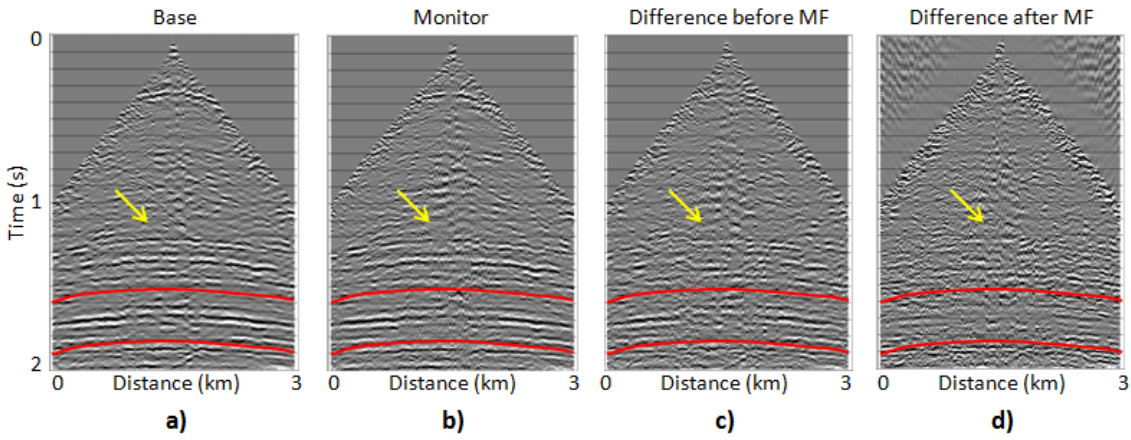

FIG.1. A shot record from the baseline survey (a), monitor survey (b), their difference before applying matching filters (c), and difference between baseline and matched monitor survey in (d). The arrow shows the approximate depth of the Cardium reservoir where CO2 is injected and the two red lines show the window where matching filters are applied.

Physical seismic modeling of a vertical fault

Jessie M. Arthur, Don C. Lawton and Joe Wong

ABSTRACT

Detecting faults and subsequent deformation zones is significant in geotechnical engineering applications, seismic hazard assessment in earthquake studies, and the petroleum industry for reservoir potential where faults act as a conduit to migrate or trap hydrocarbon flow. Fault identification is also important in shale gas development to design better productive reservoir stimulation by accounting for the slow slip of pre-existing faults during hydraulic fracturing.

This study shows seismic physical modeling results of a shallow vertical fault zone with slight vertical throw. Several physical model prototypes are created with materials which range in velocity and density to best simulate host rock and a deformed fault zone. 2D marine seismic data is acquired and processed at the University of Calgary Seismic Physical Modeling Facility. Physical model materials tested include plaster, sandstone, limestone, lard, wax, and liquid acrylic.

The post-stack imaged results are compared and it can be seen that the fault zone is resolved in both zero offset and common source data from physical modeling. An interesting by-product from the physical modeling acquisition was the identification of ghost reflections captured below the primary reflections, which can be used in 'mirror imaging', to provide better illumination of the fault zone.

The modeled fault zone images show a likeness to real 2D seismic data collected over a recent ruptured surface fault in New Zealand (Figure 1).

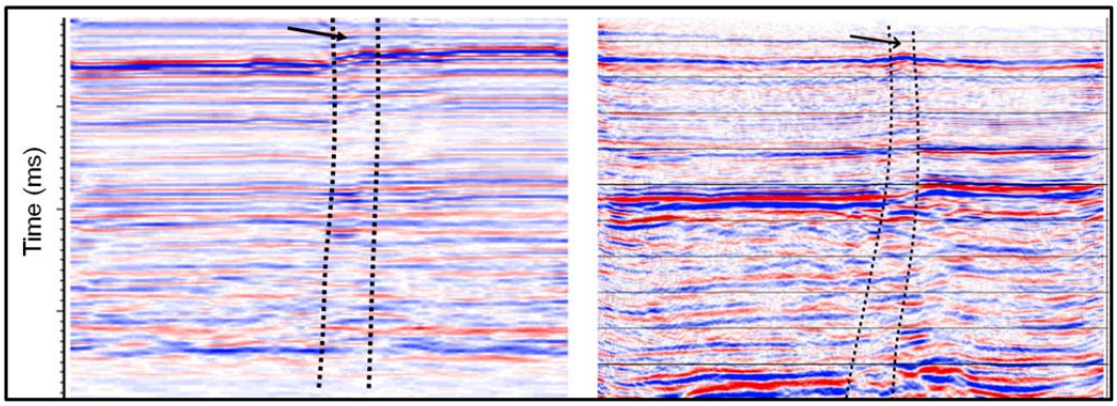

FIG. 1. Comparison of 2D final time migrated stacks of a fault rupturing the surface a) with physical modeling data and b) real data from the Greendale fault in New Zealand.

Estimation of near surface shear wave velocity using CMP Cross-Correlation of Surface Waves (CCSW)

Roohollah Askari, Robert J. Ferguson and Kristof DeMeersman

ABSTRACT

One of the challenges of converted wave processing is to estimate a good near surface shear wave velocity model for static corrections. To this end, we have enlarged upon the idea of CMP Cross-Correlation of Surface Waves to increase lateral resolution. Our approach is fast and we believe it is more robust in the presence of variable source wavelet and noise. We cross-correlate each trace of a shot record is with a reference trace that is selected from within the shot gather based on high signal to noise ration. This step removes source effect, and converts traces to zero-phase. New midpoints that relate to the correlated traces are then calculated. We calculate the phase velocity for each CMP gather, and finally, we convert the resulting dispersion curve to a vertical shear wave velocity by an inverse procedure. Putting together all the vertical shear wave velocity profiles of all the CMP gathers, 2D images of shear wave velocity are obtained for the data set. In this study, we invert for 2D shear wave profiles for two receiver lines with different geophone spacing. We have used the models to compute converted wave receiver statics, and our results illustrate the potential use of this method for computing converted wave receiver static corrections.

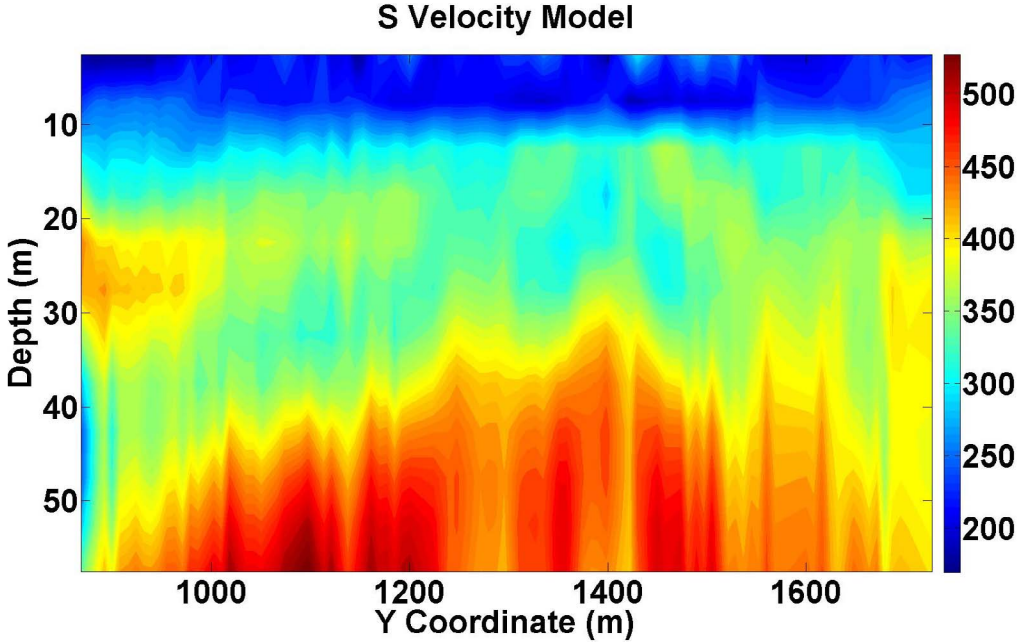

FIG. 1. Obtained S Velocity model for the first data set using CCSW.

Comments on stacking noisy data

John C. Bancroft

ABSTRACT

Stacking assumes we have seismic traces that are contaminated with noise, and that the sum of similar traces divided by the number of traces will reduce the noise by the square-root of the number of traces. This stacking process assumes the standard deviation (SD) of the noise is similar in each trace. In application where the SD of the noise varies from trace to trace, some form of weighing by each trace by its SD may improve the overall quality of the stack. In prestack migration gathers, where the noise is much greater than the data in a trace, balancing the amplitudes by dividing by the square-root of the fold may improve the stack.

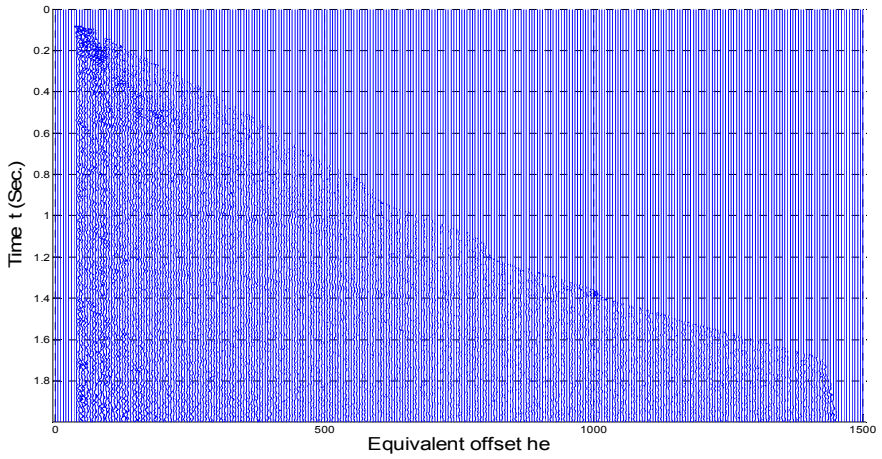

a)

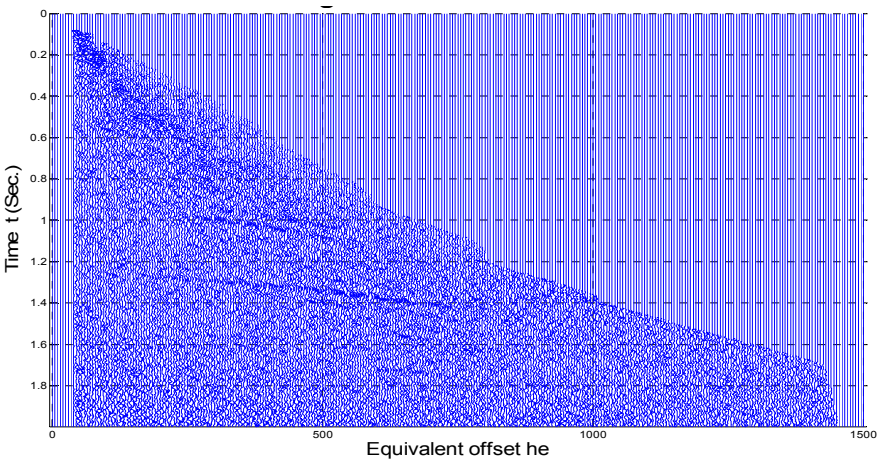

b)

FIG. 1. A CSP gather formed with a) stacking divided by the number of traces, and b) diving by the square-root of the number of traces.

An example of deconvolution after migration

John C. Bancroft

ABSTRACT

I presented a paper last year in the CREWES meeting that advocated performing a deconvolution after migration. This year, I provide additional comments and include an example of data processed commercially with a spiking deconvolution after migration.

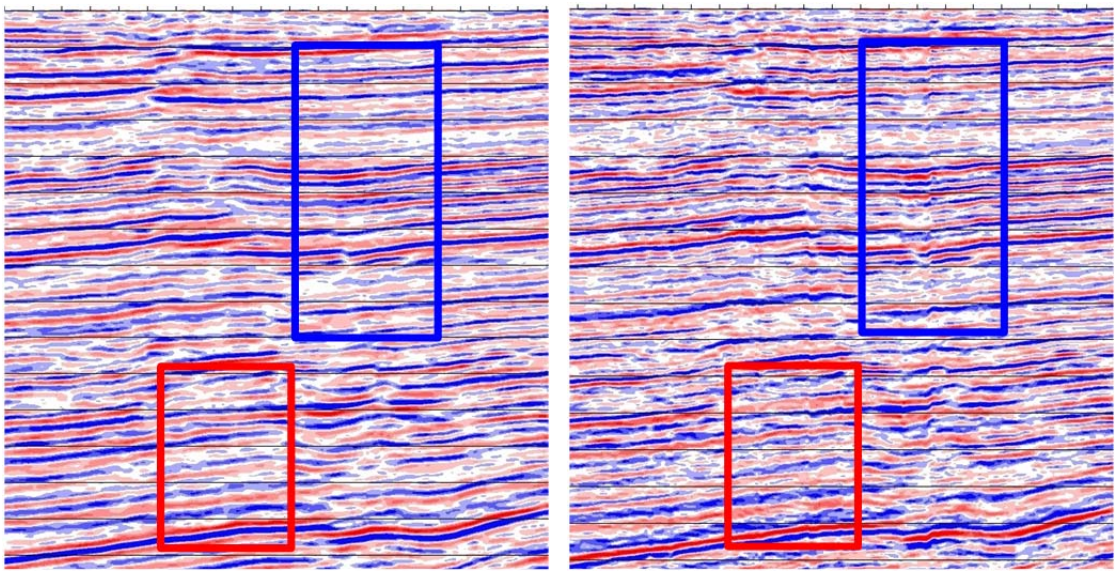

a) b)

FIG. 1. An example of the prestack migrated data with a) no deconvolution, and b) with deconvolution after the migration.

An update of MATLAB-EOM for converted wave data

John C. Bancroft

ABSTRACT

The MATLAB code of equivalent offset migration has been updated to include the processing of converted wave data. This new processing estimates a converted wave velocity that is then used to estimate a shear wave velocity that is used in the double-square-root equation. Parameter options are defined.

Some of the new parameters define a limited offset and spatial range during the gathering process to form converted wave gathers with one converted-wave velocity.

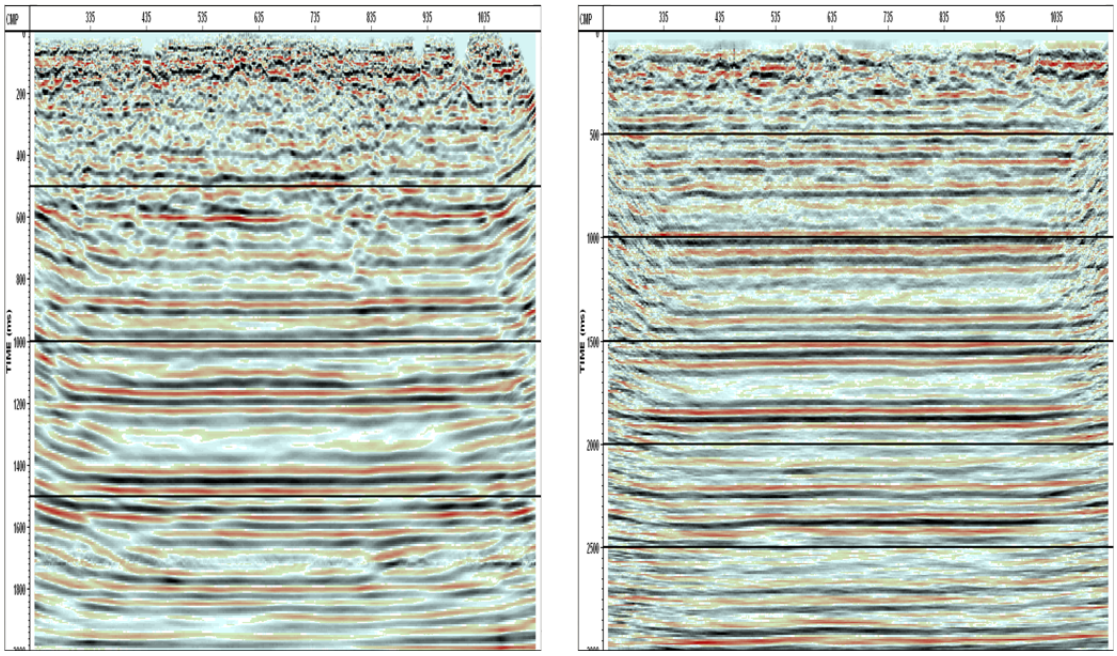

a) b)

FIG. 1. An example of the EOM processing for a) P-P data and b) P-S data. The P-P data ranges from 0 to 2 seconds and the P-S data from 0 to 3 seconds.

CREWES in the field, 2012

Kevin L. Bertram, Malcolm B. Bertram, Kevin W. Hall, Eric V. Gallant, Gary F. Margrave and Kristopher A.H. Innanen

ABSTRACT

CREWES carries out several acquisition and field experiments each year. In 2012 CREWES has completed the following acquisition projects: a) an extensive GPS survey of the often used Priddis test site; b) a pulse-probe experiment at the Priddis test site; c) the 2012 GOPH549 undergraduate Field School project with a seismic line along a road near Beaver Mines, Alberta; d) a refraction survey at the Priddis test site.

FIG. 1. CREWES has access to professional grade acquisition equipment that allow for real world data collection to be carried out at any time.

The pulse-probe experiment – a look at the Autoseis recording system

Malcolm B Bertram and Kevin W Hall

ABSTRACT

The CREWES project at the Priddis test site in July 2012 was designed to test different acquisition methods and recording systems. The project was named Pulse-Probe to describe one of the methods being tested. The equipment used were two Aries SPMLite recording systems, one with single SM7 3-component 10Hz geophones; the other with strings of 6 32CT 10Hz geophones podded and similar strings spread over 10 metres, an ION Scorpion with Vectorseis MEMS sensors, and Autoseis autonomous nodes each with 3 SM24 10Hz vertical geophones. Also tested were some 32CT 3-component geophones planted under sand bags instead of using spikes for coupling, and a single 3-component downhole geophone deployed in the well on the property. Sources for the survey were the University of Calgary Envirovibe, a Mertz M22 provided by Geokinetics, and dynamite shots of several charge sizes and depths. This paper makes some comparisons between the Aries and the Autoseis autonomous node recording systems.

FIG. 1. The receiver line looking west and the four sensors used. Top left: vectorseis, top right: SM7 3C, bottom left: GS-32CT pods, bottom right: Autoseis with SM24.

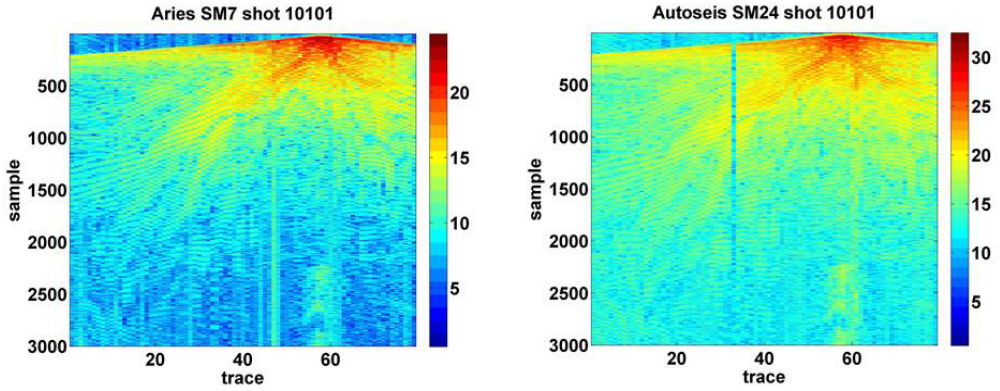

FIG. 2. Bit use plot.

Estimation of Q: a comparison of different computational methods

Peng Cheng and Gary F. Margrave

ABSTRACT

In this article, four methods of Q estimation are investigated: the spectral-ratio method, a match-technique method, a spectrum modeling method and a time-domain match-filter method. Their accuracy and the reliability of Q estimation is evaluated using synthetic data. Testing results demonstrate that the time-domain match-filter method is more robust to noise and more suitable for application to reflection data than the other three methods.

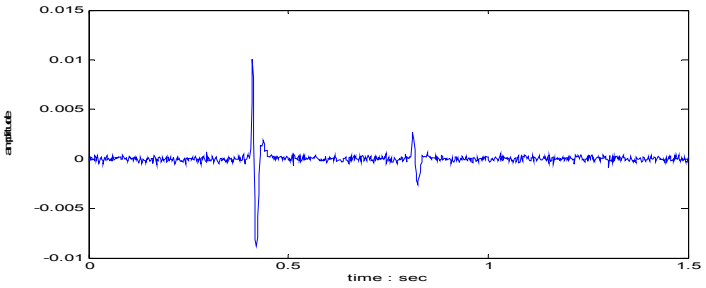

FIG. 1. An attenuated seismic trace with noise level of SNR=4 and constant Q of 80.

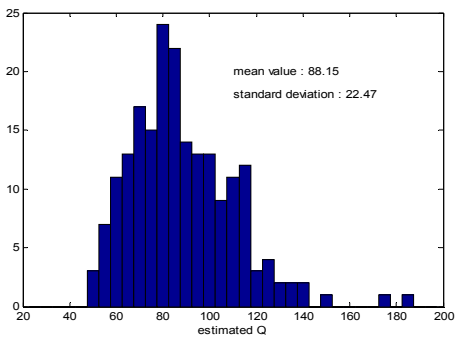

FIG.2. Histogram of estimated Q values by the spectral-ratio method using 200 seismic traces similar to the one shown in figure 1.

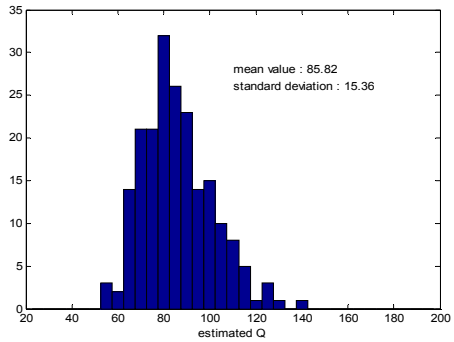

FIG. 3. Histogram of estimated Q values by the spectrum-modeling method using 200 seismic traces similar to the one shown in figure 1.

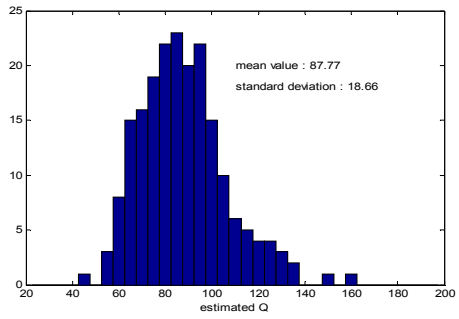

FIG. 4. Histogram of estimated Q values by the match-technique method using 200 seismic traces similar to the one shown in figure 1.

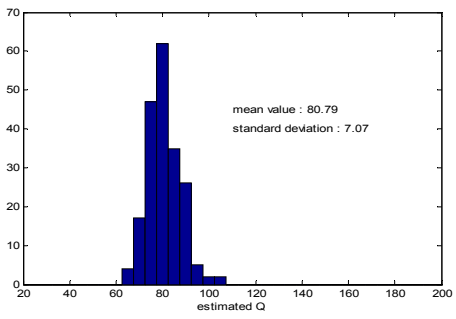

FIG. 5. Histogram of estimated Q values by the match-filter method using 200 seismic traces similar to the one shown in figure 1.

4D attenuation analysis for permeability estimates in hydraulically induced fractures

David Cho, Bill Goodway[1], Marco Perez[1], Andrew Iverson[1] and Gary F. Margrave

ABSTRACT

The effect of wave induced fluid motion between fractures and pores results in complex elastic stiffness coefficients that ultimately gives rise to frequency-dependent attenuation. Therefore, permeability estimates are obtainable through a spectral analysis of the seismic wavefield. In this study, we analyze the attenuation response associated with a time-lapse seismic survey acquired before and after hydraulic fracturing to investigate the permeability within the stimulated zone. The results obtained from the attenuation analysis were in qualitative agreement with microseismic observations and 4D seismic amplitude and traveltime anomalies, suggesting that a permeable fault diverted the energy from the hydraulic fracture treatment to re-stimulate a specific portion of the reservoir.

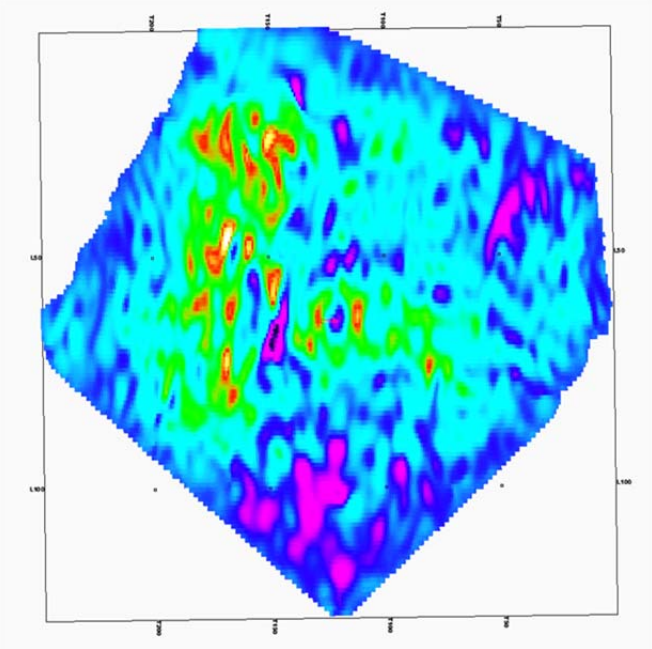

FIG. 6. Map illustrating the areal extent of the 4D attenuation anomalies suggesting fluid mobility in the stimulated zone.

[1] Apache Canada

A hybrid method for AVO inversion

David Cho and Gary F. Margrave

ABSTRACT

Global optimization algorithms are generally computationally intensive processes, where a significant amount of time is required to generate a solution. Therefore, methods to improve the efficiency are desired for problems that require its use. In this study we present a hybrid method to improve the convergence rate of an AVO inversion through implementation of a trace integration method followed by a simulated annealing optimization. The method eliminates the need for an additional model parameter to represent the layering solution and reduces the compute time of the global optimization by generation of an initial model that is close to the final solution.

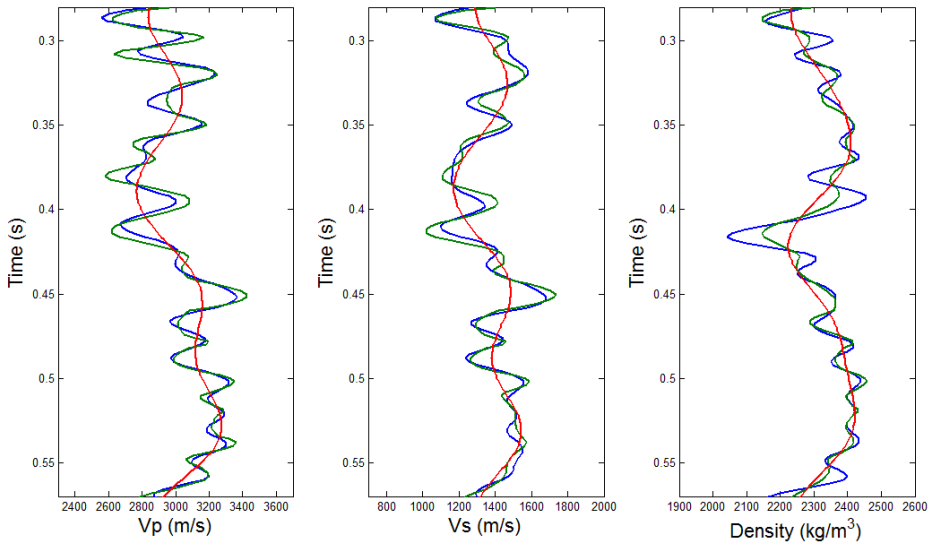

FIG. 4. Low frequency (red), true (blue) and estimated (green) model for the P- and S-wave velocities and density.

Hydraulic fracturing as a global cascade in networked systems

David Cho and Gary F. Margrave

ABSTRACT

Networked systems require the consideration of the interactions between component parts as well as the parts themselves in understanding the properties of the system. In the case of hydraulic fracturing, the process can be regarded as the spread of a fractured state through an initially unfractured network of rock elements. In this study, we implement a spreading model in networks to evaluate the dynamics of the hydraulic fracturing process in various rock types. The corresponding results regarding the stresses that must be overcome, the areal extent and energy release in hydraulic fracturing were in agreement with empirical observations.

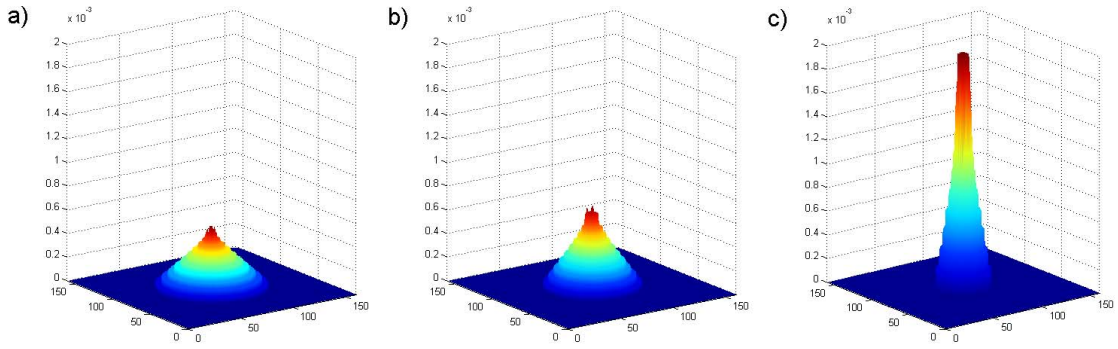

FIG. 5. Spatial distribution of total energy output for a) 70%, b) 40% and c) 10% quartz.

Cold heavy oil reservoir characterization: wormhole modeling and seismic responses

Xiaoqin (Jean) Cui, Larry Lines and Edward Krebes

ABSTRACT

Wormholes form fractural networks leading to increased reservoir permeability in the cold heavy oil production with sand (CHOPS). We extend a generalized homogeneous approach (Korn and Stockl, 1982) by presenting an algorithm of the 3D finite difference scheme with fracture parameters. We model the wormholes of CHOPS and compute synthetic seismogram responses from wormholes based on the non-welded contact theory (Schoenberg, 1980). The synthetic seismic data manifests frequency dispersion, along with amplitude, and travel time (velocity) variation for the fractal wormhole network. Therefore, Time slices of 4D time-lapse seismic data illuminates the wormhole growth, allowing us to evaluate reservoir permeability for CHOPS production and avoid invalid drilling into cold production footprints containing wormholes.

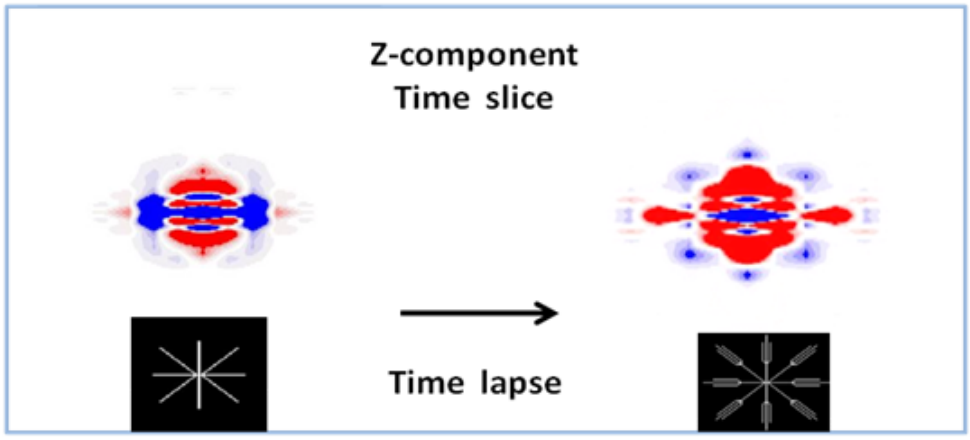

FIG. 1. Z-component time slice shows subsurface wormhole.

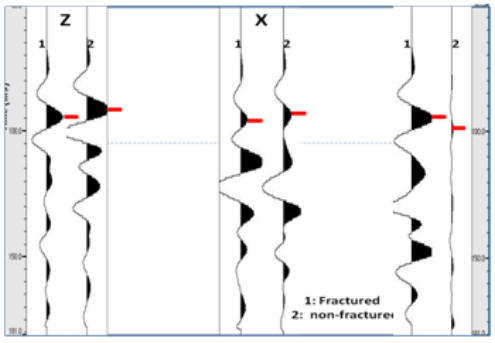

FIG. 2. x, y and z components seismic amplitude and velocity (travel time) differently vary with the direction of the fracture.

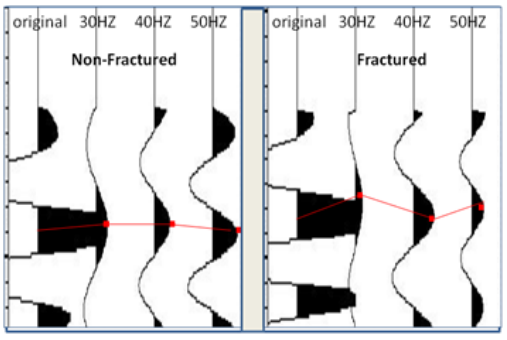

FIG. 3. Traces velocity from the non-fractured (Left) and fractured area (Right) demonstrate with and without frequency dispersion, respectively.

Numerical modeling for different types of fractures

Xiaoqin (Jean) Cui, Larry Lines and Edward Krebes

ABSTRACT

Fractures can be modeled as a non-welded contact linear slip interface (Schoenberg, 1980). In the long wavelength limit, fractured homogeneous isotropic media are equivalent to transversely isotropic media (TI). Azimuthal anisotropic parameters (Thomsen's parameters, 1986) are related to the fracture character parameters: tangential η_T and normal $\eta_N$compliances.The generalized homogenous FD scheme (Korn and Stockl, 1982)takes more physical insights into account for the fracture forward modeling because the medium and boundary conditions (BCs) are imposed explicitly The equation of motion governs the displacements outside the discontinuity interface, whereas the fracture is described as a non-welded contact boundary conditions at the discontinuity interface. We extend the generalized homogeneous algorithm modeling describing horizontal, vertical and tilted fractures as LS (linear slip interfaces) and synthetic seismic responses are exhibited for different types of the fractures (Figure 1).

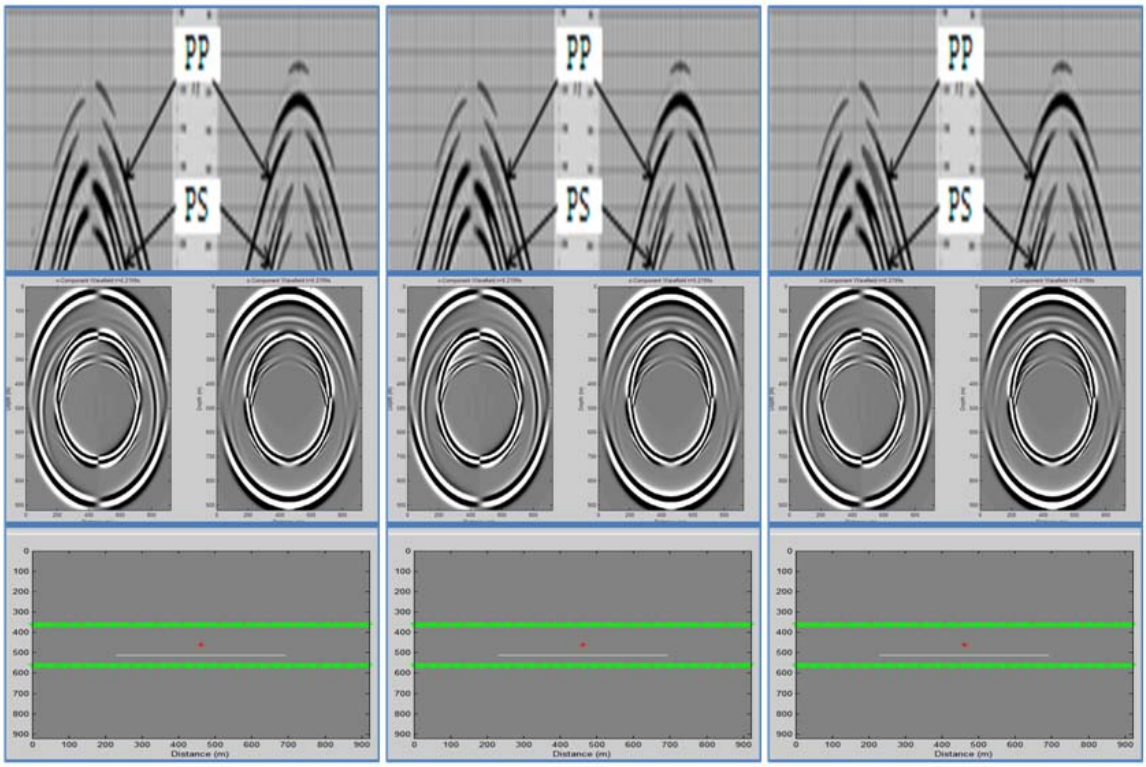

FIG.1. Numerical modeling for horizontal, vertical and tilt fractures. Three column pictures are for horizontal, vertical and tilt fractures, respectively (Left is for horizontal. Middle is for vertical. Right is for tilt). The first row shows fracture's model. The second row presents wave field propagation through the fractures. The third row displays synthetic seismograms of PP and PS without direct arrival wave.

Reflectivity modelling by finite difference

P. F. Daley and G. F. Margrave

ABSTRACT

The reflectivity method has been used for several decades to create *exact* synthetic traces for wave propagation in plane parallel layered media (e.g. Müller, 1985). For the problem of coupled P-S_v wave propagation in a radially symmetric isotropic homogenous plane parallel layered medium, the radial coordinate is temporarily removed by Hankel transforms, a Fourier time transform applied, and the resultant depth problem is handled by propagator matrix theory or variations thereof.

We take an alternate approach suggested by Mikhailenko (Mikhailenko, 1985), that uses *finite* Hankel transforms to temporarily remove the radial coordinate and finite difference methods to deal with the resultant problem in depth and time. A finite difference problem in one spatial dimension and time avoids many of the numerical difficulties inherent in problems with higher order spatial dimensions. If the additional assumption that the time dependence of the source wavelet is band limited in the frequency domain is made, the problem is fairly well defined, apart from initial and finite boundary conditions. The approach indicated here was referred to as the pseudo-spectral method in past decades. In recent CREWES volumes there are reports by P.F. Daley dealing with certain aspects of this theory. CREWES is releasing Matlab software this year that implements this theory.

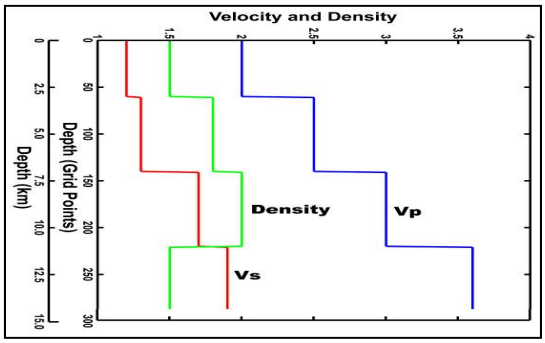

Left: FIG. 1. Velocity/Density – Depth structure (in finite difference depth points and km) for model 1, in km, km/s, and gm/cm^3. Predominant frequency of the source wavelet is 30Hz.

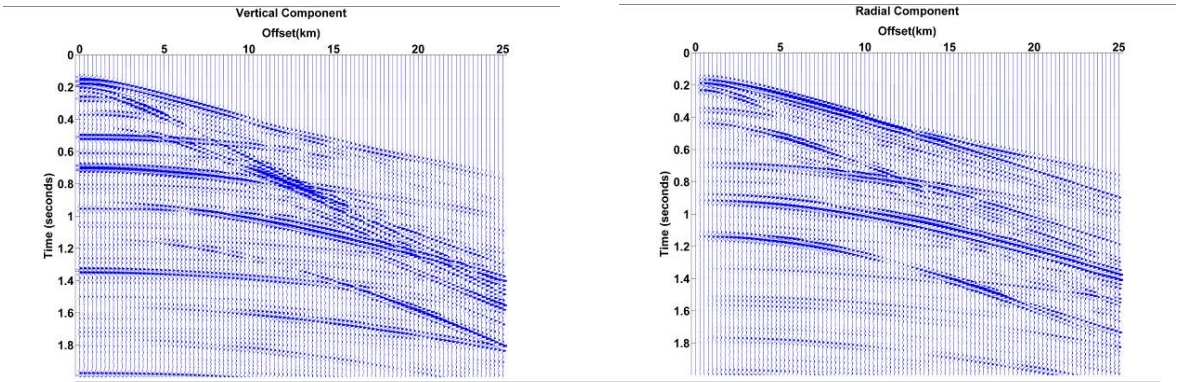

FIG. 2. Vertical (right) and horizontal (left) components of particle displacement for the model shown in Figure 1, an explosive surface point source of *P*– waves and a line of receivers at the surface. In the two figures shown the direct *P* – wave and non-geometrical surface effects have been removed.

Mikhailenko, B.G., 1985, Numerical experiment in seismic investigations, Journal of Geophysics, **58**, 101-124.

Attenuation compensation for georadar data by Gabor deconvolution

Robert J. Ferguson and Gary F. Margrave

ABSTRACT

It has been shown through previous data examples that nonstationary deconvolution,and in particular the CREWES Gabor nonstationary deconvolution, provides significant enhancement for deep georadar reflections. In many examples the improvement extends the radar image from a few meters to a few tens of meters.

We find here through controlled experiment that nonstationary deconvolution has an attenuation correction property - the frequency and phase components of attenuation loss are compensated for. Though the compensation effect is noticeable on seismic data, the effect on georadar data is quite a bit more obvious and we find that, in terms of attenuation factor Q, Q is about an order of magnitude larger for georadar than it is for seismic. We show that it this Q compensation probably accounts for the significant signal improvements that we see in georadar data.

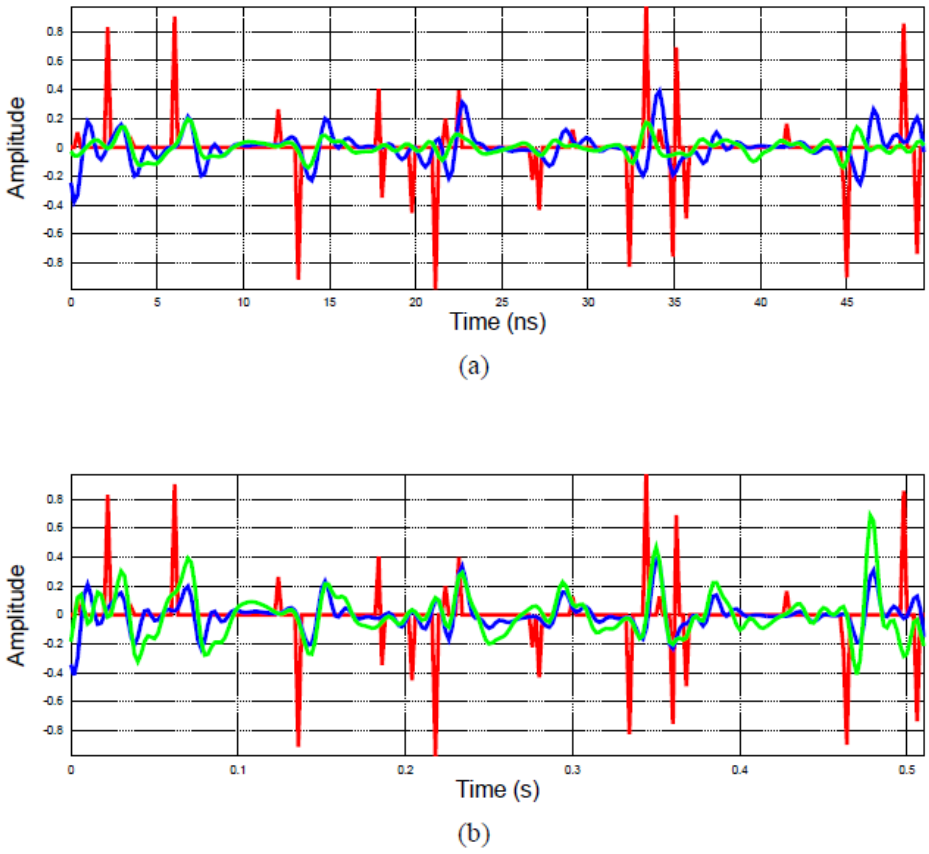

FIG. 1. Gabor decon applied to attenuated signals. Red curves are reflectivity, blue curves are the bandlimited reflectivity, and green curves are the Q restored signals. a) The georadar signal is fairly well restored with amplitude and phase departures beginning at about 20 ns. b) The seismic signal is very well restored.

Depth migration of monostatic and bistatic georadar data

Robert J. Ferguson, Matthew J. Yedlin, Christian Pichot, Jean-Yves Dauvignac, Nicholas Fortino and Stephane Gaffet

ABSTRACT

A 200 trace subset of a larger survey are compared for image quality. These data are unique in that two distinct acquisition geometries are acquired simultaneously. The first, and we will call it "bistatic", is the conventional georadar acquisition where the transmitting and recording antennae are separated by 1 meter. The second we will call "monostatic". Monostatic acquisition is unique in that the transmitting and recording antennae are exactly co-located - they are the same physical antenna, and this is a recent technical development. Monostatic acquisition reproduces exactly the geometry of the well known "exploding reflector model" of seismic imaging and therefore, zero-offset migration (ZOM) of the data is not an approximation but a legitimate imaging approach. In particular, the image of the near-surface (1 m or so) should be precisely imaged (given an exact velocity model) - bistatic data require prestack depth migration (PSDM) to achieve equal precision. PSDM, of course, is much more expensive and time consuming than ZOM and so monostatic acquisition is very desirable. Here we demonstrate a number of important differences.

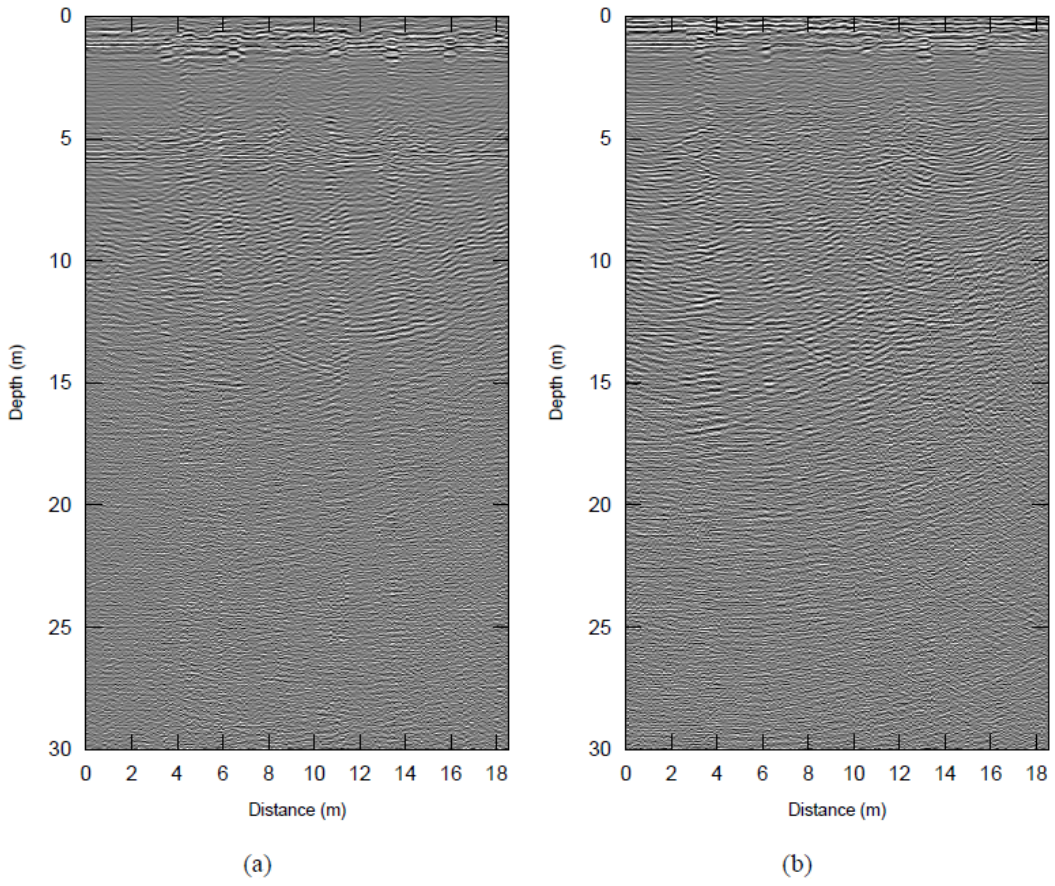

FIG. 1. Migrated georadar images. a) Monostatic antenna. b) Bistatic antenna.

Georadar data processing and imaging: paleoseismicity in the Piano di Castelluccio Basin, Central Italy

Robert J. Ferguson, Maurizio Ercoli and Alessandro Frigeri

ABSTRACT

Three lines (40, 100, and 160) are presented in a comparison between conventional georadar processing flows and flows based on the gabordecon algorithm from the CREWES toolbox. The imaging goal is to map near-surface sediments above a Quaternary fault in the Piano di Castelluccio Basin in central Italy. There is a history of earthquake risk in this region and the georadar data were acquired for infrastructure planning and as part of Probabilistic Seismic Hazard Assessment (PSHA) in Italy. The georadar data are used to tie reflection seismological fault images to the surface. We find that the gabordecon-based flow is significantly better than the conventional flow and this is likely due to Q compensation characteristics that are intrinsic to gabordecon.

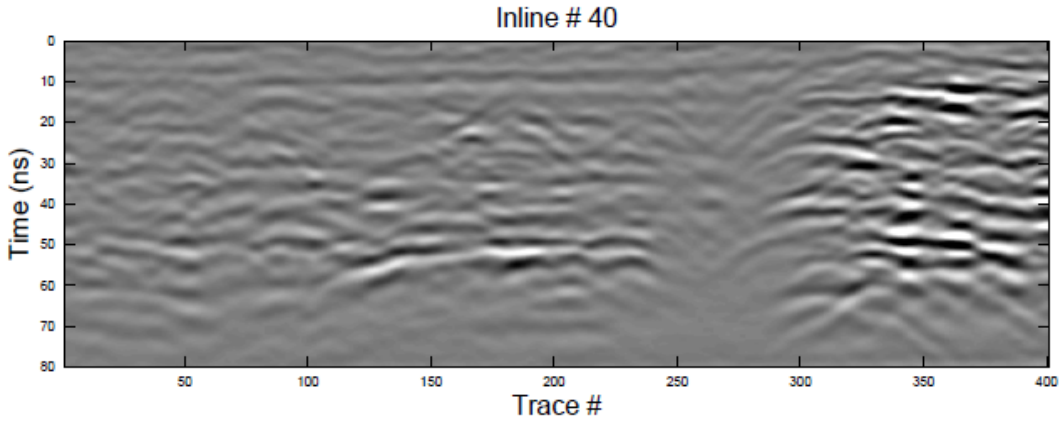

FIG. 1. Line 40 processing comparison. a) Conventional processing. b) Processing with gabordecon.

Polarity consistent geophone rotation analysis by inversion: Penn West 3D VSP

Robert J. Ferguson

ABSTRACT

The Rig-source VSP/ Offset VSP/ Walkaway VSP of Penn West Petroleum Ltd is used to demonstrate a new geophone rotation analysis. This survey employs non-gimbaled geophones in a deviated well-bore and so the orientation of all three components is required for proper wavefield separation. Three walkaway VSP source lines are recorded in a total of 45 geophone levels downhole. Data are gathered according to common receiver and first break energy is analyzed based on the new method. So that absolute measurements can be made for each receiver level, each three component recording is rotated such that all sources for a common receiver reside vertically above that receiver and then first-break analysis is used to point one of the geophone components at the source location. Within each common receiver gather very good agreement is found between sources for the dip between the geophone component and the source location and that good agreement is found for the azimuth of the two remaining components.

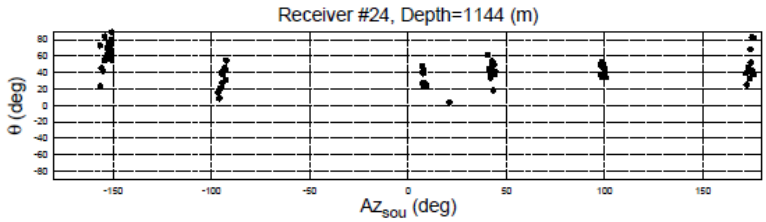

FIG. 1. Geophone azimuth estimate verses source-receiver azimuth for CRP 24.

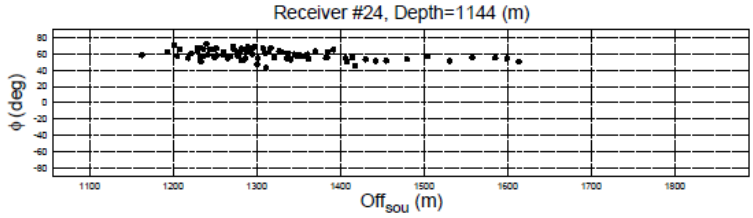

FIG. 2. Geophone dip estimate verses source-receiver offset for CRP 24.

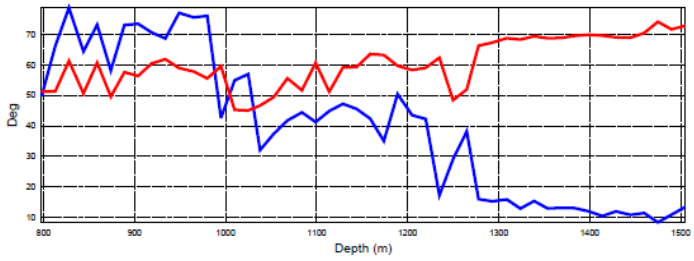

FIG. 3. Averaged estimates of θ (blue line) and ϕ (red line) for all depths.

Geophone orientation analysis in a 3D VSP survey, Alberta

Peter Gagliardi and Don C. Lawton

ABSTRACT

Geophone orientation azimuths were found from 3D and 2D VSP data, acquired near Lousana, Alberta, in order to examine any dependence of computed geophone orientation on source-well offset or azimuth. Additionally, a comparison was made between analytic and hodogram methods. The 2D dataset consisted of three lines; the standard deviation for this survey was 0.67° for all lines, 0.45° for the east line, 0.41° for the southeast line and 0.55° for the south line. Removal of sources less than 500 m (approximately 1/2 of the geophone depth) significantly improved the scatter in this dataset. Standard deviation in orientation azimuths for all lines was found to be 0.90° using the hodogram method; thus, while the both methods performed well, the analytic method produced more consistent results. The 3D dataset was divided based on source-well azimuth into bins with centers trending 0°-180°, 45°-225°, 90°-270° and 135°-315°. There appeared to be little dependence on source-well sector azimuth, which is expected for flat, isotropic geology near the well. Standard deviation in orientation azimuths were found to be 1.74° using the full 3D dataset. Offsets were binned into ranges of 0-600 m, 600-950 m, 950-1300 m, 1300-1650 m and greater than 1650 m. Scatter in rotation angles was shown to be strongly dependent on offset, with the most constrained results in the 1300-1650 m offset bin. The optimal offset range for geophone orientation calibration was found to be between 1 and 2 times the receiver depth.

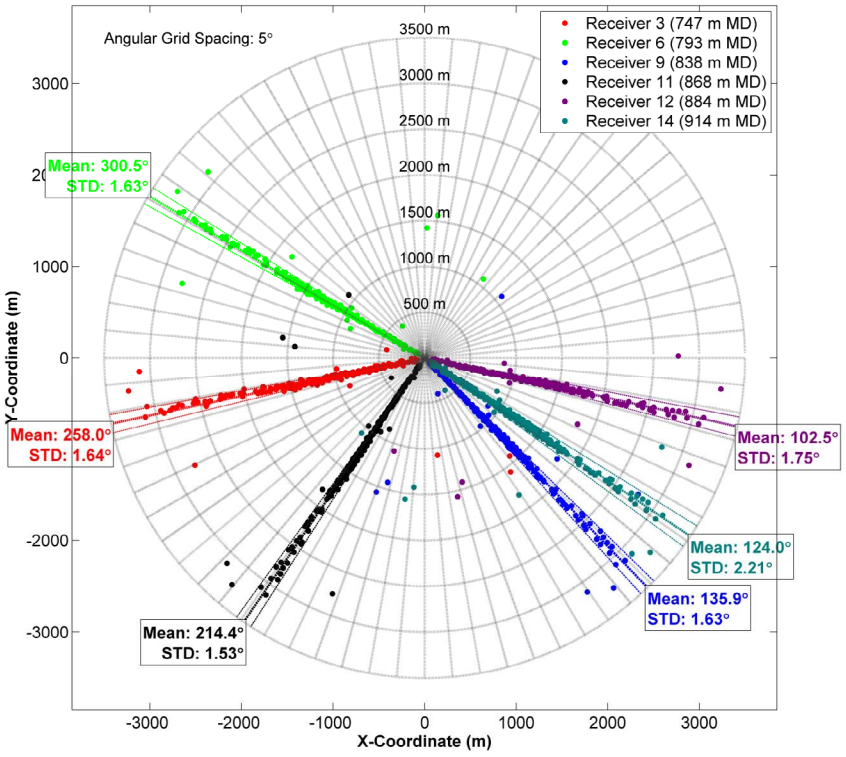

FIG. 1. Radial plot of geophone orientation azimuths for a subset of receivers. Envelope lines represent one standard deviation. Radial spacing is 500m, angular spacing is 5°.

Modelling of systematic errors in borehole geophone orientation calibration

Peter Gagliardi and Don C. Lawton

ABSTRACT

Using results from analytic and finite-difference modelling, factors affecting the orientation calibration of borehole geophones were investigated. Well deviation, lateral raybending and anisotropy were all found to produce systematic deviations in orientation analysis. Effects due to errors in a well deviation survey were found, based on analytic modelling, to produce errors of a similar magnitude on orientation analysis; specifically, errors of ±2° in inclination and azimuth angle produced scatter of 2.53° over a sample of 48 geophones. The effects due to lateral raybending and anisotropy were characterised using finite-difference models; these produced one-cycle and two-cycle sinusoidal trends when orientation was plotted against source-well azimuth. In the case of a dipping layer, errors in geophone orientation were found to be 0° along the dip direction; in the case of an HTI medium, they were found to be approximately 0° along the fast and slow directions. This suggests that acquisition design of geophone orientation calibration surveys should be guided by knowledge of the geology in the area of interest.

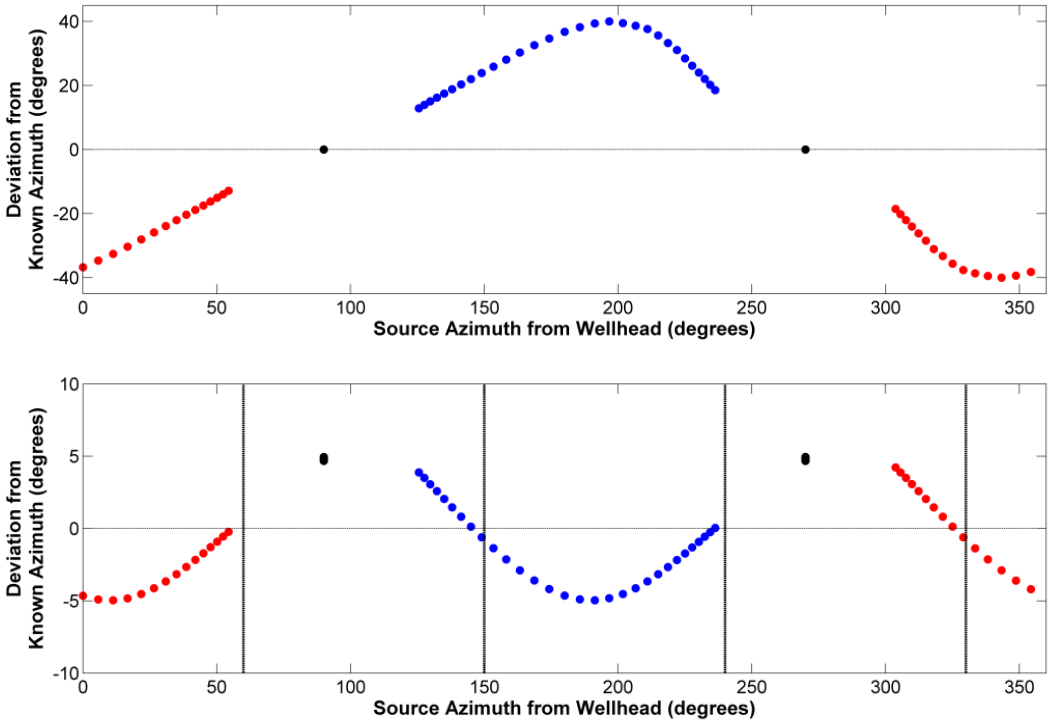

FIG. 2: Deviation of orientation angle due to a dipping layer (top) and HTI medium (bottom) plotted as a function of source-well azimuth.

Post-stack inversion of the Hussar low frequency seismic data

Patricia E. Gavotti, Don C. Lawton, Gary F. Margrave and J. Helen Isaac

ABSTRACT

The Hussar experiment was carried out in September 2011 with the purpose of acquiring low frequency seismic data to be used in inversion methods. Three wells located close to the seismic line and a dynamite-source dataset, acquired with three-component 10 Hz geophones, were used for a post-stack inversion test using commercial software. Several low-frequency cut-off filters applied to the data were tested with the 3-5 Hz model being selected as the optimum. The resultant impedance reflects lateral changes that were not present in the initial model and therefore come from the seismic reflections (Figure 1). Impedance changes in the target zone shows the general trend and relative variations, which would allow monitoring changes in the reservoir as variations in the rock properties occur. A final inversion was performed to simulate traditional approaches when the low-frequency component is absent in the seismic data. Filtered seismic-data (10-15-60-85 Hz) and an initial model with a 10-15 Hz cut-off were used for this test. The results at the well locations show a good match but the lateral variation and character of the events resemble more the initial model character (Figure 2).

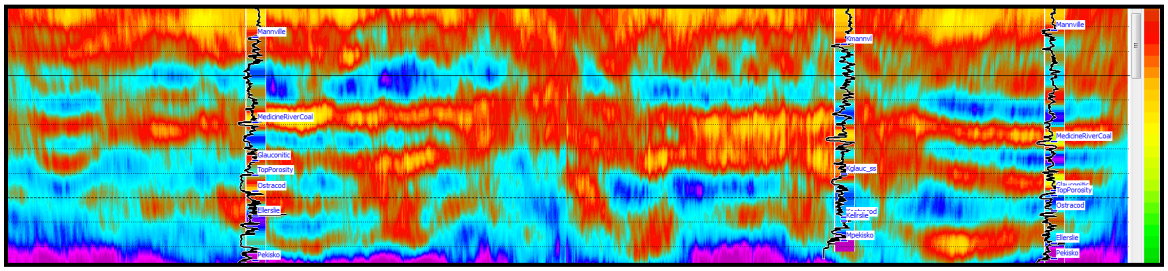

FIG. 1: Inversion result of Hussar 10 Hz dynamite dataset showing the gamma ray curve in black and the impedance log with a high-cut filter 60/85 Hz in color at the well locations for comparison.

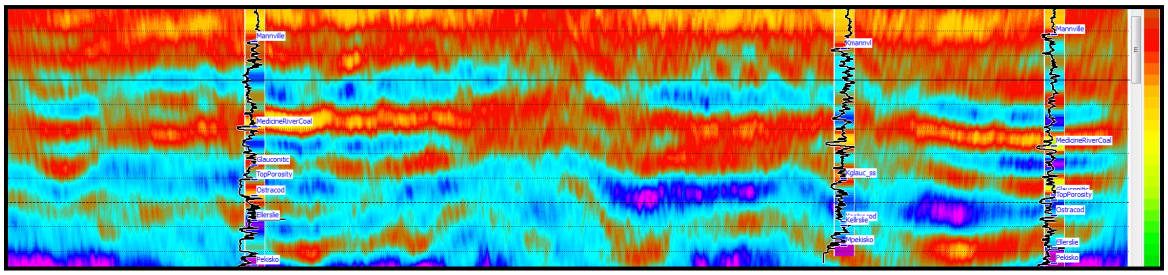

FIG. 2: Inversion result of Hussar 10 Hz dynamite dataset with a band-pass filter of 10-15-60-85 Hz showing the gamma ray curve in black and the impedance log with a high-cut filter 60/85 Hz in color at the well locations for comparison. Note the differences in continuity and character of the events with respect to the results on Figure 1.

Angle gathers for PP and PS depth images of flat and dipping reflectors

Saul Guevara and Gary Margrave

ABSTRACT

Angle gathers have been identified as an appropriate domain for prestack migration amplitude and velocity analysis, especially in complex geology settings, where other gathers appear prone to errors. This report analyses angle gathers with depth migration, applied to multicomponent data.

Shot-profile PSPI wave equation migration was the method selected for imaging. A ray based method was implemented to obtain the angle gathers, assuming a known velocity model. The characteristics of the method, and its application to PP and converted waves and to horizontal and dipping reflectors, are illustrated using two simple models, namely one with a flat horizon and the other for a dipping interface. Fig. 1 is an sketch of the method, and Fig. 2 shows an example of Ray Tracing (RT) on the dipping model, to obtain the incidence angles. Ray tracing be also used to obtain synthetic data for migration, and a Finite Difference (FD) result is used for comparison. Fig. 3 shows an Angle Gather for the horizontal layer example. Notice the limited span, related to the migration aperture. Amplitude analysis was considered. Fig. 4 shows a comparison of the amplitude vs. angle obtained after migration and the theoretical results according to the Zoeppritz equations for the dipping reflector. Qualitative agreement with the theory can be observed.

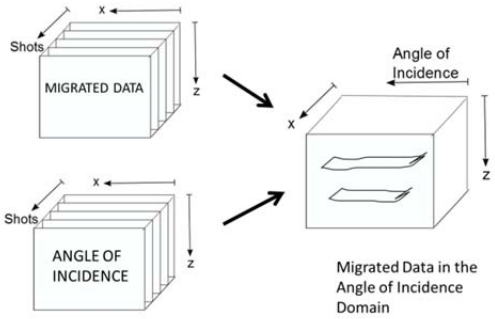

FIG. 1. Angle gathers from ray tracing.

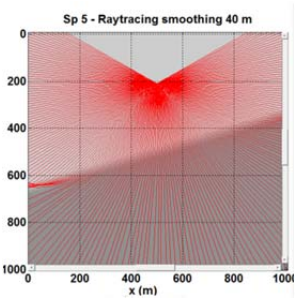

FIG. 2. Example of ray tracing- Slope model.

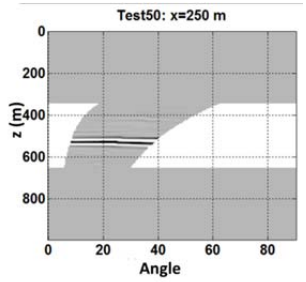

FIG. 3. Example of Image gather in the angle domain.

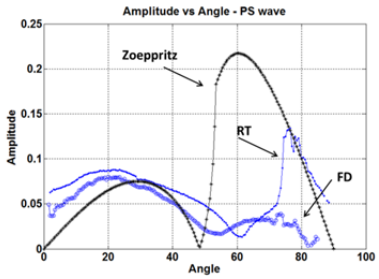

FIG. 4. PS wave Amplitude vs. Angle for the migrated data and according to Zoeppritz equations.

Estimation of shear velocity from P-P and P-S seismic data

Thais A. Guirigay and John C. Bancroft

ABSTRACT

Prestack migration of converted wave data requires accurate acoustic and shear velocities V_p and V_s. New methods to estimate the shear velocities using a single converted wave velocity V_c are shown in this paper.

The estimated shear velocity V_s is used with V_p in a full prestack migration using the equivalent offset method to form complete prestack migration gathers. This process is referred as converted wave equivalent offset migration (C-EOM). The quality of the method is demonstrated with a one real dataset.

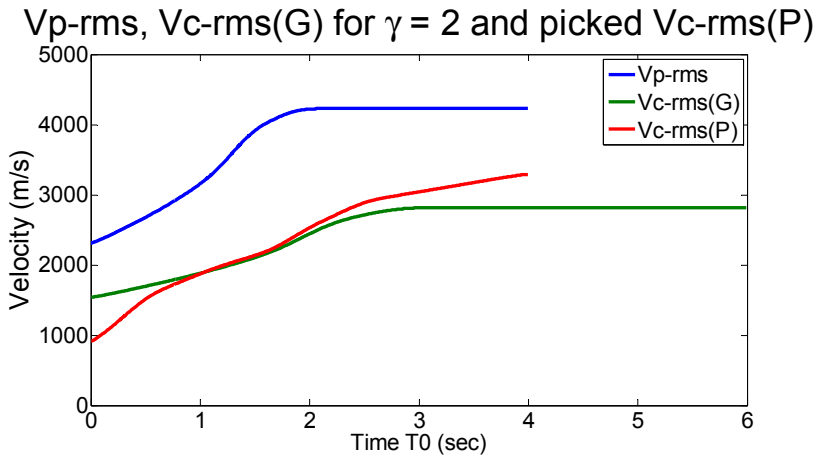

FIG 1. Mapping P and C RMS velocities.

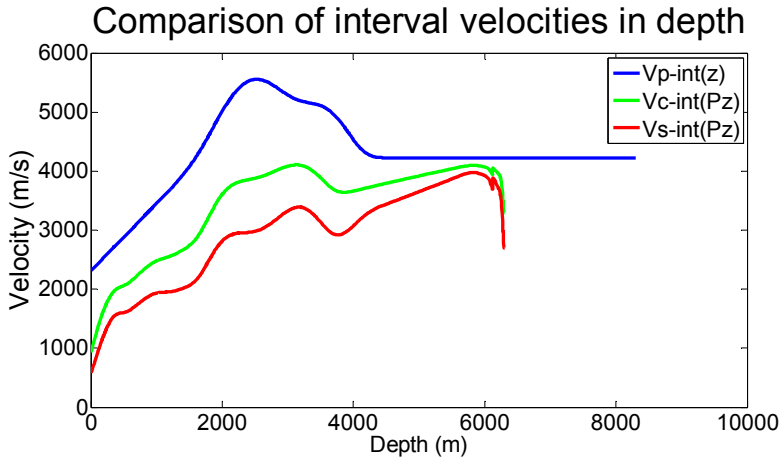

FIG 2. Plots of initial estimates of the converted wave velocity V_s with the Interval P, C and S velocities.

P-S migration using equivalent offset method

Thais A. Guirigay and John C. Bancroft

ABSTRACT

The result of applying the equivalent offset method to converted wave data is presented, along with a description of the processing sequence. The quality of the method is demonstrated for the case of one real datasets. The result show superior imaging when compared with alternative migration algorithms.

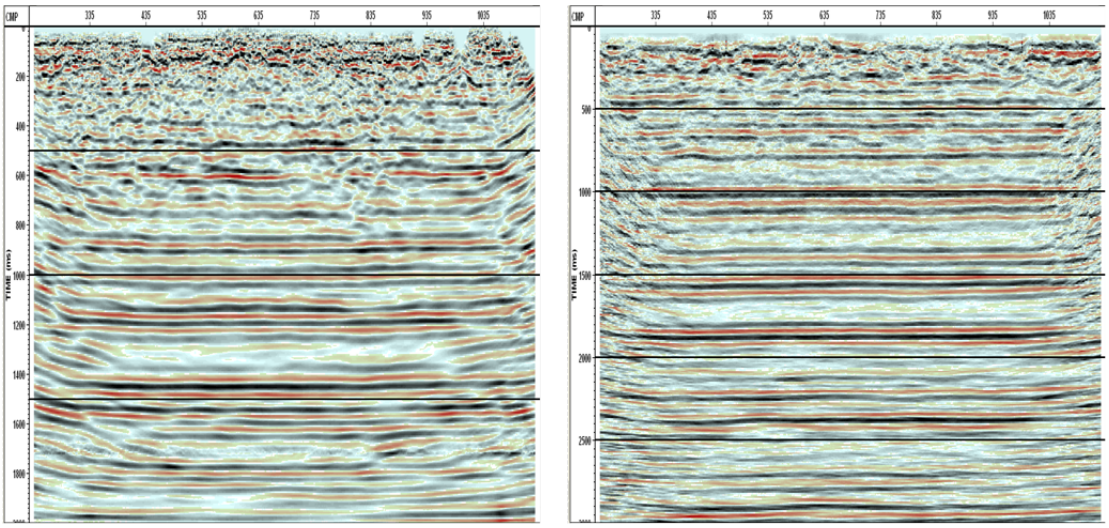

a) b)

FIG1: a) Final stacked P-P section after EOM b) and final stacked P-S section after EOM.

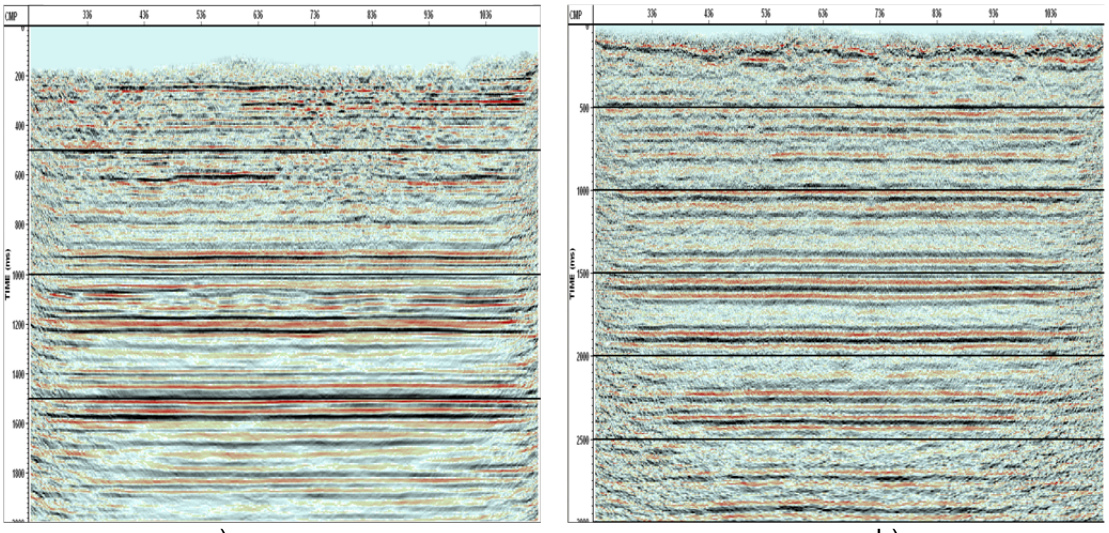

a) b)

FIG 2: Conventional processing, a) P-P poststack time migration, b) P-S poststack time migration section for comparison.

RMS velocity and average velocity ratio for P-S data processing

Thais A. Guirigay and John C. Bancroft

ABSTRACT

The prestack migration by equivalent offset and common scatter point is an alternative method to conventional prestack migration. This method may be applied to converted wave data and extends the concept of equivalent offset to include the appropriate P- and S- wave velocities. In the estimation of the total traveltime in the DSR equation, RMS velocities are required for both the P and S velocities. The P velocity is available from standard P-P processing, and the S velocity is obtained from initial estimates of a converted wave velocity that is a combination of P and S velocities. An assumption of this process is the ratio of the RMS and average velocities are similar for both the P-wave and S-wave velocities. This assumption is evaluated.

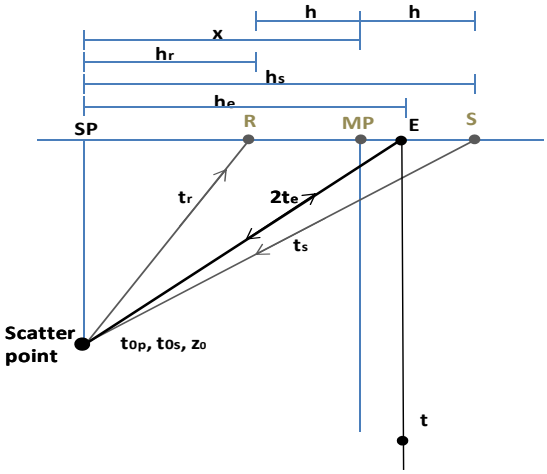

FIG 1: The raypaths and traveltime for a scatter or conversion point.

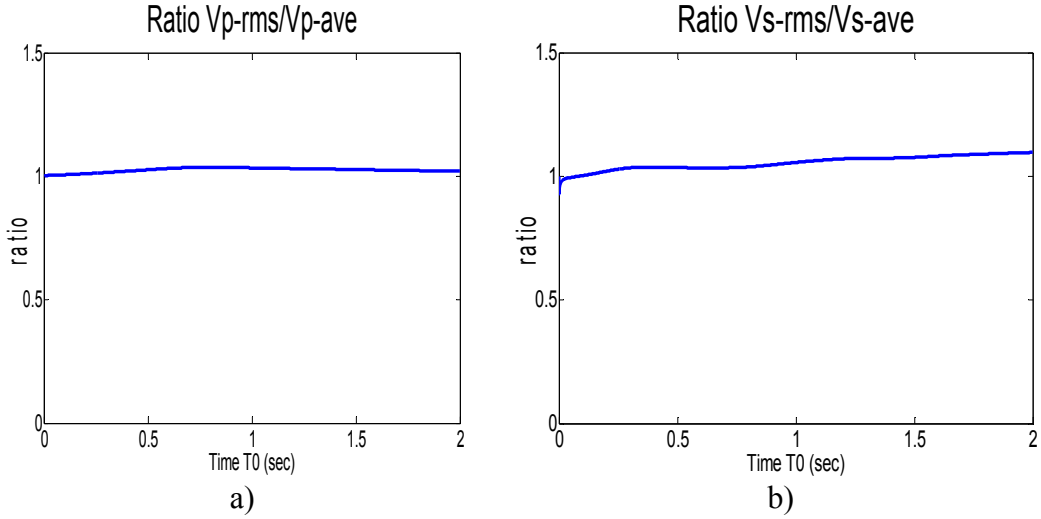

FIG 2: Ratio RMS and average velocity for a) P-wave velocities and b)S-wave velocities.

Husky 2011 walkaway 3C-VSP

Kevin W. Hall, Don C. Lawton, Dawson Holloway and Eric V. Gallant

ABSTRACT

CREWES was a participant in a walk-away vertical seismic profile (VSP) test near Cold Lake. Two-hundred and twenty-two VectorSeis accelerometers were deployed in a well at a nominal two meter spacing. Fourteen source points were acquired with dynamite and the University of Calgary's EnviroVibe source without moving the string of accelerometers in the well. P-S wavefields are observed on the radial and transverse components, and S-S wavefields are visible on the vertical, radial and transverse components for most shots. Higher amplitude down-going S-waves were generated from the vibrator source compared to dynamite. Three methods to perform automated component rotation are tested, and shown to give similar results, which are consistent between both source types. P-P and P-S brute corridor stacks are produced and compared to synthetic seismograms.

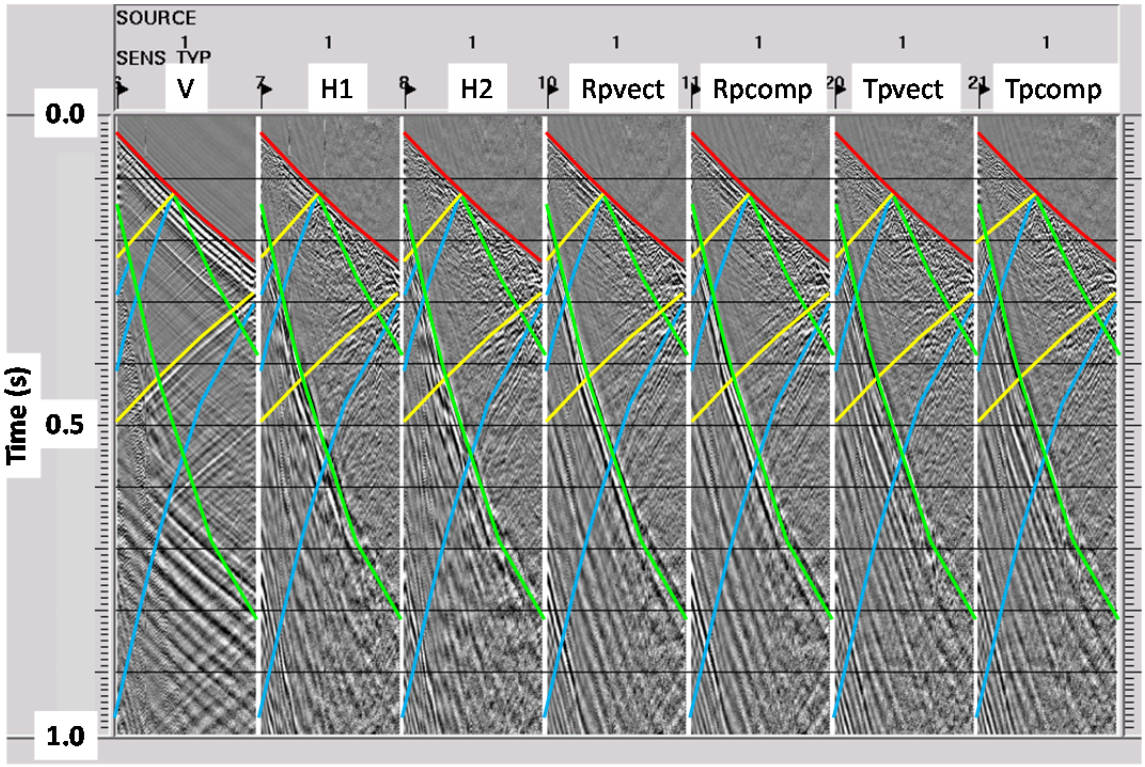

FIG. 1. EnviroVibe data for source point 1. From left to right: vertical component, horizontal 1, horizontal 2, radial from peak vector amplitude method, radial from principal component method, transverse from peak vector amplitude method, and transverse from principal component method, with 500 ms AGC for display. Red lines are P-downgoing, yellow is P-upgoing, green is S-downgoing, and blue is S-upgoing.

Towards using harmonic "contamination" as signal in vibrator data

Christopher B. Harrison, Gary Margrave, Michael Lamoureux, Arthur Siewert, Andrew Barrett and Helen Isaac

ABSTRACT

Vibroseis is currently the favoured source used for seismic land acquisition where conditions permit. A pilot signal generates a sweep of designed length and frequency range which drives the vibrator to impart a signal into the earth. Due to non-linearity in the vibrator hydraulics and mechanical systems, as well as near surface non- linearities, higher order harmonics of the pilot signal are generated, "contaminating" both sweep and the seismic record. Traditionally these higher order harmonics have been targets for attenuation during acquisition and processing. In 2011, CREWES and POTSI developed algorithms to decompose these harmonics from a vibrator sweep.

In this paper we examine the use of these higher order harmonics as correlation operators. We first look at the relative root mean power of each harmonic as compared to the original sweep and error/noise. This analysis shows, on average, that the third harmonic (H3) and upwards have power near noise levels. We then test the fundamental (H1), second harmonic (H2), third harmonic (H3) and forth harmonic (H4) as correlation operators on several increasingly complex synthetic traces. These results indicate, in a synthetic case, that H2 resolves closely spaced reflectors better than the other tested harmonics. Finally, we utilize uncorrelated field data supplied by Statoil to compare a basic pilot correlated seismic image with a time domain Gabor decomposed second harmonic correlated seismic image (FIG. 3). These seismic results indicate that using the second harmonic as a correlation operator has potential to reveal more shallow thin bed information than the pilot correlated trace.

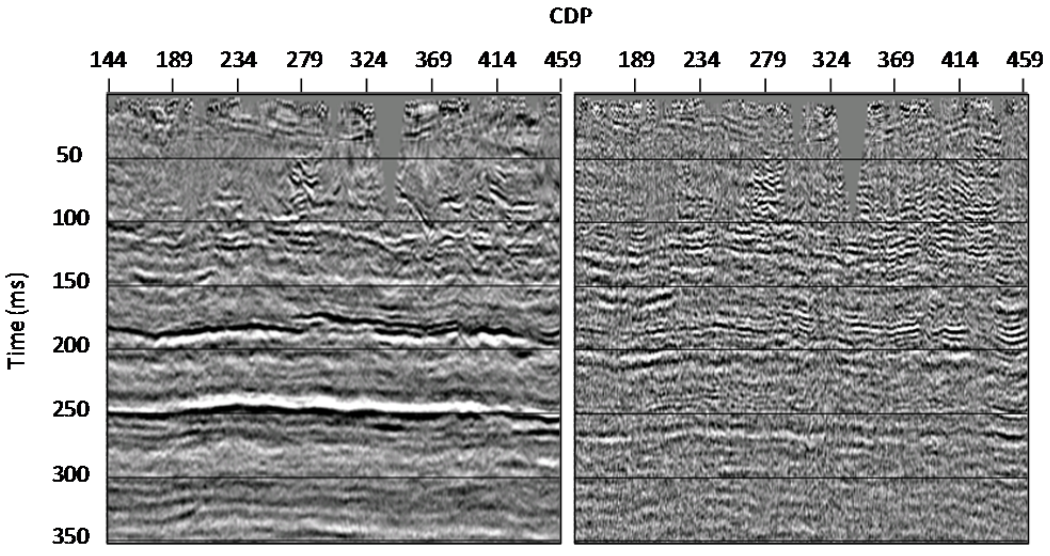

FIG. 3. Pilot correlated seismic image (left) and the near-offset (0-350m) second harmonic (H2) correlated seismic image (right).

Interference and the art of static correction: raypath interferometry at Hussar

David C. Henley

ABSTRACT

The technique known as raypath interferometry has been developed specifically to provide static corrections for seismic data from areas where surface-consistency is not valid, and where near-surface conditions complicate reflection event arrivals. The new technique is also compatible with surface-consistent data, however, and can increase effective redundancy for static corrections in general. Furthermore, the interferometry process itself, which involves inverse filtering, can apparently broaden the band of the resulting stack image. We demonstrate raypath interferometry on a subset of data from the 2011 Hussar Low-frequency experiment, providing static corrections for both PP and PS data. The result for PP data appears to be at least as good as conventional statics, while that for PS data is at least comparable to the conventional results over key horizons.

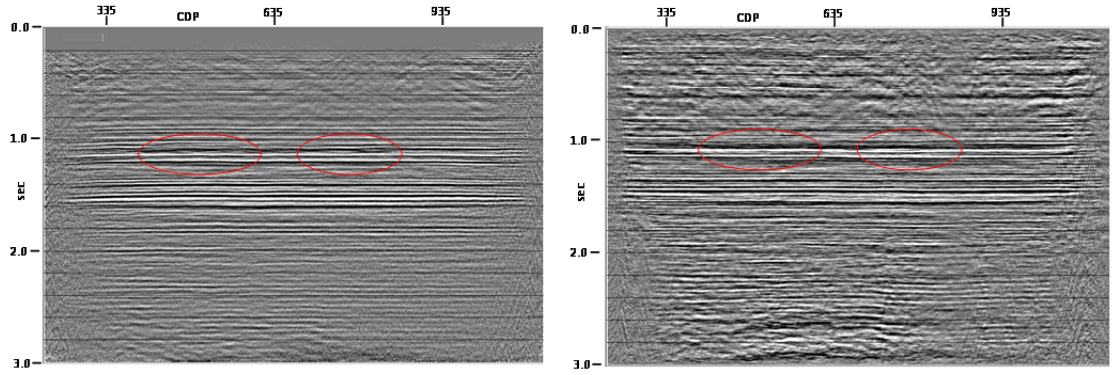

FIG.1. CMP stack of conventionally processed Hussar vertical component dynamite data (left) vs. CMP stack of the same vertical component data after raypath interferometry (right).

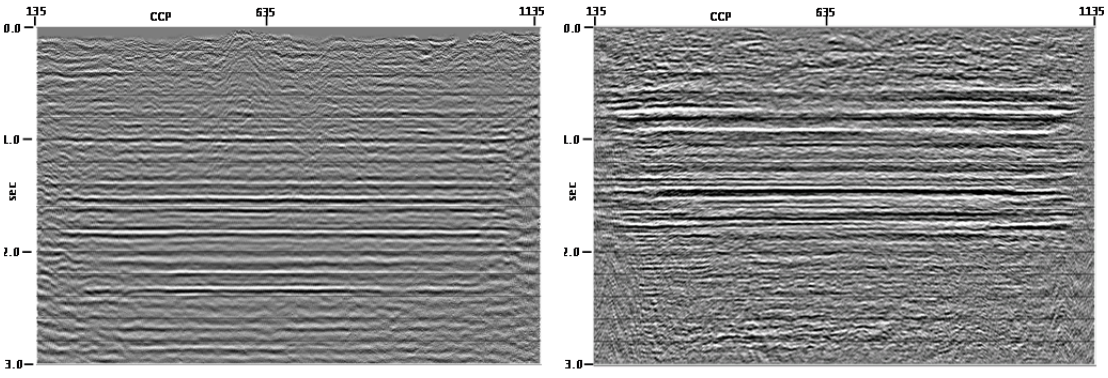

FIG. 2.CCP stack of conventionally processed Hussar radial component dynamite data (left) vs. ***approximate*** CCP stack of the same radial component data after raypath interferometry (right).

Time-lapse by the numbers: elastic modeling of repeatability issues

David C. Henley, Joe Wong and Peter M. Manning

ABSTRACT

An important emerging application for seismic reflection imaging is the remote monitoring of hydrocarbon production from a formation, or the injection of a fluid like CO2 for sequestration underground. In this application, it is important for seismic data acquisition and processing to be reliably repeated at regular intervals, over a period of time sufficient to provide a 'difference anomaly' history of the monitored process. One way to explore the detectability of this anomaly is to model the time-lapse process numerically. Since elastic modeling is probably the most realistic way to simulate the earth response to a seismic survey, a state-of-the-art elastic modeling program was used to generate seismic surveys corresponding to several 'baseline' and corresponding 'time-lapse' 2D earth models. Each time-lapse model differed from its baseline only in a small subsurface zone, where properties were altered to simulate fluid exchange. This work explored the detectability of the time-lapse anomaly relative to various acquisition and processing parameters. With identical acquisition parameters for a baseline model and its matching time-lapse model, the detectability of the anomaly was surprisingly robust in the presence of both random and coherent noise. In the presence of significant simulated 'seasonal' statics variations, the anomaly remained detectable, with suitable processing.

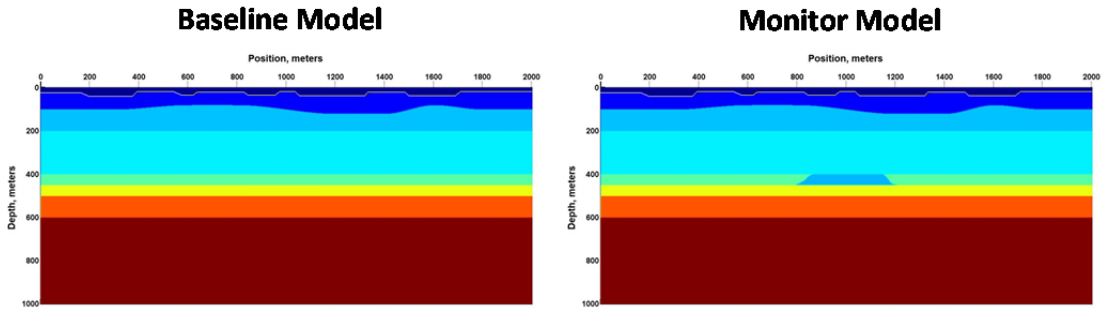

FIG. 1. Schematic representations of two models used in this time-lapse model study. Fluid-induced anomaly is visible in the 'monitor' model.

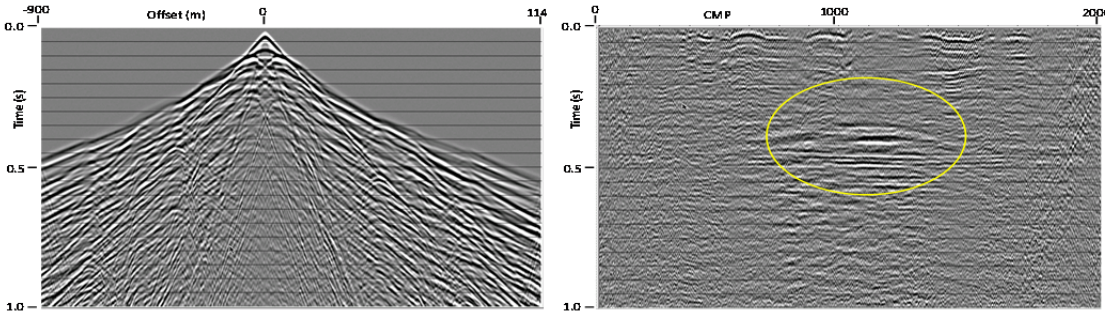

FIG. 2. Typical vertical component shot gather from baseline model (left), and difference image for CMP stacks of baseline and monitor models above.

Where in the earth are the low frequencies?: comparison of sources at Hussar

David C. Henley

ABSTRACT

Recent increased interest in full-waveform inversion of seismic reflection data has motivated attempts to broaden the spectrum of reflections recorded at the earth's surface. Of particular importance is the low frequency portion of the spectrum, which contributes significantly to the 'character' of reflections and to the ability to tie seismic data to well logs. An obvious way to boost the low-frequency spectrum is to increase the amount of low frequency source energy penetrating the earth during seismic acquisition, and to employ sensors optimized for detecting low frequencies. The objective of the Hussar experiment, performed by CREWES and some of its sponsor companies in 2011, was to test acquisition configurations designed to enhance low-frequency energy content of seismic surveys. Early results for these data compared the low-frequency spectra of the various sources on unprocessed trace gathers or on fully processed stack images. Here, in a different approach, we compare two low-frequency-optimized surface sources (Vibroseis) with buried dynamite on single source gathers from two different arrays of sensors. By separating the coherent surface-wave noise from the source gathers, we show that a larger proportion of the low-frequency source energy for the two surface sources appears as surface-wave energy, compared to dynamite. Single-fold dynamite data demonstrate both higher S/N and a broader reflection spectrum than corresponding Vibroseis data. Subsequent processing, including high-fold stacking and migration may diminish these differences, but it appears that dynamite is more effective in propagating low frequency energy into useful reflections than the surface sources tested, much of whose low-frequency output seems to preferentially excite surface waves.

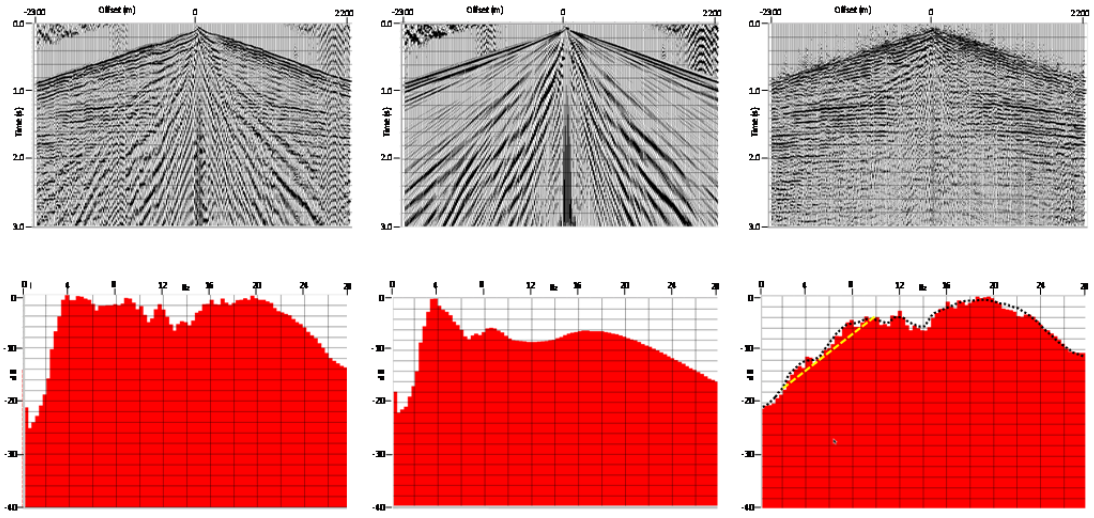

FIG. 1. Vertical component dynamite shot gather from Hussar from 4.5Hz geophones. Left: raw shot, centre: noise estimate, right: shot after noise subtraction. Average power spectra over the range 0-28Hz posted beneath each gather. Noise power peaks at 4Hz with these 4.5Hz phones.

Application of internal multiple prediction from synthetic to lab to land data

Melissa Hernandez and Kris Innanen

ABSTRACT

Multiple reflections represent a serious problem in the field of seismic processing. Multiple events can be mistaken for primary reflections, and may distort primary events and obscure the task of interpretation. In particular, internal multiples can be very problematic because they mask information from seismic data, which is very harmful in sophisticated analysis such as AVO. In this work we will focus in the prediction of internal multiples and we will illustrate how the inverse scattering internal multiple algorithm introduced by Weglein and Araujo in 1994, is capable to attenuate internal multiples without any a priori information about the medium through which the waves propagate. One of the advantages of this method over other is its ability to suppress multiples that interfere with primaries without attenuating the primaries themselves. I consider the version of the algorithm for 1D normal incidence case.

In this work we promote a stepped approach to predicting multiples in a given field data set: first, by carrying out synthetic/numerical examples; second by carrying out tests on laboratory physical modeling data; and finally by testing prediction of a field data set suspected to be strongly contaminated with internal multiples.

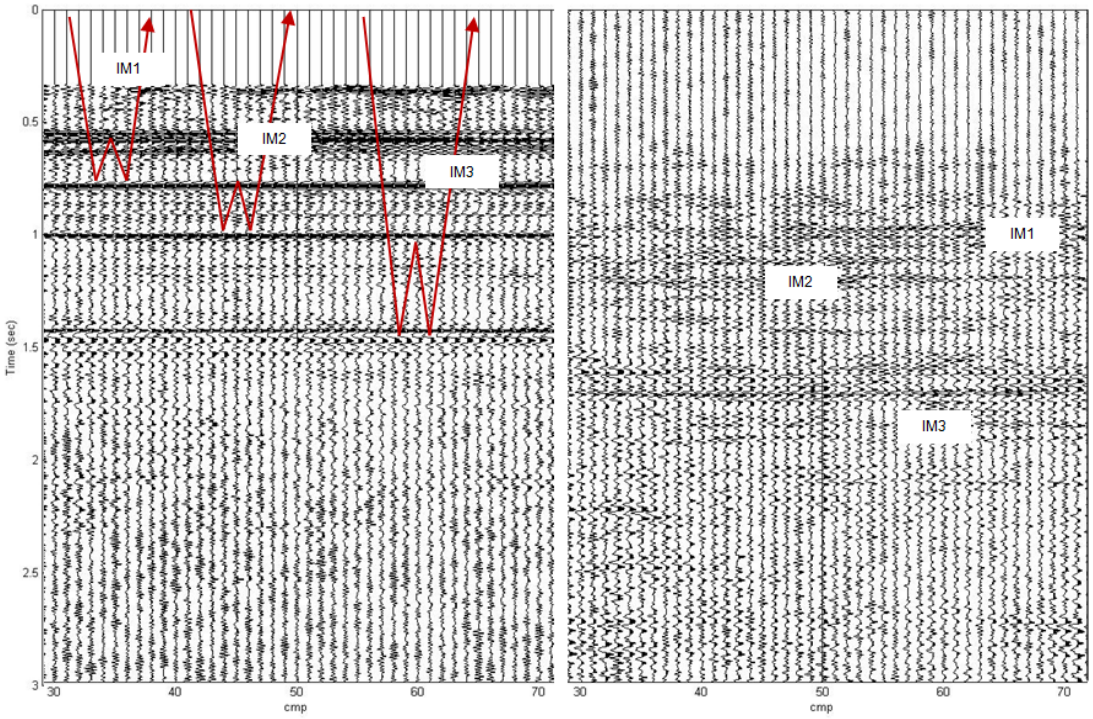

FIG. 1.Comparison between input data (left side) and output prediction (right side),field data.

1.5D internal multiple prediction in MATLAB

Kris Innanen

ABSTRACT

We present a 1.5D MATLAB implementation of the inverse scattering series internal multiple prediction algorithm developed by Weglein and collaborators in the 1990s. We discuss the transformation of the data from the space and time domain to those of wavenumber and pseudo-depth, and the subsequent prediction operation, and illustrate the procedure with a synthetic example. Our plan forward is to apply with the 1.5D algorithm the methods developed by Hernandez for the 1D algorithm (in this report), which involve stepping from synthetic, to laboratory, and finally to land data.

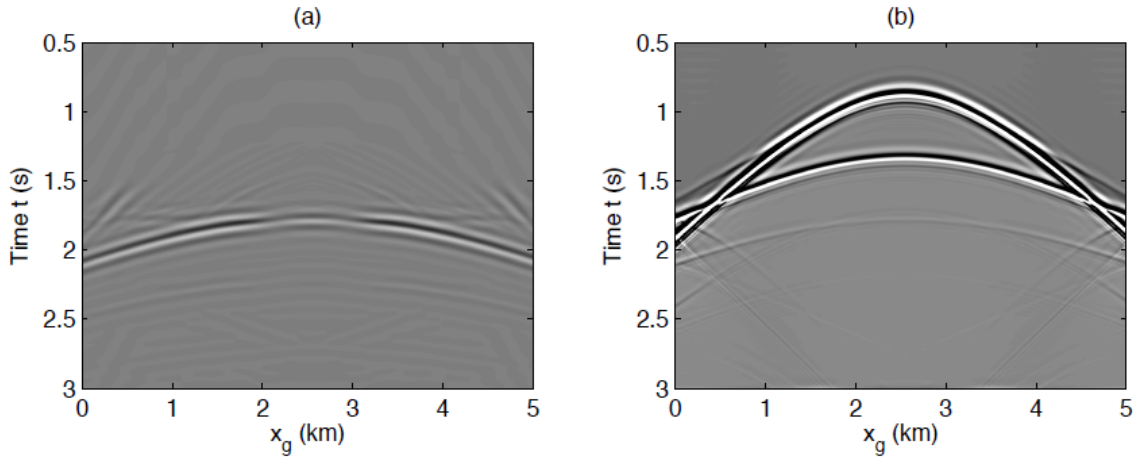

FIG. 1. The output of the 1.5D internal multiple prediction. (a) The prediction, in which two multiples are predicted. (b) The original data with both primaries and internal multiples.

The acoustic Lagrangian density and the full waveform inversion gradient

Kris Innanen

ABSTRACT

The Euler-Lagrange equations relate the Lagrangian density $\mathcal{L}$ for a system of particles or fields with the associated equations of motion or field equations. A central problem of field theory is to postulate an $\mathcal{L}$ from which the correct equations derive. The problem may be posed in reverse also: known equations of motion can be used as a starting point from which to deduce the associated $\mathcal{L}$. This is useful primarily as a pedagogical exercise. However, the $\mathcal{L}$ for acoustic continua is proportional to the acoustic Fréchet derivative, a crucial quantity in seismic full waveform inversion which often must be laboriously calculated. If Fréchet derivatives and thereby FWI gradients are derivable directly from the appropriate continuum mechanical Lagrangian densities, in addition to opening an avenue for physical interpretation of inversion iterates, a considerable savings in calculation would likely be available.

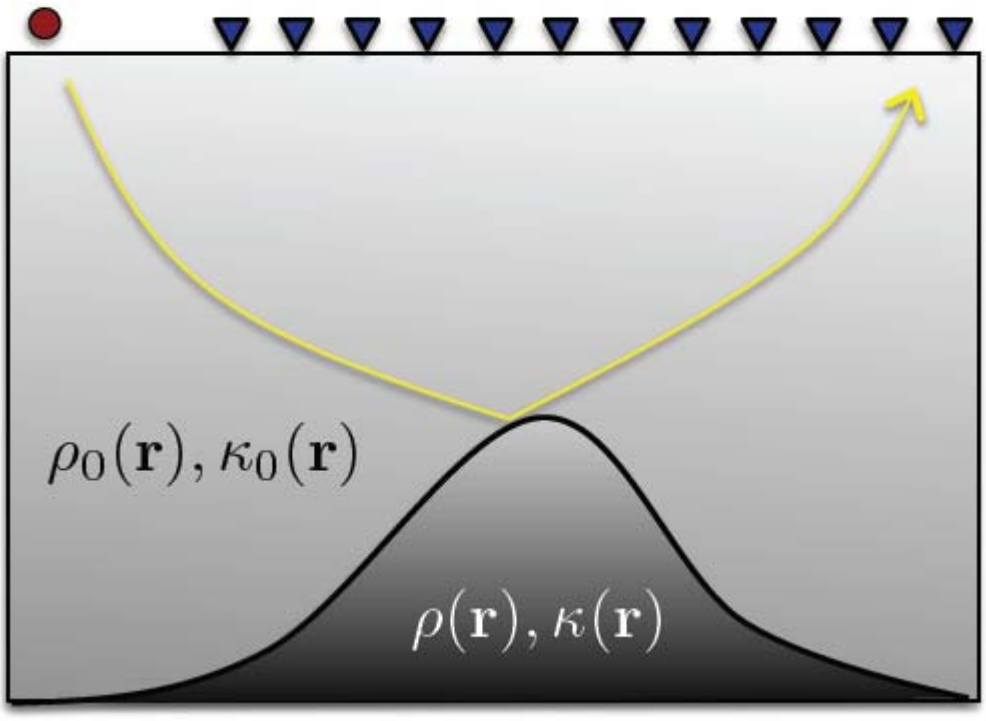

FIG. 1. The acoustic seismic reflection problem.

Anelastic AVO approximations continued

Kris Innanen

ABSTRACT

We write down linearized anelastic AVO approximations appropriate for problems involving both elastic and anelastic incidence media. Variations in the anelastic properties of the Earth across the reflecting boundary are expressed in terms of reflectivity- and relative change-type quantities. R_{PP}, R_{PS} and R_{SS} coefficients are each investigated. There is a wide range of degrees of accuracy produced by this set of formulas and no obvious pattern. We conclude it is best to have all of the forms "on hand" to fit anelastic AVO situations as they arise.

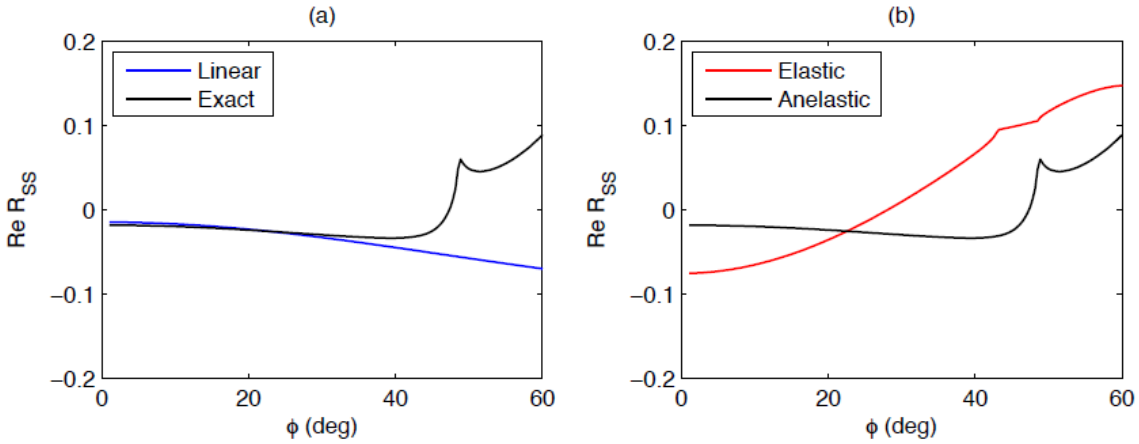

FIG. 1. RSS approximation for elastic incidence media in terms of the relative change in anelastic parameters across the reflecting boundary. (a) Exact anelastic R_{SS} (black) vs. linear approximation (blue). (b) Exact anelastic R_{SS} (black) vs. exact elastic R_{SS} (red) assuming entirely elastic media.

Blurring the line between intrinsic and scattering attenuation by means of the Shannon entropy

Kris Innanen

ABSTRACT

We compute a version of the Shannon entropy S of snapshots of a seismic wave field as it propagates. S is argued to be a measure of the degree of either multiple scattering, or attenuation, or both, experienced by the wave, evolving similarly regardless of which process dominates in a given example. Invoking it, therefore, forces us to reject the distinction between intrinsic and extrinsic attenuation, and allows us to place thin-bed reverberations above and below the resolving power of the experiment on an equal footing should we decide to do so. S is easily computable, as is shown with both synthetic ("wave in a box") examples and a field VSP example. It relies on stable estimates of the histograms of wave amplitude values, and the best way of doing this is still under investigation.

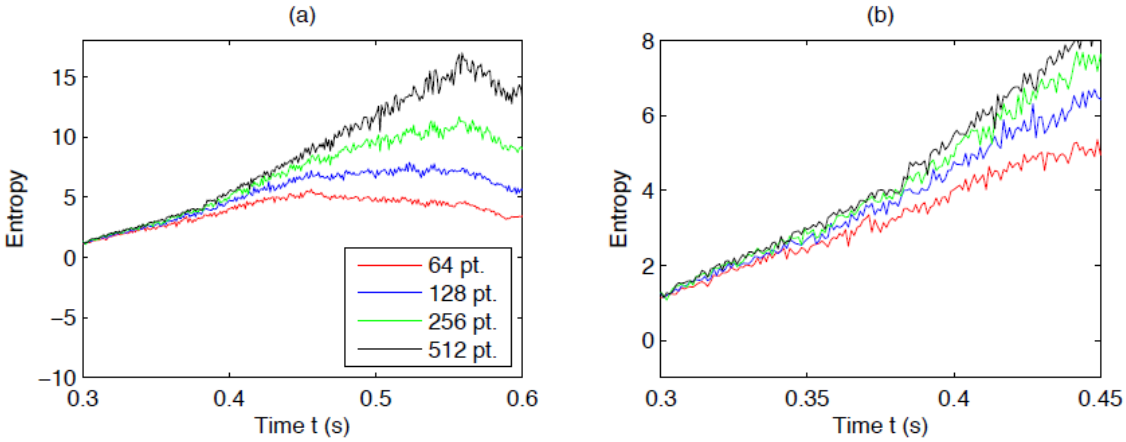

FIG. 1. The Shannon entropy of the zero offset Ross Lake data. (a) S calculated using four different bin lengths and sizes for the full time history in which the direct wave is detected in the VSP data; (b) zoom in on early times.

Hagedoorn's +/- method and interferometric refraction imaging

Kris Innanen

ABSTRACT

Hagedoorn's plus/minus method involves the calculation of sums and differences of first arrivals in refraction data sets. These quantities can be used to estimate subsurface velocities and the depths of curved refractors. Since seismic interferometry is, in a sense, a formal way of adding and subtracting traveltimes, it follows that the +/- method should be expressible in the form of an interferometric procedure. An algorithm for refractor imaging, expressed in terms of interferometric calculations on forward and reverse shot records, is derived heuristically and tested with a simple synthetic data set.

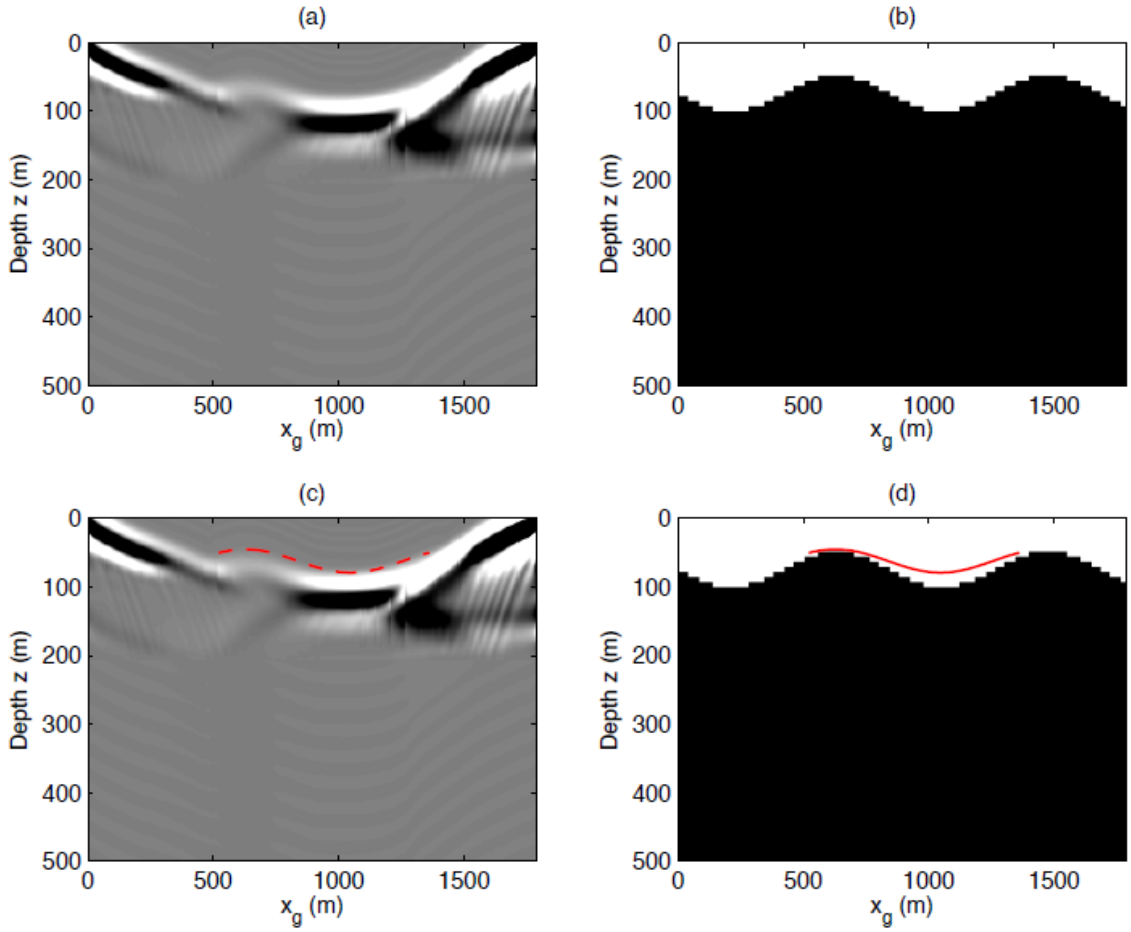

FIG. 1. Imaging with the interferometric plus field. (a) The plus field is plotted agains the scaled depth axis. (b) The original model is plotted for comparison. (c) Within the +/- window the first arrival is picked (red dashed line). (d) The picked line is re-plotted against the actual model (red solid line).

Nonlinear AVO in the lab

Kris Innanen and Faranak Mahmoudian

ABSTRACT

The nonlinearity of the seismic amplitude-variation-with-offset (AVO) response in the presence of large relative changes in acoustic and elastic medium properties is investigated with physical modelling data. A procedure for pre-processing reflection data, acquired using the CREWES-University of Calgary physical modelling facility, is enacted on a reflection from a water/plexiglas boundary. The resulting picked and processed amplitudes are compared with exact solutions of the plane-wave Zoeppritz equations, as well as first, second, and third order R_{PP} approximations. We conclude that in the angle range 0 - 20°, the third order approximation is sufficient to capture the nonlinearity of the AVO response to within roughly 1% from a liquid-solid boundary with V_P, V_S and ρ contrasts of 1485 - 2745m/s, 0 - 1380m/s, and 1:00 - 1:19gm/cc respectively. This is in contrast to the linear Aki-Richards approximation, which is in error by as much as 25% in the same angle range.

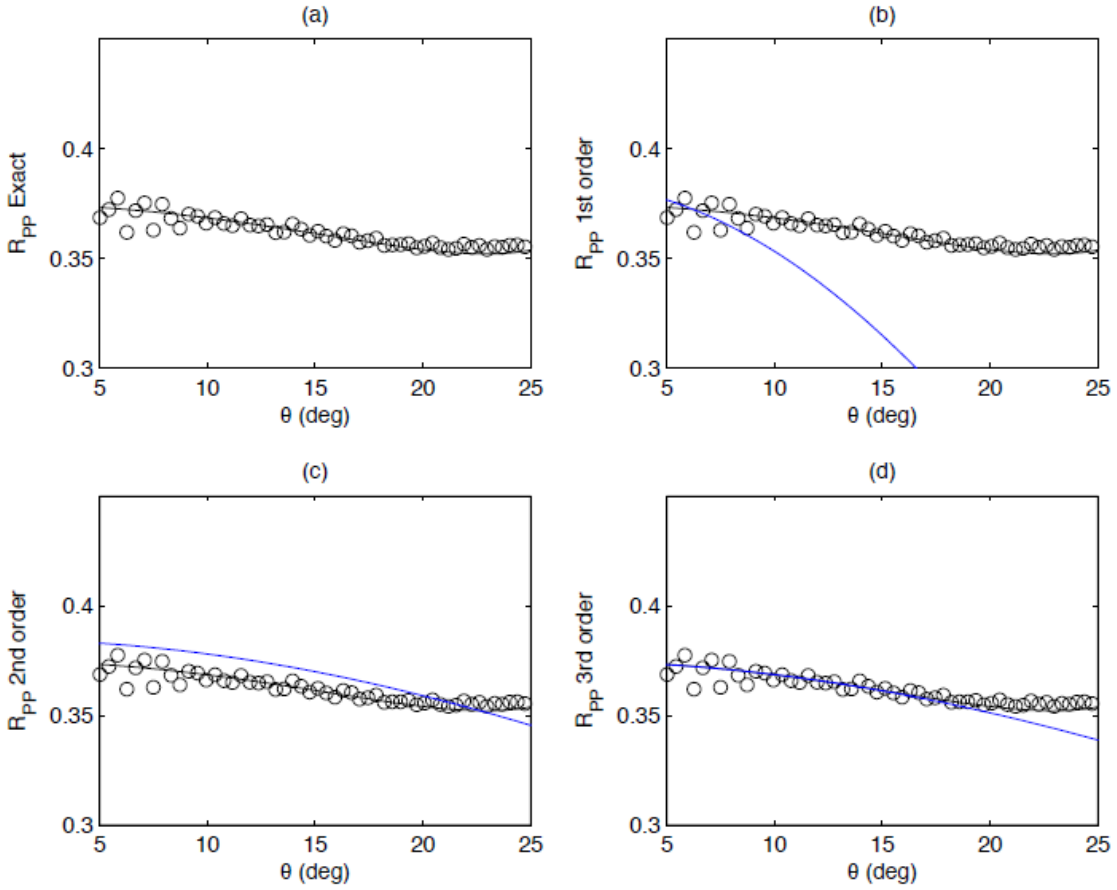

FIG. 1. Modelled data vs. lab data. (a) Exact solution for R_{PP} is plotted as a solid line, as are measured lab data. (b) First-order (linearized) R_{PP} approximation is plotted in blue against the same measurements. (c)-(d) Second- and third-order approximations plotted agains the lab data similarly.

Nonlinear seismology: the Priddis pulse-probe experiment revisited

Kris Innanen, Gary Margrave and Malcolm Bertram

ABSTRACT

One of the objectives of the 2012 Priddis pulse-probe experiment was to revisit the idea of measuring nonlinear seismic responses on the exploration/monitoring scale. In this initial study, we consider the difference between seismic responses from (1) the CREWES mini vibe as a lone source carrying out a linear sweep, (2) a standard (Geokinetics Mertz 22) vibe as a lone source vibrating at a fixed 25Hz, and (3) the two simultaneously. We show examples of the uncorrelated data for these sweeps, as well as compare the sizes of the data sets with and without the background signal.

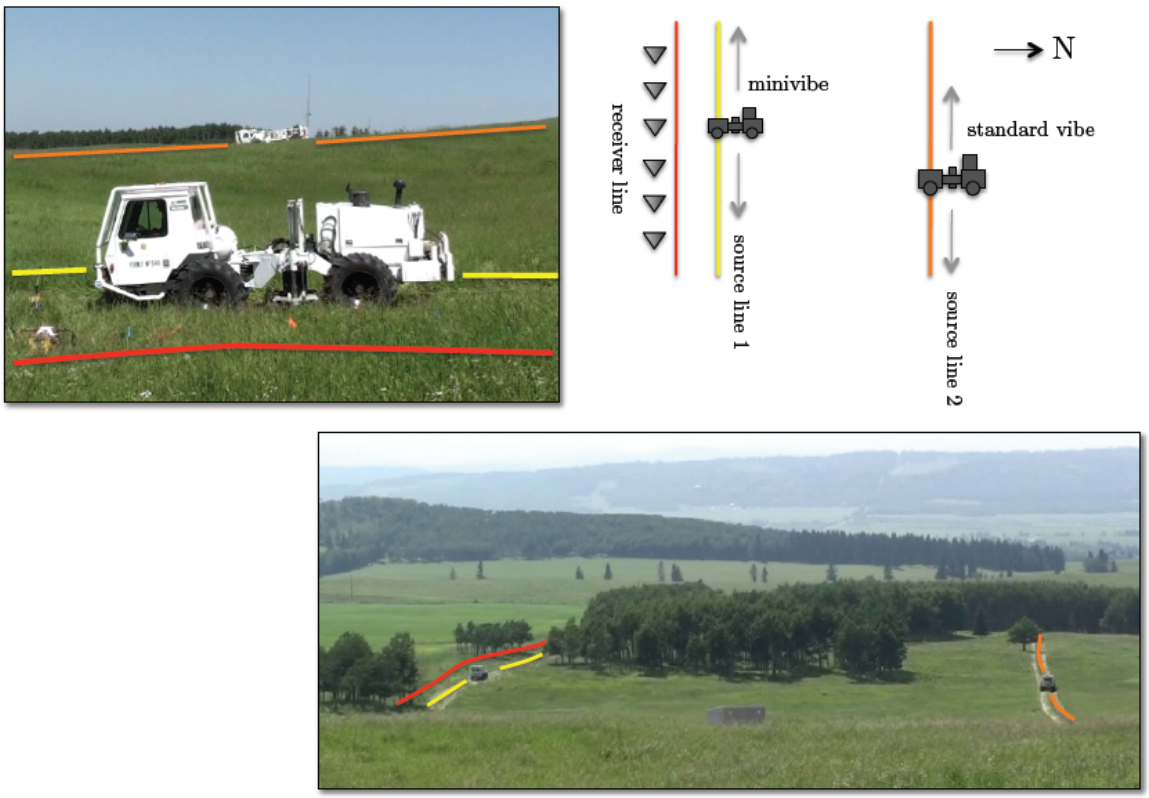

FIG. 1. Schematic illustration of the 2012 Priddis pulse-probe experiment. Two vibes are activated as sources on parallel source lines (yellow and orange); the CREWES Envirovibe on the receiver line and the standard vibrator on the 100m offset line. The offset vibe excites a fixed 25Hz wave in the Earth, and the Envirovibe carries out a linear sweep with and without this background wave field.

Potentials for anelastic scattering

Kris Innanen

ABSTRACT

Previous efforts to characterize the scattering problem for anelastic waves have been carried out in the anacoustic regime, and in the full anelastic regime but for single reflectors (i.e., the anelastic AVO problem). Here we begin to frame the full anelastic scattering problem, focusing on some key issues: transformation of anelastic scattering potentials to the P-, Sv-, and Sh- potential domain, and the consequences to that transformation of moving from an elastic reference/anelastic perturbation model to an anelastic reference/anelastic perturbation model. We use the scattering potentials thus derived to produce sensitivity kernels for full waveform inversion iterates wherein V_P , V_S, ρ updates are carried out in elastic target determination, and Q_P and Q_S updates are added in anelastic target determination.

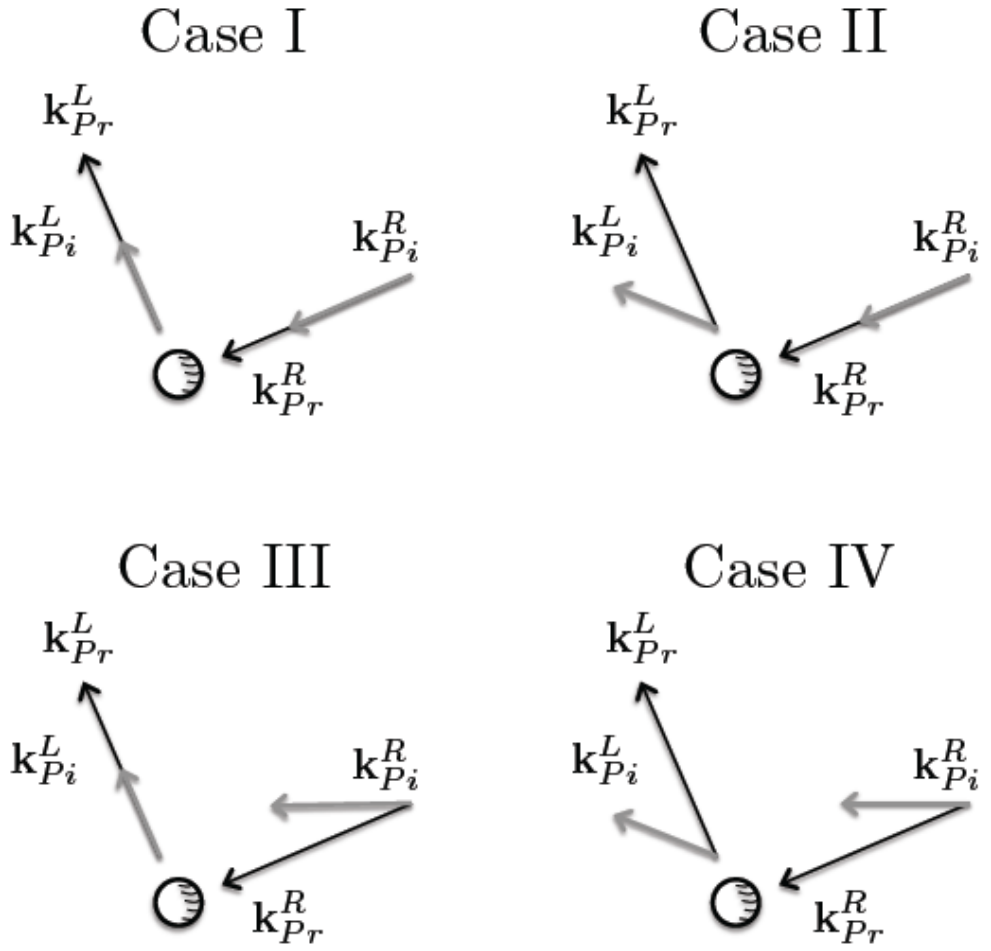

FIG. 1. Schematic diagram for incoming and outgoing waves in anelastic reference media. Case I: homogeneous incoming and outgoing waves. Case II: homogeneous incoming and inhomogeneous outgoing waves. Case III: inhomogeneous incoming and homogeneous outgoing waves. Case IV: inhomogeneous incoming and outgoing waves.

Wave propagation and interacting particles continued: plane waves at oblique incidence

Kris Innanen

ABSTRACT

We continue the development of a model of seismic data based on the idea of particles, or groups of particles, undergoing collision and disintegration interactions—rather than seismic wave events reflecting and transmitting. Here we admit plane waves which propagate obliquely with respect to the spatial axis along which they are observed (which we have thus far fixed to be the depth axis, e.g., the well in a VSP experiment). We consider both harmonic and transient waves. Acoustic and multi parameter problems demand the inclusion of additional particles in order that boundary conditions are honoured.

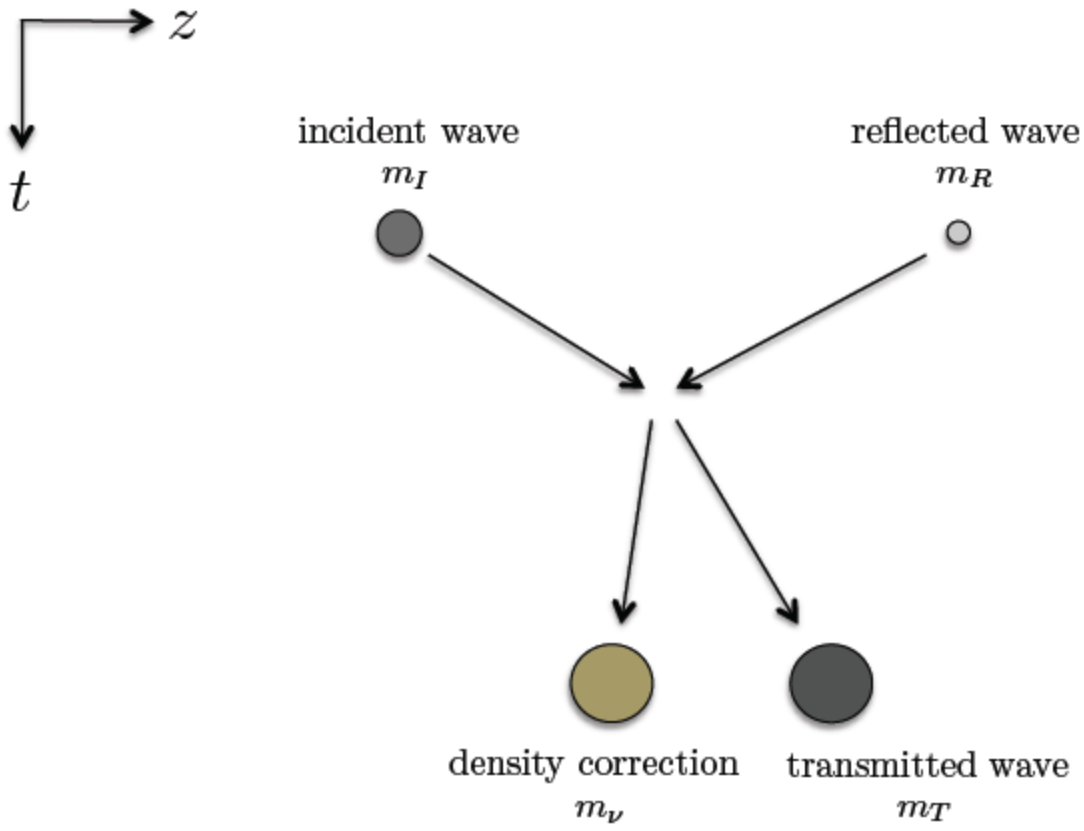

FIG. 1. Multiparameter problems. The simple direct relationship between conservation of momentum and rate of motion along the time axis is a consequence of scalar boundary conditions. To maintain the particle model in a velocity/density problem we must introduce an unmeasured ghost particle ν to carry off a portion of the apparent momentum.

Hussar converted-wave data processing and analysis

J. Helen Isaac and John C. Bancroft

ABSTRACT

We processed and inverted converted-wave data acquired during the low-frequency shoot at Hussar, Alberta in September, 2001, generated from dynamite and low-dwell vibroseis sources and recorded on 3C 10 Hz geophones. The data processing included radial filtering and Gabor deconvolution. The stacked dynamite and vibroseis data both show strong converted-wave reflections. Receiver statics were derived successfully by flattening an horizon picked on a stack of receiver gathers.

Comparison of the stack of vibroseis data obtained through conventional NMO, common conversion point (CCP) stack and post-stack migration and the equivalent offset migration (EOM) stack of the same data show that the EOM method successfully produced a stack of comparable quality. The converted-wave velocity model derived through common scatter point analysis was similar to that obtained through semblance analysis of common conversion point gathers. Thus, EOM shows considerable promise as a method for converted-wave data velocity estimation and migration.

Joint PP-PS model-based inversion was only partially successful. The character ties between the migrated PS data and well data were not easy to make and the registration of the PP and PS data shows that the character match between the two datasets is poor. However, since we clearly have converted-wave data in this area, the dataset will be useful for testing converted-wave processing procedures such as velocity determination, statics estimation and migration, and PP-PS data matching and registration.

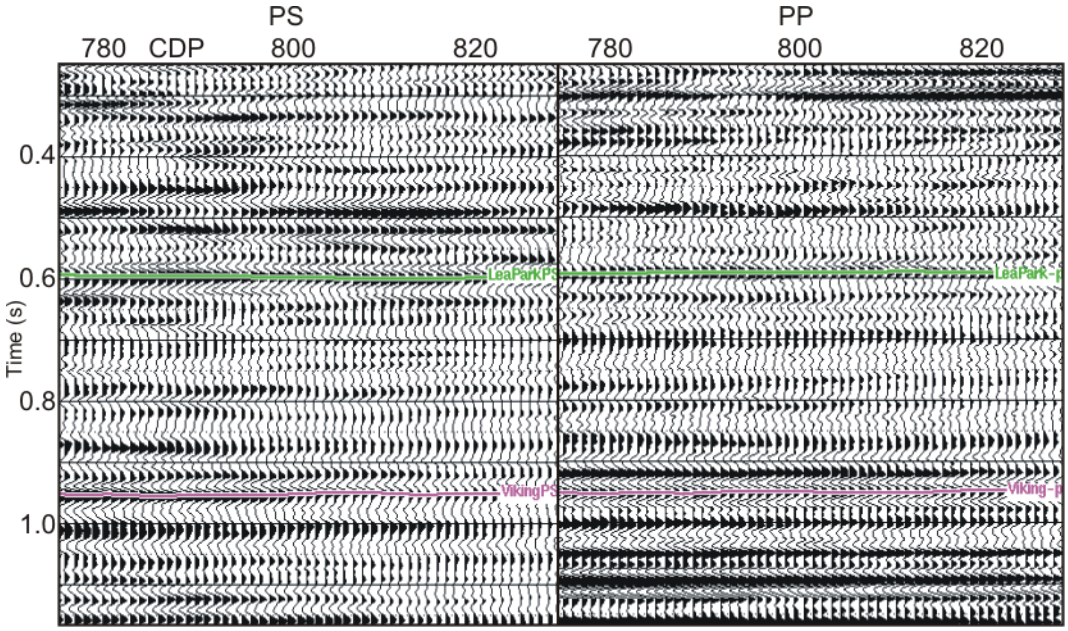

FIG. 1. Registered PS and PP dynamite data with the correlated horizons. The PS data have been scaled to PP time.

Processing and analysis of Hussar data for low frequency content

J. Helen Isaac, Gary F. Margrave, Monika Deviat[1] and Pam Nagarajappa[1]

ABSTRACT

Seismic data acquired by CREWES at an experimental low frequency shoot at Hussar, Alberta, in September 2011 were processed to attenuate unwanted noise and wavetrains and to retain or even enhance the low frequency content. We analyze the stacked data by creating plots of lateral phase-coherency versus frequency.

The initial unprocessed data show strong coherency down to 7.5 Hz and weak coherency to 5 Hz but nothing below that. After processing by CREWES with radial filters and Gabor deconvolution, the data show good phase-coherency to 3 Hz but little in the range of 0-3 Hz. Stacks of the same dataset processed by CGGVeritas with much more noise attenuation display coherency in the lowest frequencies of 1-5 Hz. Efficient noise attenuation appears to be the greatest factor in attaining high coherency at the lowest frequencies.

The phase-coherency plots are affected by processing procedures such as AGC and the amount of muting before stack. AGC adversely affects the coherency while the mute should not be so harsh as to remove desired frequency content. Geophone instrument response compensation does not appear to enhance coherency at the lowest frequencies.

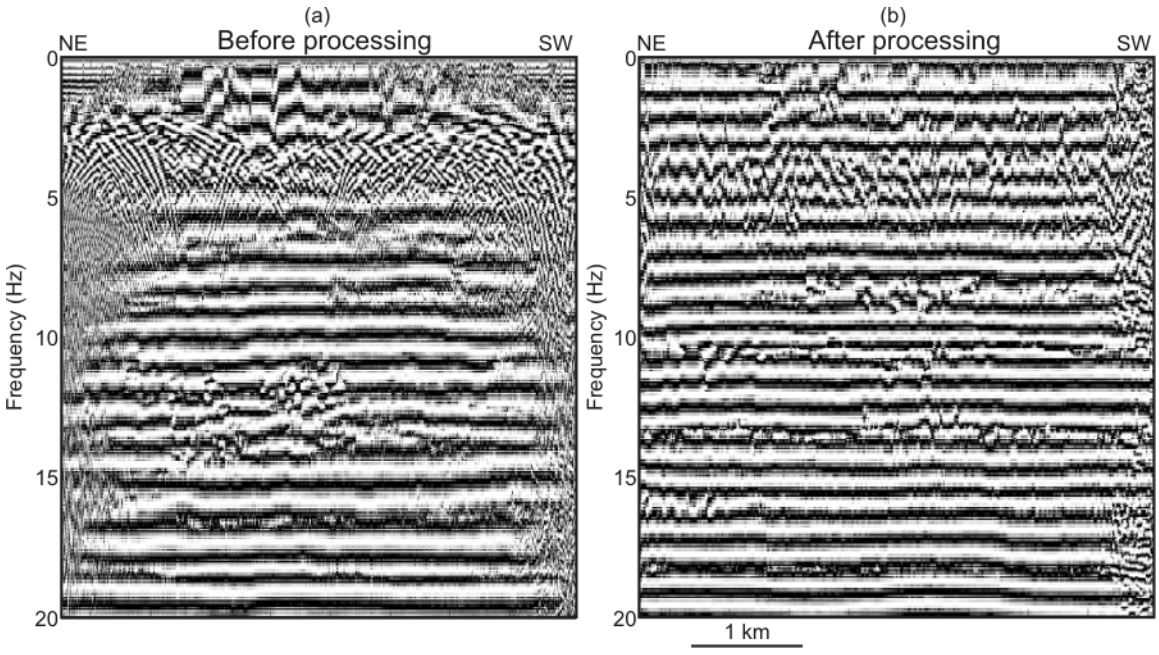

FIG. 1. Phase-coherency plots of stacked dynamite data before (a) and after (b) processing to remove undesired groundroll, converted-wave energy and noise. These plots show the coherent frequency content of signal in the 0-20 Hz band.

[1] CGGVeritas

Towards full waveform inversion: A torturous path

J. Helen Isaac and Gary F. Margrave

ABSTRACT

Full waveform inversion (FWI) can be viewed as an iterative cycle involving forward modelling, pre-stack migration, impedance inversion and velocity model updating. At each stage of the process there are many factors affecting the outcome. Among the most important are the type of modelling (acoustic versus elastic), derivation of the initial velocity model, the inherent differences between field data and numerically modelled data, and the conditioning of the field seismic data to be inverted.

Our attempts to derive an initial velocity model suggest that the integration of a refraction tomography velocity model with well log data provides a better initial velocity model than well log data alone. Initial comparisons of field and modelled shot gathers confirm that conditioning of the field seismic data plays a large role in the successful matching of field and modelled data. We hope to experiment with shot gathers having different processing techniques applied to determine the optimum processing to apply.

We know there are many factors that affect the field data that cannot be accounted for in the numerical modelling, even if elastic modelling is used. Our future work will include analysis of data with different processing to assess the suitability of the processing for data intended for input into FWI. CREWES has access to several FD modelling codes and would like to test them all with the same velocity model to assess their applicability to FWI.

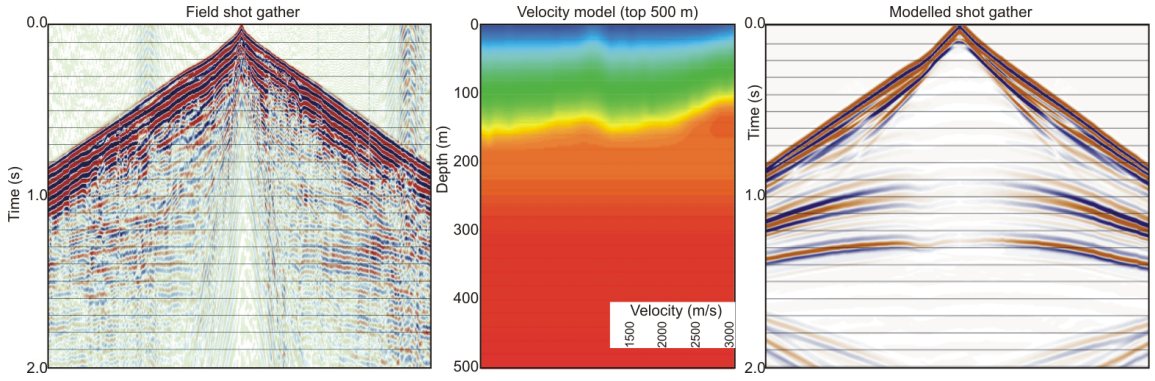

FIG. 1. Field shot gather from the Hussar low frequency dynamite dataset, velocity model that integrates the tomography model and well data, and the shot gather modelled by an acoustic finite difference algorithm. The velocity model was developed to provide the closest match between the field and modelled first break picks. It is necessary to include the sub-weathering velocities in the model.

Q Estimation via Continous Wavelet Transform

Hormoz Izadi, Kris Innanen and Michael P. Lamoureux

ABSTRACT

In seismic signal analysis, irregular structures and points of sharp variation contain critical information, thus making the study of a signal's local properties an appropriate mechanism for obtaining information from seismic data. The local regularity of a seismic event is determined by the wavelet transform modulus maxima and the associated Lipschitz exponent. As a means of classifying regularities of a signal and estimating the associated Lipschitz exponent, the linear and non-linear Mallat-Hwang-Zhong (MHZ) signal model based on the wavelet theory is reviewed and developed.

For practical settings, in particular band-limited signal events, the more complex nonlinear MHZ signal model must minimised in order to estimate the local regularity and the additional smoothness parameter. Based on synthetic vertical seismic profile (VSP) modelling, a relatively complicated mathematical mapping between the Lipschitz exponent and seismic quality factor Q is obtained. However, analysing the smoothness parameter results in an invertible power law relation between the aforementioned parameter and Q.

Applying the non-linear MHZ model to Ross Lake VSP field data captures the general absorption trend estimated by Zhang and stewart (2006). Furthermore, the power law relation provides relatively reasonable Q values comparable to the estimated values using traditional methods, such as the steepest descent. However, for a more robust mathematical relation between the Lipschitz exponent, smoothness parameter and seismic quality factor Q, additional theoretical and field data analysis is required.

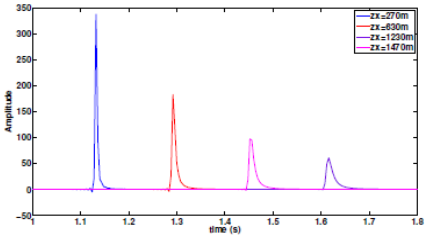

(a)

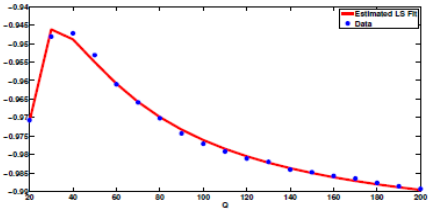

(b)

FIG. 1. (a) Direct arrivals corresponding to receivers located at z = 270m, z = 630m, z = 1230m and z = 1470m respectively with Q = 20 (b) Plot of α vs Q for z = 270m.

A framework for accurate approximation of difference reflection data from monitor to baseline survey in a time-lapse problem using AVO analysis

Shahin Jabbari and Kristopher A. H. Innanen

ABSTRACT

Perturbation theory has been used widely in many applications in seismology, more recently for time-lapse problems. Time-lapse is a cost-effective approach for monitoring the changes in the fluid saturation and pressure over a period of time in a reservoir. The difference data during the change in a reservoir from the baseline survey to monitor survey are described through applying the perturbation theory. We defined a form for the difference reflection data, ΔR_{PP}, in order of physical change or baseline interface contrast and time-lapse changes. A framework for linear and non linear time-lapse difference data is formulated using amplitude variation with offset (AVO) methods. The linear forms are equivalent to those of Landro (2001) and higher order terms represent corrections appropriate for large contrasts. We conclude that in many plausible time-lapse scenarios increase in accuracy associated with higher order corrections is non-negligible. The results are summarized in Figure 1.

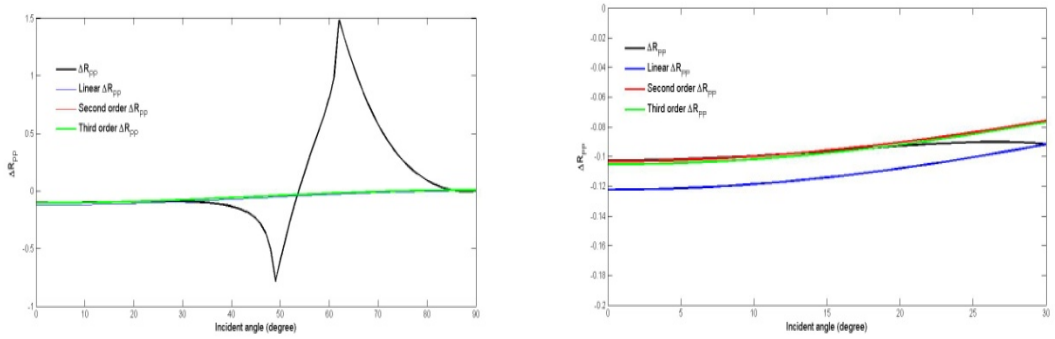

FIG. 1. ΔRPP for the exact, linear, second order, and third order approximation. Elastic incidence parameters: V_{P0} =3000 m/s, V_{S0} = 1500 m/s and ρ_0 = 2.000 gm/cc ; Baseline parameters: V_{PBL} = 4000 m/s, V_{SBL} =2000 m/s and ρ_{BL} = 2.500 gm=cc ; Monitor parameters: V_{PM} = 3400m/s, V_{SM} = 1700m/s and ρ_M =2.375 gm/cc.

A physical modelling study of time-lapse AVO signatures

Shahin Jabbari and Kris Innanen

ABSTRACT

Physical modeling can be used to validate the reflectivity predicted with different theoretical methods. We acquired a physical model experiment simulating a time lapse problem to investigate our theoretical results. The baseline survey has been modeled with plexiglass and PVC slabs resembling the cap rock and reservoir. The PVC slab has been replaced with a phenolic slab to resemble the monitor survey in which the reservoir had been gone under geological-geophysical changes during the time. Picked amplitudes from plexiglass-PVC and plexiglass-phenolic interfaces are corrected for geometrical spreading, emergence angle, free surface, transmission loss, and radiation patterns. The results for baseline survey, monitor survey, and their difference representing the difference data in time-lapse are analyzed. The linear and higher order approximations for difference data derived theoretically using perturbation theory and Zoeppritz equations were provided from the companion paper (Jabbari and Innanen 2012). These approximations are compared with the model data for validation. Results showed that the higher order approximations are more comparable with the model data which emphasizes on including higher order terms for the difference data in time-lapse (Figure 1).

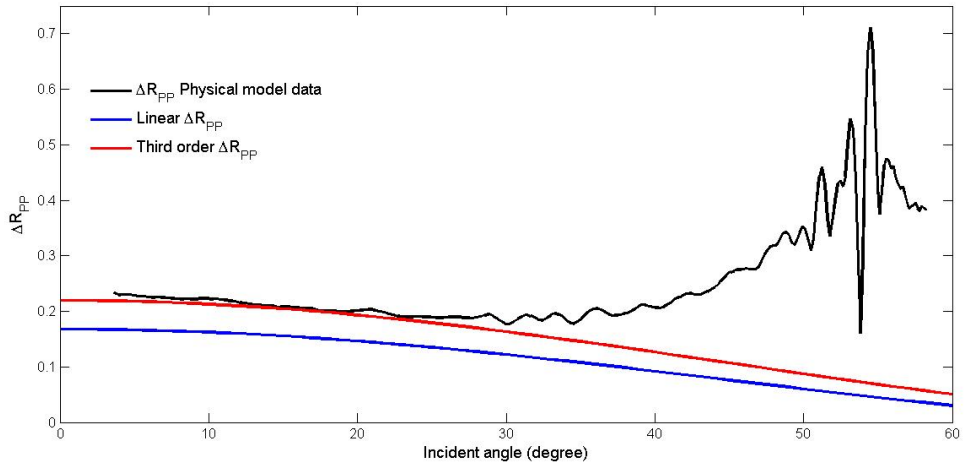

FIG. 1. The difference physical model data for difference data in a time-lapse problem are compared with the linear and third order approximation.

AVO effect of elastic wave modelling

Zaiming Jiang, John C. Bancroft and Laurence R. Lines

ABSTRACT

Reflection coefficients are studied from 2D P-SV cases of wave-equation based elastic wave modelling. The modelled results are compared to analytical results obtained from Zoeppritz equations.

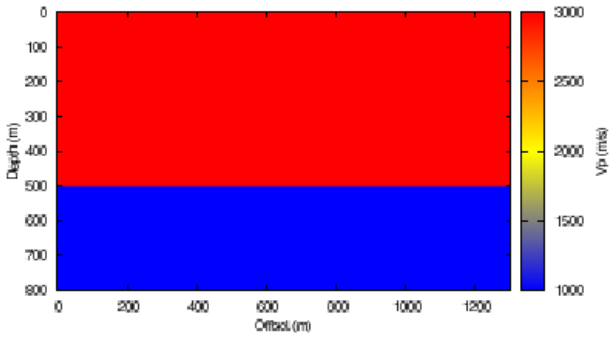

FIG. 1. A two-layer subsurface model.

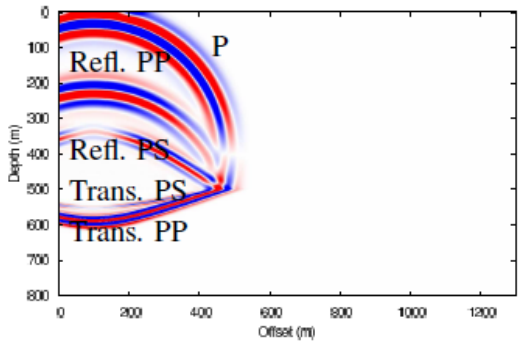

FIG. 2. A snapshot of vertical component at time 0.15s.

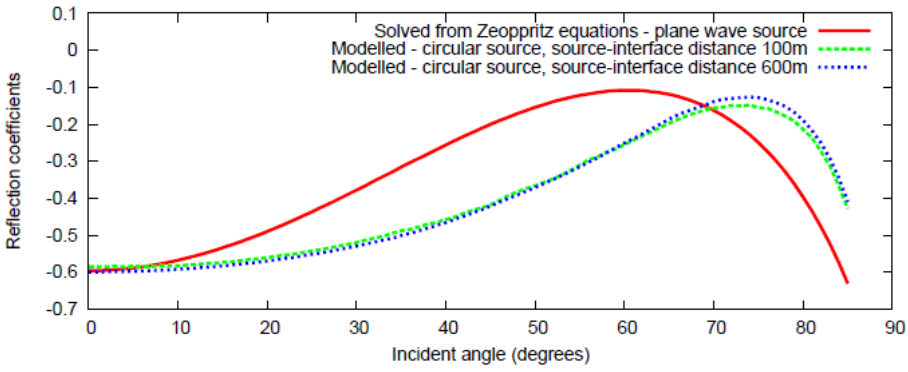

FIG. 3. Reflection coefficients calculated from Zoeppritz equations versus those measured from modelling results.

Elastic imaging conditions based on Helmholtz decomposition

Zaiming Jiang, John C. Bancroft and Laurence R. Lines

ABSTRACT

This report demonstrates Helmholtz decomposition performed on particle velocity wavefields with a staggered-grid FD scheme. In addition, Helmholtz decomposition is used in elastic reverse-time migration, and PP, PS, SP, and SS images are obtained.

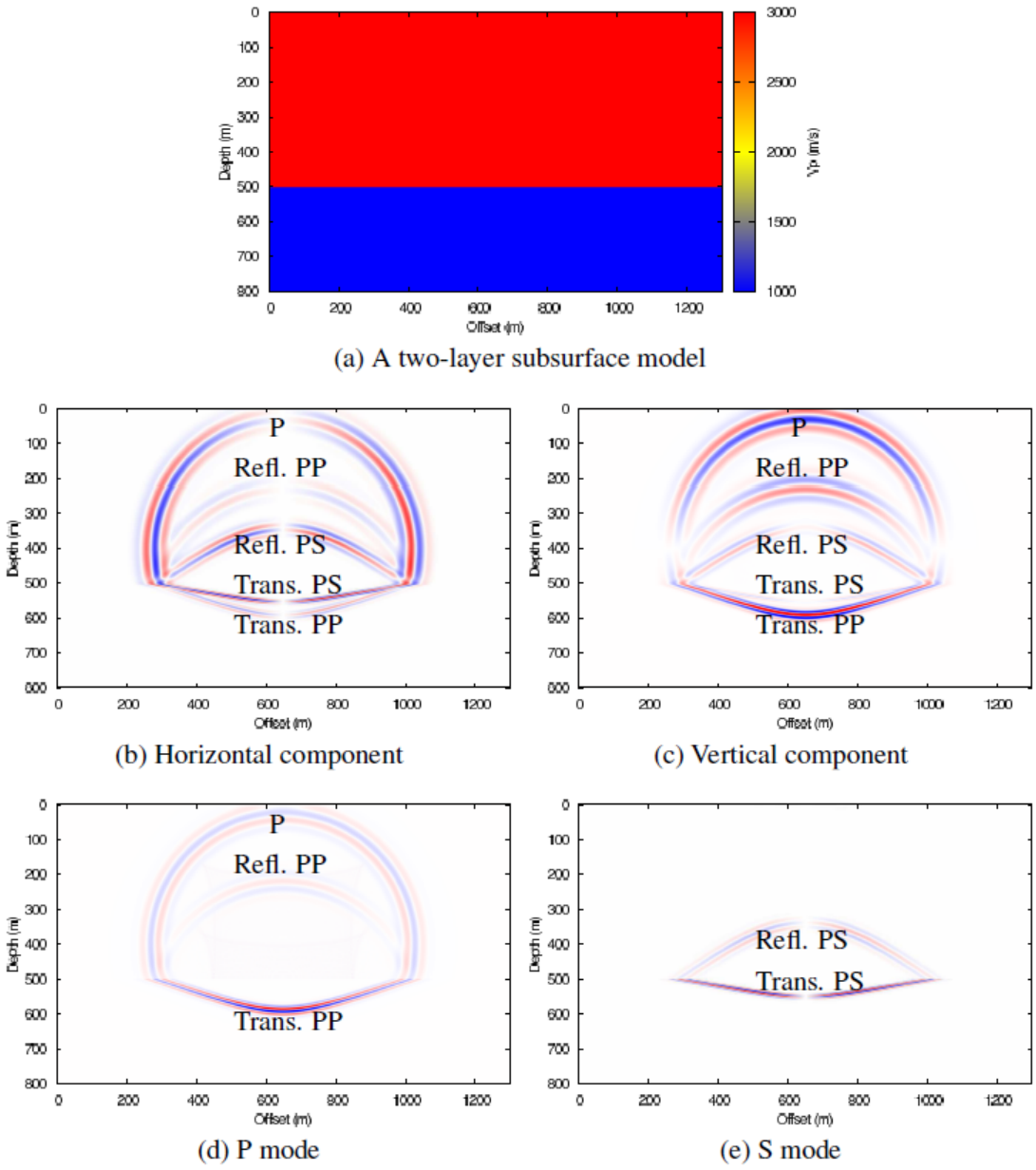

(a) A two-layer subsurface model

(b) Horizontal component

(c) Vertical component

(d) P mode

(e) S mode

FIG. 1. Two components of a wavefield is decomposed into P and S modes. (a) is P-wave velocities of an elastic subsurface model. (b) and (c) are two components of a particle velocity wavefield modelled with a P-wave source at (650m, 400m) in (a), (d) and (e) are P and S modes obtained from (b) and (c) by Helmholtz decomposition approximations.

Elastic reverse-time migration

Zaiming Jiang, John C. Bancroft and Laurence R. Lines

ABSTRACT

Two aspects of elastic reverse-time migration are addressed. First, a new method of imaging conditions is proposed and compared to two popular methods. The comparison is done using a point reflector subsurface model, and the proposed method is used in migration of a shrunk Marmousi2 model. Second, a prestack reverse-time migration workflow is proposed and tested with a shrunk Marmousi2 model. The processing workflow is very different from the traditional seismic data processing workflow. For example, it is not necessary to remove ground roll from surface records.

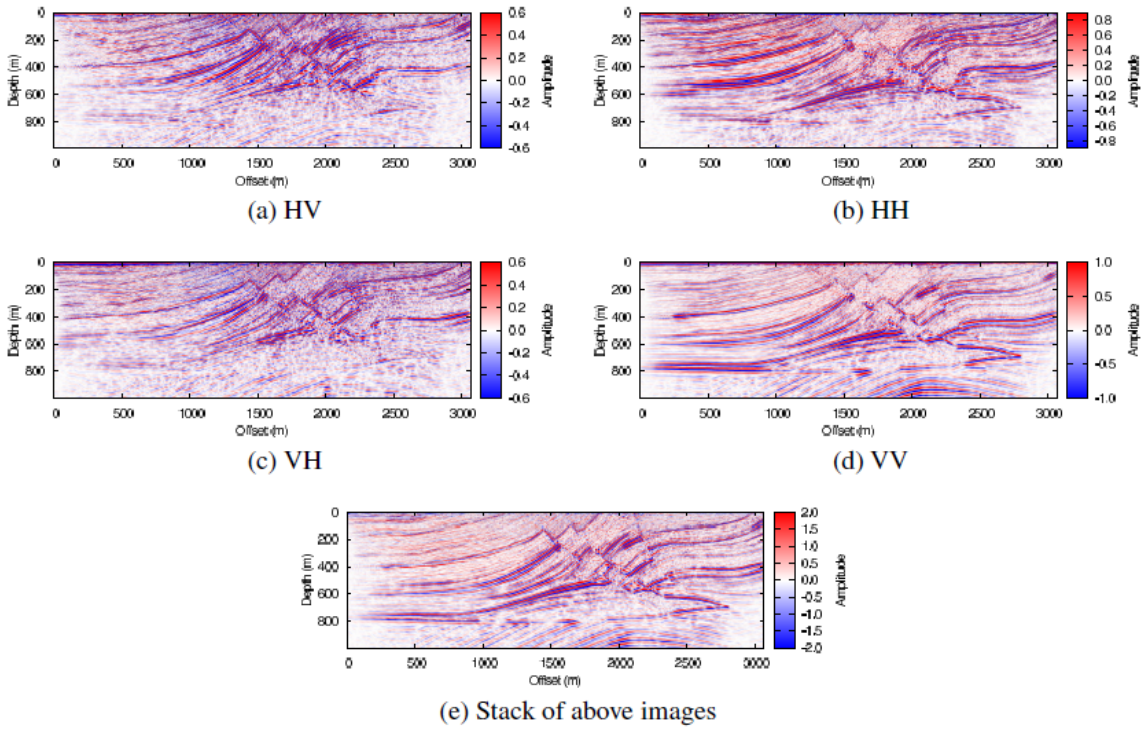

FIG. 1. Migrated image for shrunk Marmousi2.

Interpretation of time-lapse seismic data from a heavy oilfield, Alberta, Canada

Byron M. Kelly and Donald C. Lawton

ABSTRACT

Two 3-D seismic datasets and their difference volume were interpreted and analyzed for the presence of amplitude anomalies and time delays related to the injection of steam into a shallow, heavy oil reservoir. High amplitude anomalies were observed on the monitor data in conjunction with apparent time-thickening of the reservoir interval due to a decrease in the P-wave velocity. The decrease of velocity was interpreted to be due to the increase in reservoir temperature and decrease in differential pressure created from the injection of high temperature steam into the McMurray Formation reservoir. An analysis of the amplitude anomalies yielded a spatial display of reservoir steam chamber distributions (Fig 1).

The attenuation of high frequencies beneath steam chambers was observed within the monitor survey, characterized by low-frequency shadows, observable on the Devonian reflection underlying the amplitude anomalies.

Geological well log information was integrated with the geophysical observations. McMurray Formation channels sands were observed within the seismic data through the analysis of the semblance attribute, as well as within the geological data as low gamma ray values on well log cross sections. The channel sands were observed to intersect amplitude anomalies with the monitor volume. Outside of the amplitude anomalies, the channel sands were bound by muddy IHS bedding, creating baffles to steam flow.

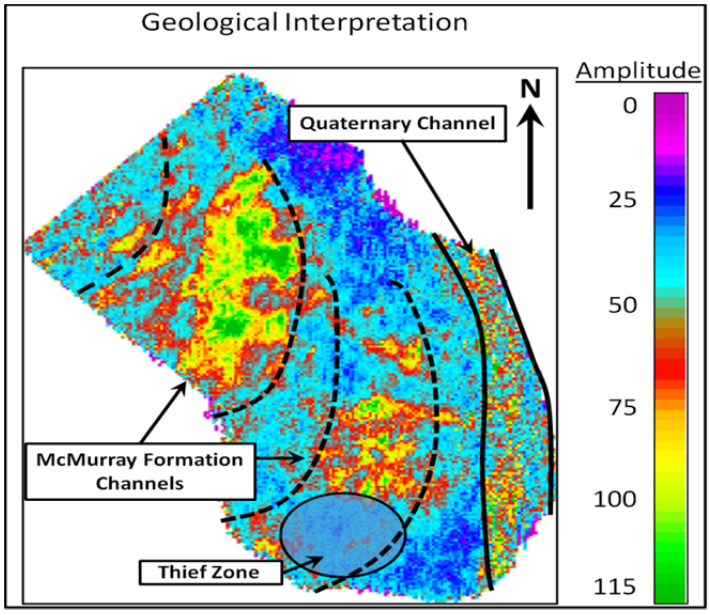

FIG. 1. Combined geological and geophysical interpretation of two McMurray channels, with interpreted boundaries overlain on amplitude anomalies.

Simultaneous P-P and P-S waveform inversion algorithm using Pre-Stack time imaging method

Hassan Khaniani, John C. Bancroft and Eric von Lunen

ABSTRACT

Conventional approach of elastic full waveform inversion requires a forward modeling and a depth migration. The forward modeling engine, which usually is based on finite difference solution of elastic wave equation, computes the data residual that compares the data driven from current model with the real data from the true model. Migration is an adjoint operator of the forward modeling, which usually is based on Reverse Time Migration (RTM) on the data residual, finds the gradient function from current model toward the true model.

Numerically, this scheme suffers from huge computational costs associated with time stepping of forward modeling and the migration. Assuming multiple free data and smooth lateral variation of subsurface properties, this work serves as an introduction to elastic waveform inversion using Pre-Stack Time imaging Migration (PSTM) and the corresponding forward modeling.

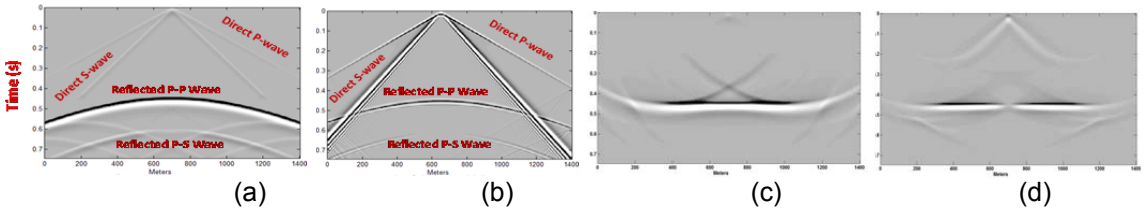

FIG. 1. P-P and P-S forward modeling and migration using Kirchhoff operator, a) P-P and P-S waves obtained from Kirchhoff solution, b) P-P and P-S obtained from finite difference solution, c) P-P time migrated d) P-S time migration on P-P time.

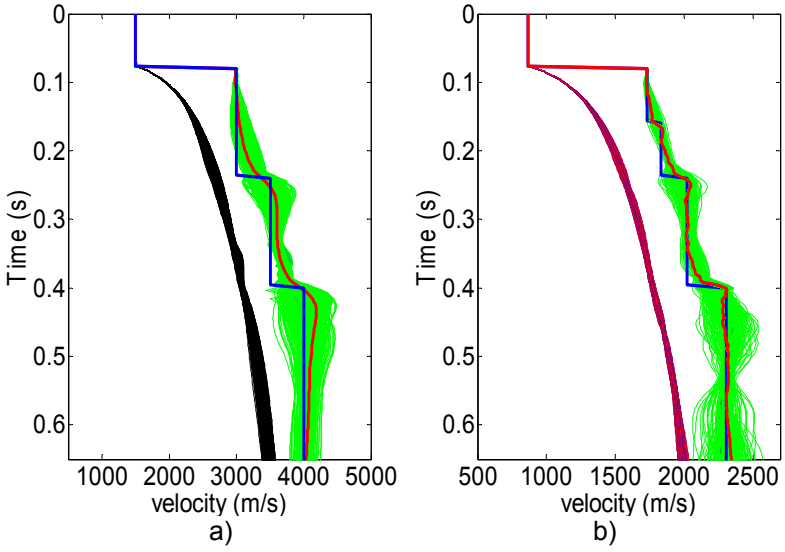

FIG. 2. Simultaneous P-P P-S inversion algorithm. FIG. 3. Velocity inversion for a) P and b) S.

Characterization of poroelastic targets for P- and S-waves using linear and non-linear AVO methods

Steven Kim and Kris Innanen

ABSTRACT

AVO is one aspect of seismic analysis that is largely used in industry. In this report, an examination of amplitude modelling, as typically viewed from a surface seismic acquisition experiment, is performed. The basis of this work is driven primarily by the research by Russell, Gray and Hampson and their *f* - *m* - *r* equation where he shows a linear poroelastic AVO formulation that quantifies fluid in the target medium. We would like to extend that formulation by showing the method in which non-linear poroelastic AVO approximations are derived in terms of models using two different sets of model parameters. The first that will be shown is in terms of perturbation and the other is reflectivity. Their analytical expressions will be shown for 1st order (linear), 2nd order (non-linear), and 3rd order (non-linear). Once we have shown all six poroelastic approximations, we will display the results against a synthetic model to view the variations that occur between each approximation. We will also show the stability that each approximation holds in an exercise that tests various modelling parameters.

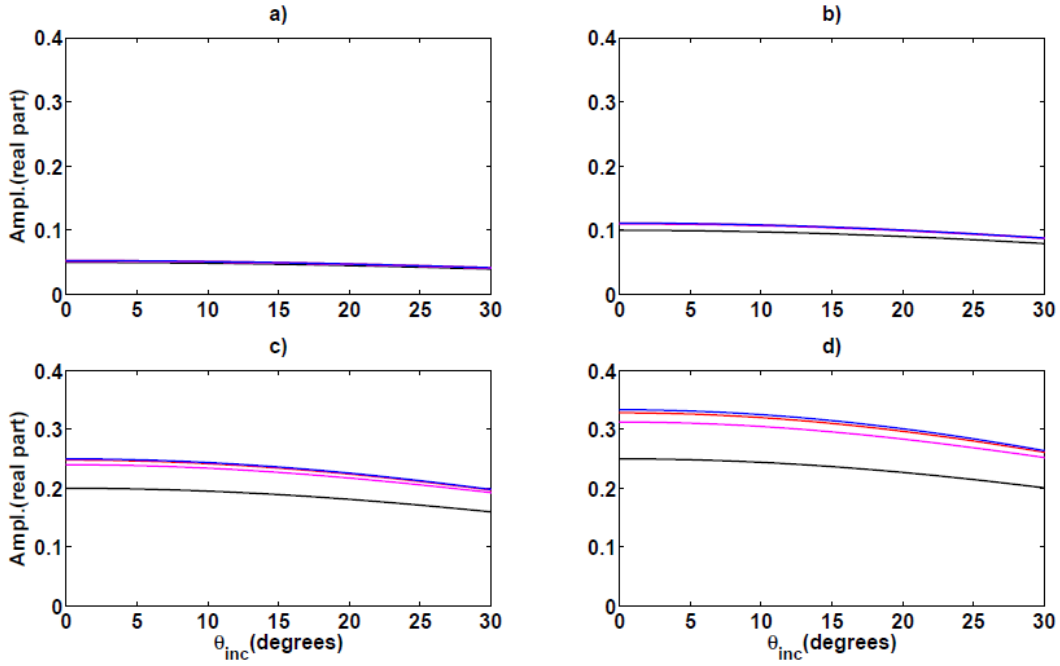

FIG. 1. All four panels have chosen a consistent perturbation each in a_f, a_μ, and a_ρ. The top left panel uses a perturbation of 0.1. Then it increases from one panel to the next in the top right panel to 0.2, 0.4 in the bottom left and 0.5 in the last panel. The blue curve represents synthetic data that is the Zoeppritz equations while the black curve represents the first order approximation, the magenta curve represents second order, and the red curve represents third order.

Re-expressing frequency dependent reflection and transmission coefficients for P-waves incident on porous fluid-filled media

Steven Kim and Kris Innanen

ABSTRACT

There are various parameterizations of reflection and transmission coefficients for poroelastic media. These expressions are also typically non-linear. From the perspective of inversion, non-linearity can cause an extra complexity to the problem of solving for unknown petrophysical parameters as an example. Therefore, we would like to present a framework of equations based off of previous findings of normal incidence, frequency dependent reflection and transmission coefficients. A linearized form for these coefficients would provide a computationally faster measure of inverted poroelastic parameters. Future investigations of the accuracy and precision of these inverted parameters would be desired.

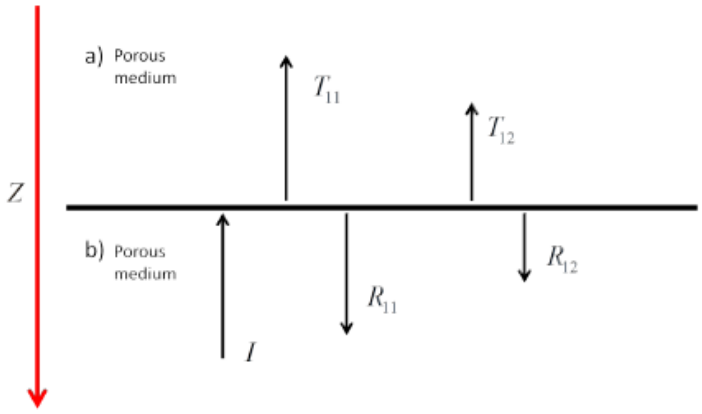

FIG. 1. A representation of an incoming P-wave in layer b. The reflection and transmission coefficients are for P-waves only and the subscripts indicate a fast P-wave (1) and Biot's slow wave (2).

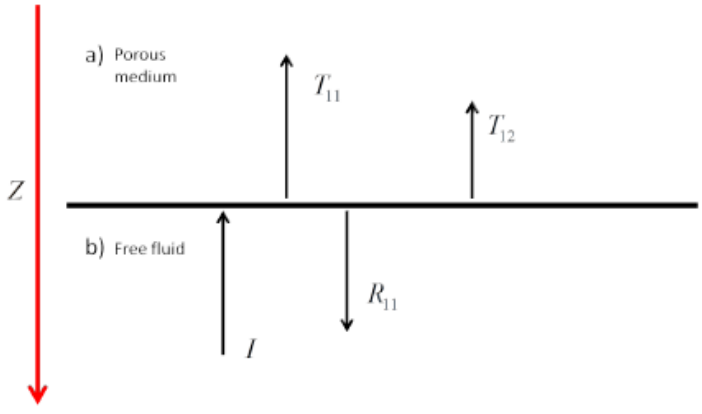

FIG. 2. A second representation of an incoming P-wave in layer b which is instead a free fluid. The reflection and transmission coefficients are for P-waves only and the subscripts indicate a fast P-wave (1) and Biot's slow wave (2).

Reflection coefficients through a linear velocity ramp, in 1D

Michael P. Lamoureux, Peter C. Gibson and Gary F. Margrave

ABSTRACT

A seismic wave propagating from one region of constant velocity to another, through a smooth transition zone, will differentially reflect or transmit across the zone, depending on the relative sizes of the transition zone and the wavelength of the propagating wave. This work presents an exact analytic solution for the case of a linear ramp velocity in the transition zone, and demonstrates that for long wavelengths, the ramp looks essentially like a jump discontinuity in the medium, with the corresponding reflection and transmission coefficients. For short wavelengths, the ramp provides essentially 100% transmission and no reflection. Energy conservation is verified for all wavelengths. A careful consideration is given to the two cases of varying the velocity parameter, one via variations in the density of the propagation medium, the other in varying the modulus of elasticity. The results are different, in particular there is a sign difference in the reflection coefficient, and a large amplitude difference in the transmission coefficient. We also present the numerical result for the transmission and reflection of a delta spike through the velocity ramp, and observe the reflection is a broadened "boxcar" response, while the transmission results in a spike.

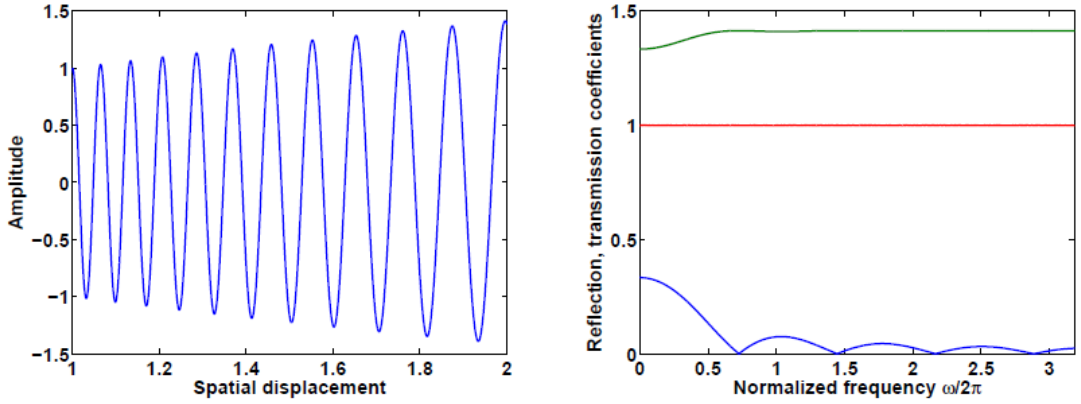

FIG. 1. Waveform in a linear velocity ramp, and reflection/transmission coefficients.

Reflections on PS – an interactive discussion

Don C. Lawton, Gary F. Margrave and Robert R. Stewart

ABSTRACT

Multicomponent seismic data are being recorded more often now than a decade ago, but the analysis and interpretation of the converted-wave (PS) data still lags that of P-wave data. Anecdotal evidence suggests that horizontal-component data are being recorded but not necessarily processed concomitantly with vertical-component data, except in some marine surveys. In some cases, the horizontal-component data are being shelved until value-added propositions are realized. This is due, to a considerable extent, to the many challenges that face the acquisition and processing PS-wave data and the current, immature status of joint P-wave and PS-wave interpretation methods. Acquisition issues include survey design, geophone coupling, efficacy of geophone orientation, group versus point receivers, and low S-wave velocities in irregular and highly heterogeneous near-surface layers. Key processing topics are receiver statics, velocity analysis, deconvolution, binning, migration/inversion, and anisotropy. Interpretation challenges are related to difficulties in P-wave and PS-wave registration, differential S-wave versus P-wave attenuation, P-wave and PS-wave phase, PS-wave amplitude versus offset analysis and joint P-wave and PS-wave inversion, and anisotropy.

However, a surface or near-surface energy source excites a very rich elastic wavefield in the subsurface. Figure 1 shows the raw, radial-component data of an offset vertical seismic profile (VSP) shot gather recorded into a dense 3-component geophone array. The fine receiver sampling interval allows easy observation of families of elastic waves present in the data.

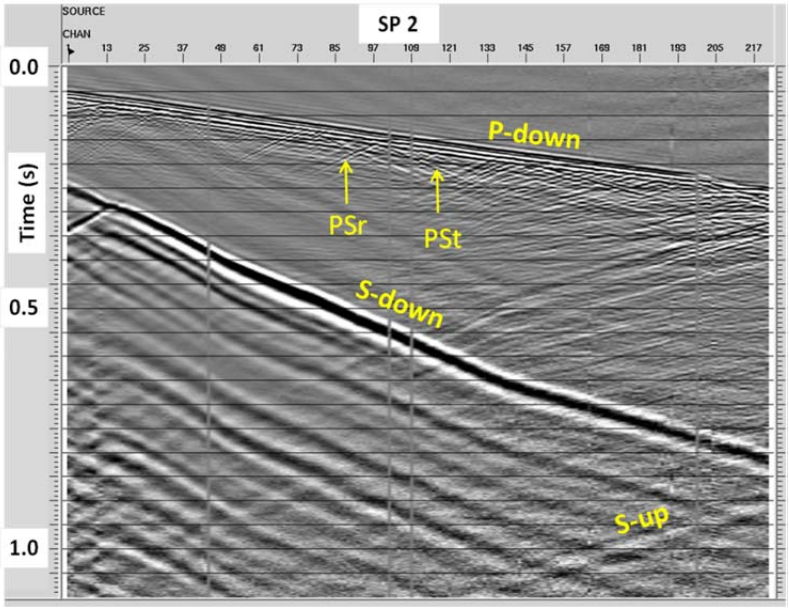

FIG. 1. Some wave modes identified in the radial component of a walkway VSP shot gather. PSr = P-S mode conversion upon reflection; PSt = P-S mode conversion upon transmission.

Synthetic seismograms, synthetic sonic logs, synthetic core

Laurence R. Lines and Mahbub Alam

ABSTRACT

In geophysics, we often model or "synthesize" measurements in order to enhance our interpretation of geophysical data. Synthetic seismograms utilize sonic and density logs to model reflection seismograms - so that we can identify reflections on real seismic data. Synthetic sonic logs, as originally described by Lindseth (1979), utilize seismic data in order to estimate acoustical impedance variation between wells. Both synthetic seismograms and synthetic sonic logs have been widely used in petroleum exploration.

Synthetic core modeling uses well log data and geological templates of depositional systems in order to synthesize core. Alam describes the procedure in his 2012 M.Sc. thesis (University of Calgary) which described the interpretation of data from a Saskatchewan heavy oil field (denoted here as P-field). While well logs and seismic data were available, there was no core available for P-field. Hence, a model of core was synthesized. To do this, Alam first computed Thomas-Steiber shale volume estimates using from gamma ray logs and density logs. He then used a series of templates corresponding to facies from different depositional environments, where each template had different shale volumes - as shown in Figure 1. Core from neighboring fields, which were also described by these facies templates were used as surrogate models for core that did not exist in P-field. Alam is doing self-validation on existing core in other fields and intends to include seismic data for shale volume calculations in future core modeling.

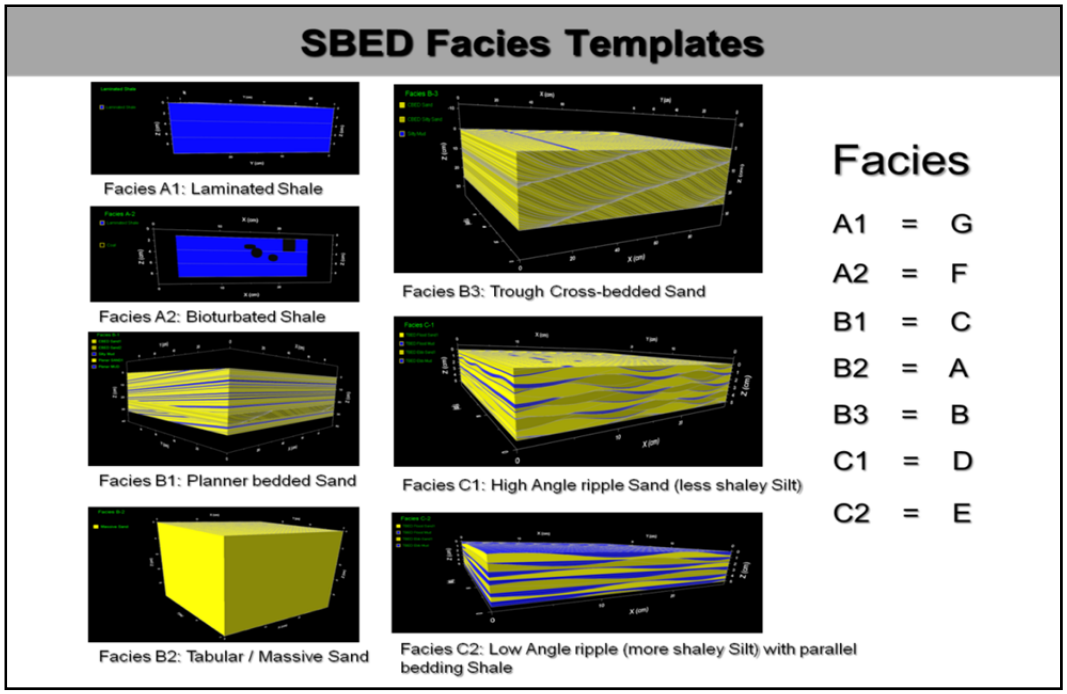

FIG. 1. Sedimentary structures for a heavy oil field are described by SBED facies templates of varying shale volumes. Core from neighboring fields are also described by these facies templates and these were used to synthesize missing core for the field under study (Alam, 2012).

Acoustic impedance inversion using stacking velocities: Hussar example

Heather J.E. Lloyd and Gary F. Margrave

ABSTRACT

In band-limited acoustic impedance inversion low frequencies must be provided from a non-seismic source. Impedance logs, estimated at wells from standard sonic and density logs, are commonly used however other sources such as impedance sections created from stacking velocities can be used. Stacking velocities must first be conditioned by interpolating on a grid that is the same size as the seismic data. For this purpose the PCHIP (Piecewise Cubic Hermite Interpolating Polynomial) algorithm was used. The next step is to convert the stacking velocities to interval velocities. Densities can be estimated using Gardner's equation and the interval velocities and from there an impedance section can be calculated by multiplying the densities and interval velocities. Information from this impedance section in the 0-2 Hz band was combined with the seismic data from Hussar using the BLIMP (Band-Limited IMPedance) algorithm. The inversion has high lateral variation so a second inversion was calculated using the mean of the impedance section. The mean inversion had a percent error of 11% between 0.2 and 1.05 seconds where as the regular inversion had a percent error of 12% in the same interval. Good results were obtained using the stacking velocities from standard processing but these had sparse picks. Better results are likely to be obtained with finer stacking velocity picks and constraining the conversion of stacking velocities to interval velocities.

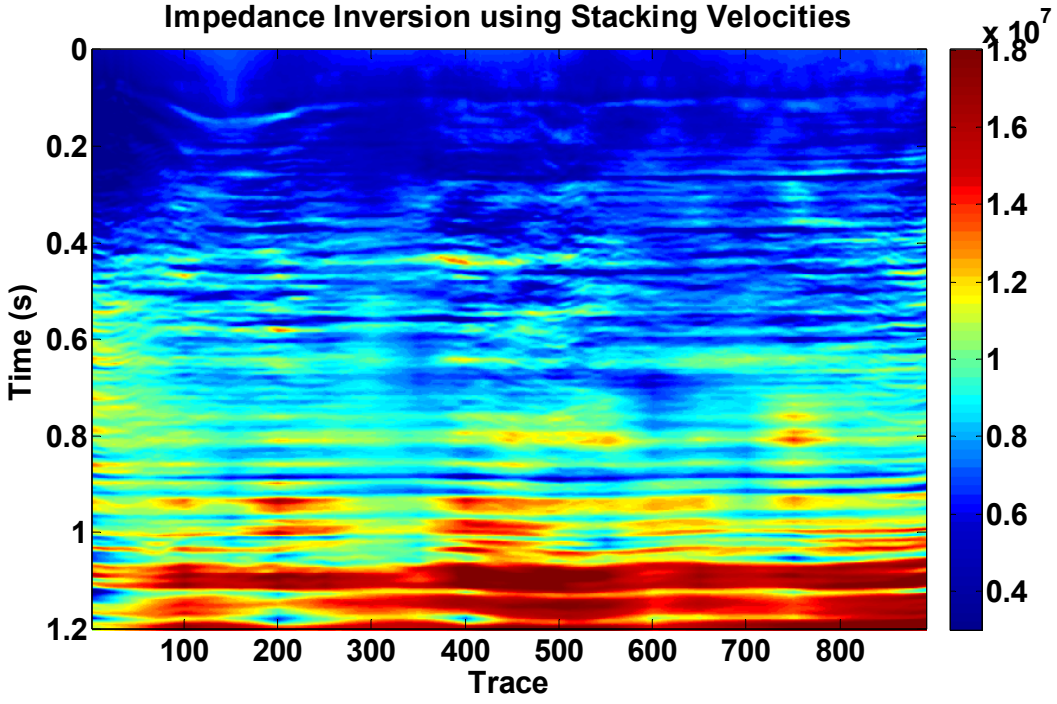

BLIMP impedance result using 2 Hz of low frequencies from the stacking velocity impedance section.

Incorporating spectral colour into impedance inversion

Heather J.E. Lloyd and Gary F. Margrave

ABSTRACT

Most seismic data processing flows try to shape seismic data into a white spectrum during deconvolution. This choice of white spectra is largely a statistical convenience and most natural occurring reflectivity sequences do not have white spectra. Shaping the seismic spectra to that seen in reflection coefficients computed from well logs is known as colouring. By colouring the seismic data we are potentially rewarded with a more realistic data set. A colouring operator can be devised by dividing a modeled trace spectrum with a modeled well reflectivity spectrum. We experimented with a variety of spectral models for both data and reflectivity. We choose to model the trace spectra using a 4^{th} order polynomial fit to the log amplitude spectrum. Alternately, we model the well reflectivity log amplitude spectrum with a 4^{th} order polynomial log frequency. The ratio of these spectral models is our colour operator which can then be applied to the seismic data. The coloured seismic data are then input into acoustic impedance inversion using the BLIMP (BandLimited IMPedance) algorithm. The 10Hz geophone dynamite Hussar data was used in this study. When the coloured operator was applied to the seismic data, 0.2 to 0.6 seconds was overwhelmed by noisy high frequencies. These high frequencies also carried over into the impedance inversion. It seems likely that the seismic data spectrum is nonstationary and our spectral models, based on stationary spectra, are not appropriate. Further work needs to be done to perfect this method to produce quality inversions for the entire section.

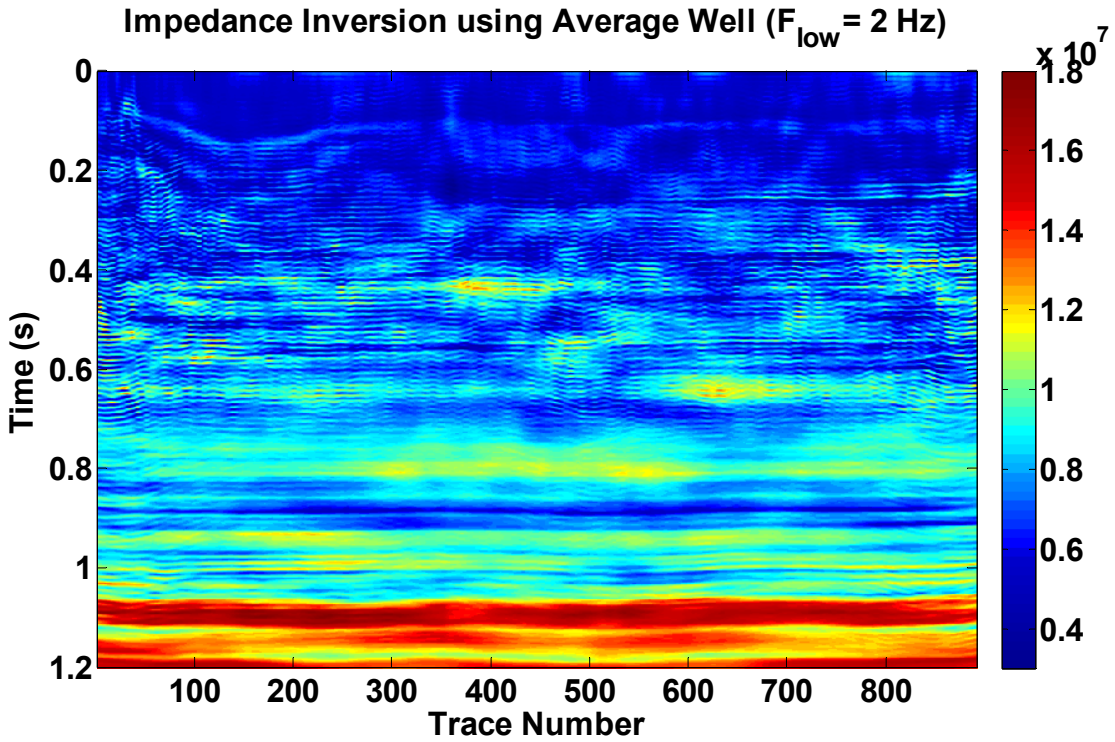

Coloured inversion section using the average well impedance and a low-frequency cut-off of 2Hz.

Investigating methods to transform acoustic impedance inversions into depth

Heather J.E. Lloyd, Roy O. Lindseth and Gary F. Margrave.

ABSTRACT

The prime use of seismic reflection data is to map subsurface time structure. Attribute analysis seeks to extract or refine information about the nature of the subsurface. Seismic data can be used for attribute analysis but by converting it into impedance the inherent properties of rock layers can be analyzed. Seismic data, when converted into depth, becomes easier to interpret and easier for geologists and engineers to work with. Depth conversions are usually completed using sonic logs or check shots but impedance sections can also be used.

Impedance is the product of velocity and density so if density can be approximated then velocity remains. In 1974, Gardner et al. found a relationship between density and velocity which can be used to estimate the density from impedance using the original stationary parameters. Densities can also be provided from nearby wells and by creating non-stationary Gardner parameters. Once the velocity has been separated from the density it can be used to transform the section into depth. Formation tops from the Hussar seismic data were converted to depth and compared to the formation tops from nearby wells. This allowed each method to be evaluated for accuracy and precision. The standard Gardner method had a mean error of 131 ± 66 m averaged over all wells. The log density method had a mean error of a mean error of 115 ± 48 m. The time variant Gardner method had similar results of 86 ± 39 averaged over all wells.

Even though the time variant Gardner's rule produced a depth conversion where the tops varied less with depth the top picks were different from the well picks ranging 50 to 120 meters. Further investigation must be done to limit these errors which could be reduced by better inversions in the overburden and better density estimation methods.

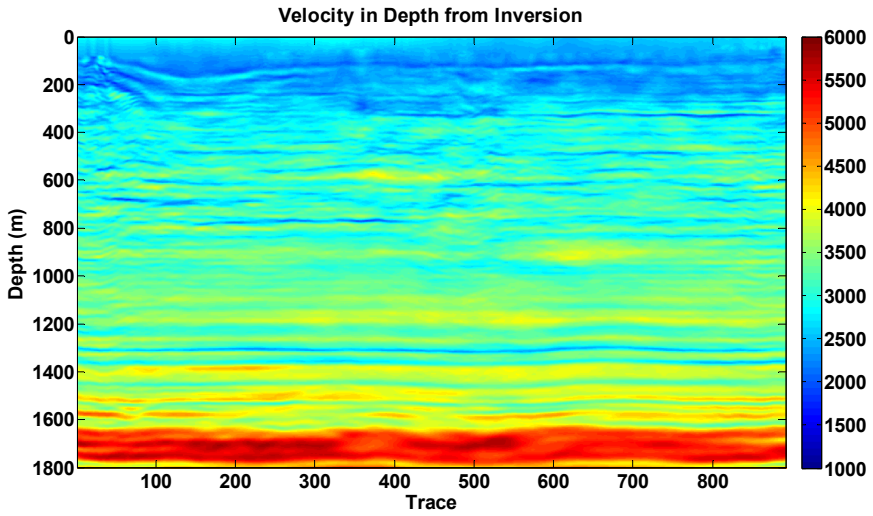

The velocity section after converting to depth, using nonstationary Gardner's rule.

Investigating the low frequency content of the Hussar data with impedance inversion

Heather J.E. Lloyd and Gary F. Margrave

ABSTRACT

Acoustic impedance inversion can easily be computed by the BLIMP (BandLimited IMPedance) algorithm. This algorithm uses well logs to fill in the low-frequency information that is missing in bandlimited seismic data. The transition from well log low-frequency information to the seismic data spectrum is marked by a cut-off frequency, f_c. The choice of f_c depends on the low-frequency content of the seismic data, and it is generally desirable to push f_c as low as possible to make the inversion less dependent on well control. For the Hussar data, with 10 Hz geophones and dynamite sources, an f_c as low as 2 Hz gives good results. This is relatively low compared to the 5 to 10 Hz that is commonly chosen for most seismic data. Three wells intersect the Hussar line and all were used to calculate inversions as well as a well log that was prepared by averaging the three impedance logs. The average log was found to produce the best inversions with a mean impedance error of 8.5% from .2 to 1.05 seconds, where wells 12-27, 14-27 and 14-35 produced errors of 11%, 10% and 10% respectively over the same interval. Other cut-off frequencies were also examined and the best choice appears to be non-stationary, as frequencies down to 1.5 Hz can be trusted in the shallower section. This study has shown that the Hussar data set has trusted frequencies down to 1.5 - 2 Hz.

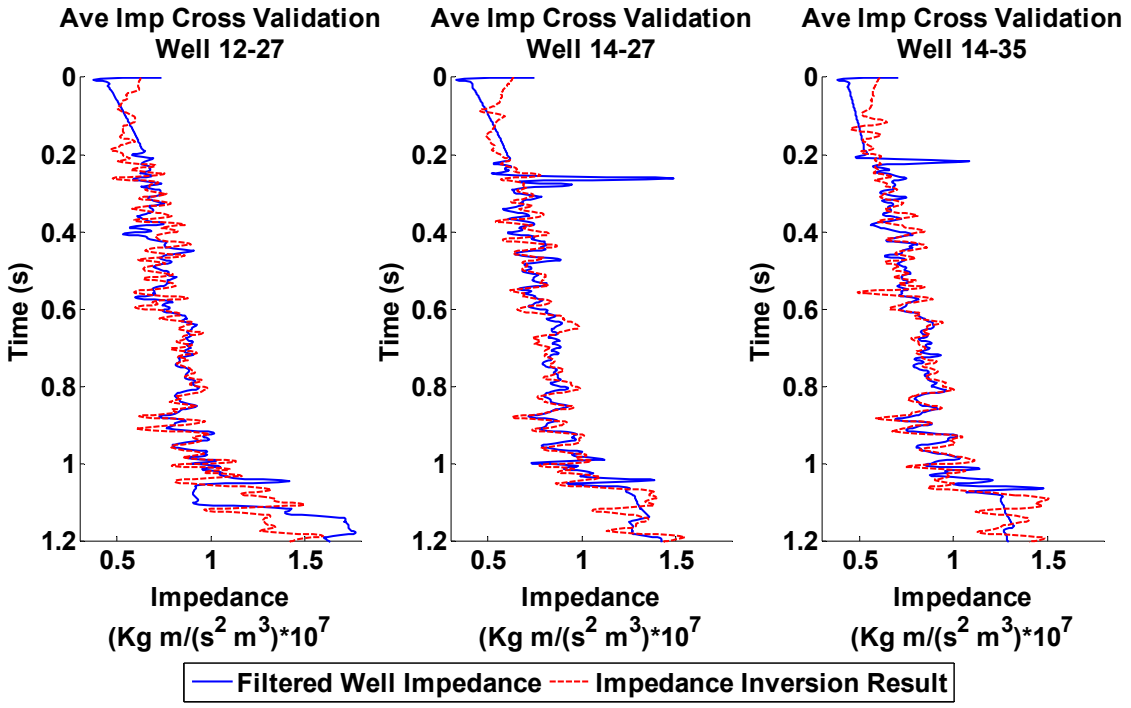

FIG 1: Cross validation plot that compares the inversion calculated using the impedance log from the average well with the filtered well impedances. The low-frequency cut-off that was used was 2 Hz.

Well tying and trace balancing Hussar data using new MATLAB tools

Heather J.E. Lloyd and Gary F. Margrave

ABSTRACT

In September 2011, CREWES recorded a data set in southern Alberta near Hussar. The purpose of this survey was primarily to compare receiver types (four types of receivers) and source types (four types of sources) at very low frequencies. Data processing by CGGVeritas resulted in a final section for 10Hz vertical component geophones and dynamite source and this was used in this study. Three wells intersected this line, two near the south (12-27 and 14-27) and one towards the north (14-35). An overburden and underburden, derived from the stacking velocities, was applied to the sonic logs. An overburden and underburden was also applied to the density log using the stacking velocities and Gardner's equation. The next step was to estimate a wavelet by fitting a fourth order polynomial to the decibel amplitude spectra of a seismic average trace.. Synthetic traces were then prepared at each well location. A rough tie of well 12-27 was completed and the seismic data was balanced with a time-variant scaling operator. To create a good tie between the seismic data and the synthetic traces the sonic logs of the wells were stretched until key events matched. An average trace was prepared from averaging five traces located at each well location after the traces were aligned as a slight dip is evident in the seismic data. An average synthetic trace was prepared by aligning, balancing and averaging the synthetic seismograms at each well location. The reflectivity and Impedance for these wells were also aligned and averaged. It is helpful to have a reference impedance section which was created by a weighted average of the well impedance logs.

This study found that producing well ties that match the seismic data is not trivial and is very important for accurate inversions. StretchWell and WaveletEstimator were two programs created for this study with graphical user interfaces used in tying the wells. StretchWell is used to modify the sonic logs and WaveletEstimator is used to create wavelets. Each of these programs is explained at the end of this paper.

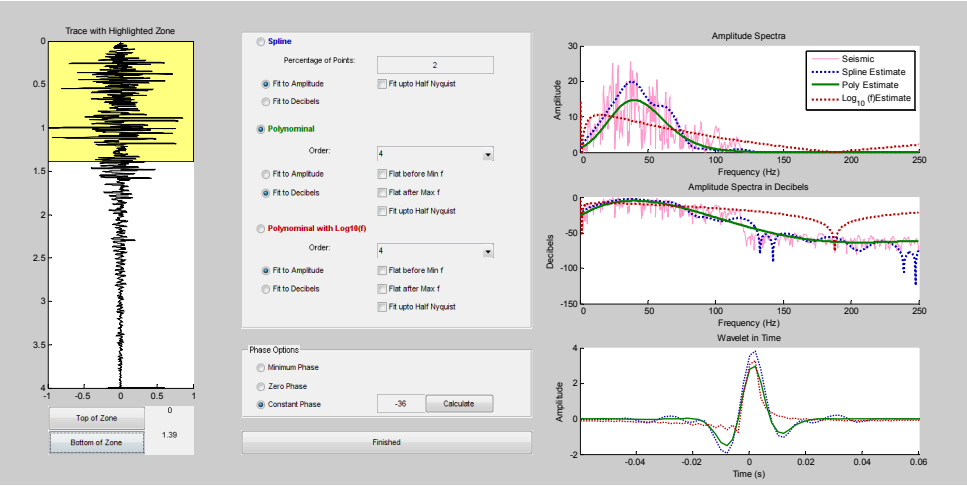

WaveletEstimator Interface

AVAZ inversion for fracture orientation and intensity: a physical modeling study

Faranak Mahmoudian and Gary Margrave

ABSTRACT

We present a pre-stack amplitude inversion of P-wave data for fracture orientation and intensity. We test the method on multi-azimuth multi-offset physical model reflection data acquired over a simulated fractured medium. Our simulated fractured medium is composed of phenolic material with controlled symmetry planes, and its elastic properties have already been determined using traveltime analysis; this experimental model represents an HTI layer. We follow Jenner (2002) amplitude inversion on small incident angle data to extract the fracture orientation (direction of isotropic plane of the medium), and estimate the fracture orientation with remarkable accuracy. Knowing the fracture orientation, we have modified the linear PP reflection coefficient equation by Rüger (2001) to invert for anisotropy parameters ($\varepsilon^{(V)}$; $\delta^{(V)}$; γ). We incorporated some constraints on the vertical velocities and density in the inversion process. Large-offset data are required for the azimuthal amplitude inversion of the simulated fractured layer, as the material shows only slight azimuthal amplitude variations. The results for all three anisotropy parameters from AVAZ inversion compare very favorably to those obtained previously by a traveltime inversion. This result makes it possible to compute the shear-wave splitting parameter, γ, (historically determined from shear-wave data) which is directly related to fracture intensity, from a quantitative analysis of the PP data.

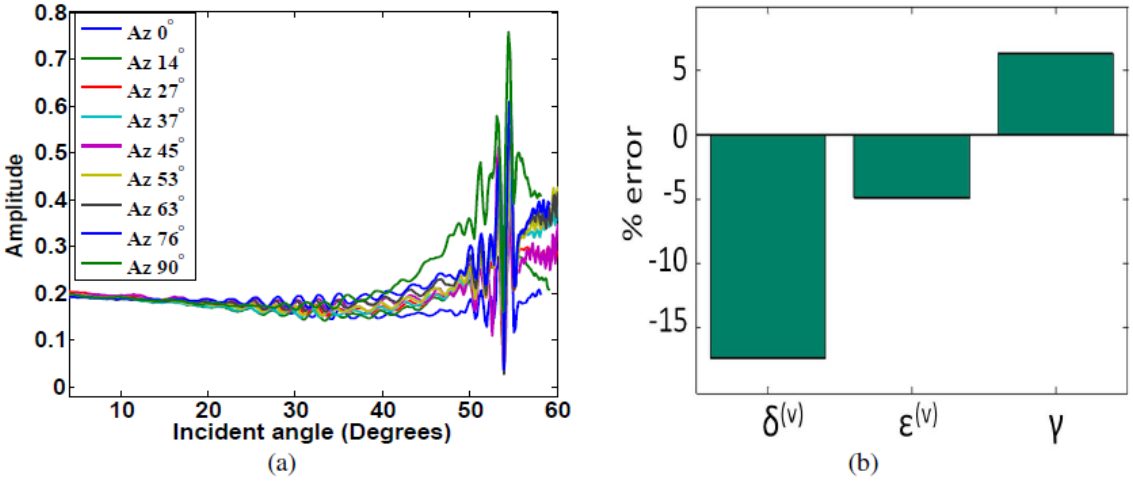

FIG. 1. (a) Input to AVAZ inversion, corrected amplitudes reflected from the interface of an isotropic material (plexiglas) and simulated fractured medium, along azimuths between 0° and 90°. (b) Three anisotropy parameters from the constrained AVAZ inversion.

Azimuthal AVO over a simulated fractured physical model medium

Faranak Mahmoudian, Gary Margrave, and Joe Wong

ABSTRACT

We have verified the suitability of seismic data from a physical model for a quantitative amplitude analysis of anisotropic targets. Physical model data have often been used for traveltime analysis, while incorporating them in an amplitude analysis was limited due, in part, to the large size, highly-directional physical model transducers employed as sources and receivers. We acquired multi-offset, multi-azimuth, seismic data over a simulated fractured layer overlain by two isotropic layers with the most top layer being water. We simulated the fractured medium by constructing a physical layer, with horizontal transverse anisotropy (HTI), from phenolic material. Acquisition was designed to avoid the overlapping of the primary and ghost events. We treated the large-size transducers as seismic arrays and employed an array-type correction to compensate for their effects on seismic amplitudes. The PP reflection amplitudes from the top of the simulated fractured layer, after required AVO corrections, reveal a clear azimuthal variation caused by the simulated fractured layer and agreed with amplitudes predicted theoretically.

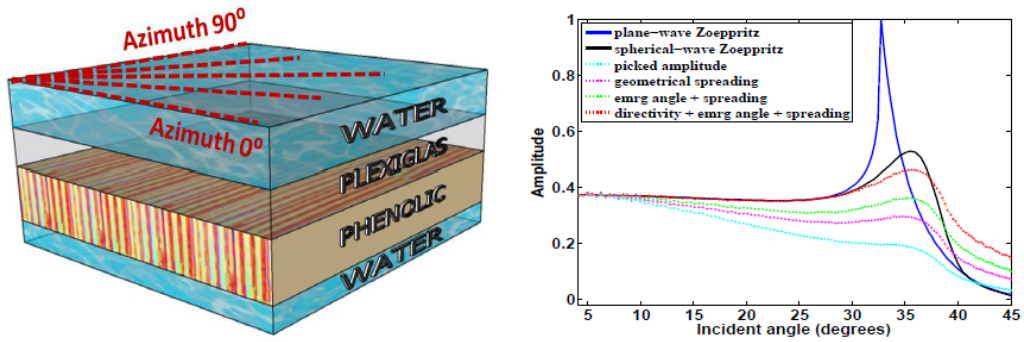

FIG. 1. (left) The four-layered earth model used in physical modeling acquisition. (right) Waterplexiglas reflector amplitudes, raw amplitudes and corrections.

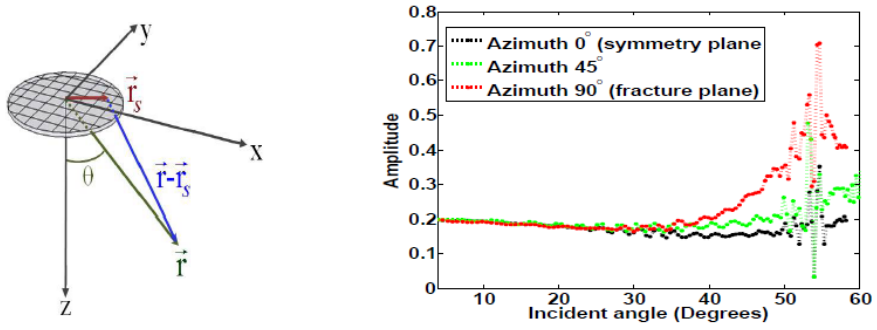

FIG. 2. (left) A circular source transducer as source array, with the point receiver at location $\vec{r}$. Fracture top corrected reflection amplitudes from three azimuths.

Estimation of stiffness coefficients of an orthorhombic physical model from group velocity measurements

Faranak Mahmoudian, Gary Margrave, P.F. Daley, and Joe Wong

ABSTRACT

Physical model data have been used for many years to simulate exploration targets, as in the example of a fractured medium. Yet, physical modeling is challenging for at least two reasons; (1) the initial characterization of the medium is difficult, and (2) the large highly-directional transducers used as sources and receivers cause distortions. We present a straightforward method to characterize a physical model, composed of phenolic material, by employing the highly accurate group-velocity measurements in estimating the orthorhombic stiffness coefficients of the medium. The large physical model transducers effect is discussed in another paper in this year's report. We measured the qP, qSv , and qSH wave-mode group velocities from direct-arrival traveltimes on physically modeled 3C transmission gathers. An approximate orthorhombic group velocity expression is used to estimate the off-diagonal stiffness coefficients. We show that estimates of the stiffness coefficients are consistent with measured velocity data. Theoretically predicted group velocities from the estimated stiffness coefficients are very close to the measured velocities. The stiffness coefficients values suggest that the experimental physical layer approximates a weakly anisotropic HTI layer. Hence our model simulates a vertically fractured transversely isotropic layer for physical modeling of fractured reservoir characterization, and for testing new anisotropic seismic data processing algorithms.

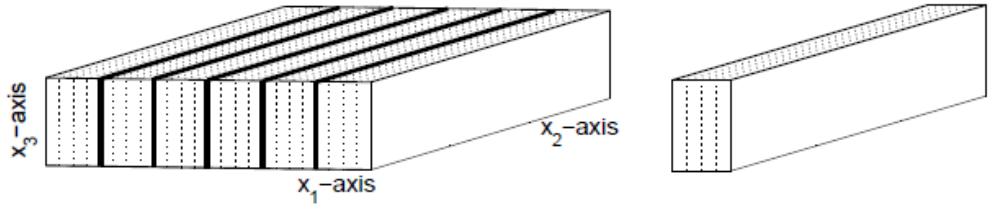

FIG. 1. (left) The simulated fractured medium in this study with an area of 57 × 57cm^2 and a thickness of 7cm. (right) A slab of phenolic material with dashed lines displaying the linen planes.

Table 1. Density-normalized stiffness coefficients of the simulated fractured layer. They have the units (km/s)^2.

8.70 ± 0.41	4.9 ± 0.21	4.96 ± 0.21	0	0	0
	12.67 ± 0.49	5.58 ± 0.23	0	0	0
		12.25 ± 0.49	0	0	0
			2.89 ± 0.12	0	0
				2.34 ± 0.11	0
					2.28 ± 0.11

If we treat the simulated fractured layer as a HTI medium with x1-axis as the symmetry axis, the Rüger's parameters (α, β, $\varepsilon^{(V)}$, $\delta^{(V)}$, γ), are: $\alpha = V_{P0} = 3500$ m/s, $\beta = V_{S0} = 1700$ m/s, $\varepsilon^{(V)} = -0.145$, $\delta^{(V)} = -0.185$, and $\gamma = 0{:}117$.

A Tiger user manual

Rolf Maier

ABSTRACT

A brief description of instruction on using tiger, a 3D anisotropic seismic modeling package, is presented. The HTML file on the CREWES website fills in gaps in the documentation and details the setup of a user environment and the format and creation of earth model files in seismic Unix (SU), tiger's preferred format. The help document contains a still growing section on the conversion of data formats and layouts, and on using SU to first create models in, and then to create displays or PDFs and plots from tiger's output. A description of the capabilities and limits of tiger's nice but not always fully described GUI is also offered. A tutorial based on a 2D line over part of the SEG salt model has lately been made available, and others should follow and will be added, together with notes on limits causing failures for reasons not yet tested by the GUI.

Figure 1 below shows an unscaled shot of a model with shallow, low velocity pockets, causing wobbly events and reduced amplitudes, and another, deeper pocket which does not show without scaling.

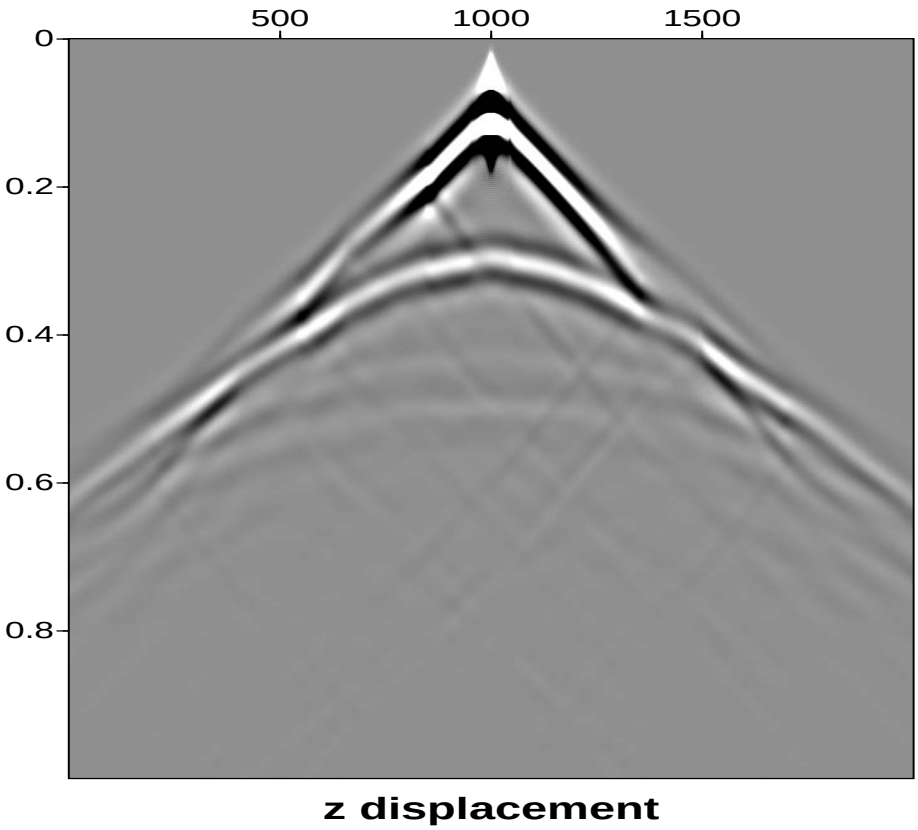

FIG 1: Shot showing the effects of low velocity pockets near the surface.

Tests of sand-bags to couple geophones to the earth's surface

Peter M. Manning

ABSTRACT

Sandbags were used as a means of coupling geophones to the ground as part of the Priddis shoot in July of 2012. The main object was to see if better shear wave data could be obtained. Twenty older geophones were deployed at ten metre intervals along a short portion of the main test line, and their response was recorded for all the source tests that were done. A source line of dynamite charges was used to match the two data sets, but very little shear wave data could be found. The investigation was continued by comparing ground-roll data, where the sand-bag data seemed to be more consistent than the comparable spike-phone data. From this it was concluded that further tests should be done, with a larger number of geophones in an area of high data quality.

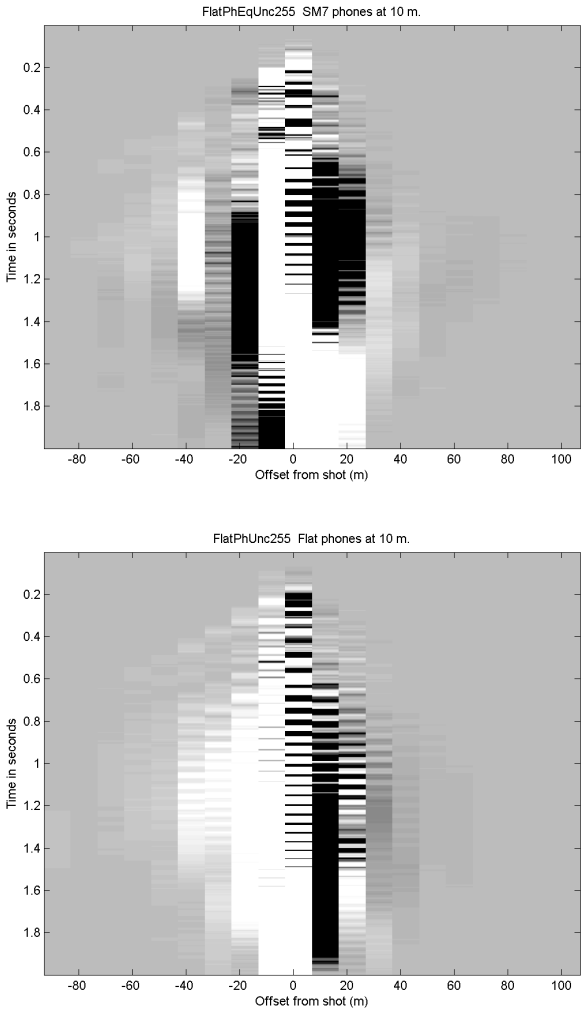

Ground-roll analysis plot on the spike line (above) and the sand-bag line (below). There is a much stronger indication of retrograde motion on the sand-bag line, implying that the in-line shear wave recording is more realistic.

A Perspective on Full-Waveform Inversion

Gary F. Margrave, Kris Innanen and Matt Yedlin

ABSTRACT

We examine and compare the standard seismic inversion methodology, denoted SM, and full-waveform inversion, denoted FWI. We find many parallels but also interesting differences. Both methods produce a detailed impedance model (or impedance image) as the end product but differ in how this is created. SM first produces a reflectivity image (i.e. a migrated section) that is then converted to impedance, in a step called impedance inversion, by incorporating low-frequency information from an external source, typically well control. In a preparatory step, the reflectivity image is calibrated by comparing it to synthetic seismograms at well locations. We call this well validation and it serves to estimate the seismic wavelet whose removal matches the seismic reflectivity image to the well reflectivity. Alternatively, FWI creates an impedance image as the result of an iteration which gradually adds detail into an initial impedance model. The impedance update at each iteration comes from a type of migration of the data difference, which is the difference between the recorded data and synthetic data predicted by the impedance model as it exists at the iteration's beginning. This migrated data difference is derived from theory as the gradient of the data misfit function, or sum-of-squares of the data difference. Essentially the impedance model is calibrated by comparing synthetic data to recorded data, and we call this data validation.

Both methods require low frequency information but FWI requires this in the data while SM incorporates wells. Both methods require knowledge of the source waveform, but SM achieves this by deconvolution and tying to wells which FWI commonly estimates this in the iteration. SM validates the model at wells and never attempts to predict synthetic data. FWI validates the model through data prediction and comparison to the raw data but does not incorporate well control. SM produces a migrated reflectivity image while FWI uses migration to estimate the gradient of the misfit function. However, we show that this gradient is actually a rather poor migration which lacks gain correction.

FWI is the method of the future but we suggest that a viable step forward is iterative modelling, migration, and inversion or IMMI. Such an approach can incorporate any migration method and can use both well validation and data validation.

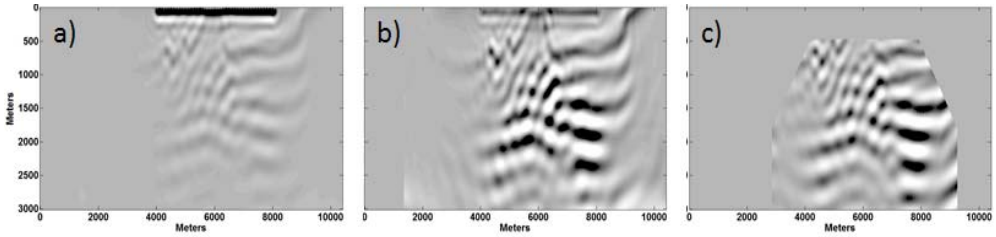

Consider a series of 40 shots taken over the center of the Marmousi model. For the frequency band 0-5 Hz, a) shows the gradient of the misfit function as prescribed by FWI theory, b) shows the same as a) but gain has been applied, c) is a conventional prestack depth migration using a deconvolution imaging condition with mute applied.

Galerkin methods for numerical solutions of acoustic, elastic and viscoelastic wave equations

Matt A. McDonald, Michael P. Lamoureux, Gary F. Margrave

ABSTRACT

The numerical modelling of wave equations is a common theme in many seismic applications, and is an important tool in understanding how the physical systems of interest react in the process of a seismic experiment. We apply state-of-the-art numerical methods based on domain-decomposition combined with local pseudospectral spatial discretization, to three physically realistic models of seismic waves, namely their propagation in acoustic, elastic, and viscoelastic media. The Galerkin formulation solves the weak form of the partial differential equation representing wave propagation and naturally includes boundary integral terms to represent free surface, rigid, and absorbing boundary effects. Stability, accuracy, and computation issues are discussed in this context along with direct comparison with finite difference methodologies. This short paper is a summary of highlights from the 2012 MSc thesis of the first author, which aims to bridge the gap between the development of accurate physical models to represent the real world, as seen in seismic modelling, and the implementation of modern numerical techniques for the accurate solutions of partial differential equations.

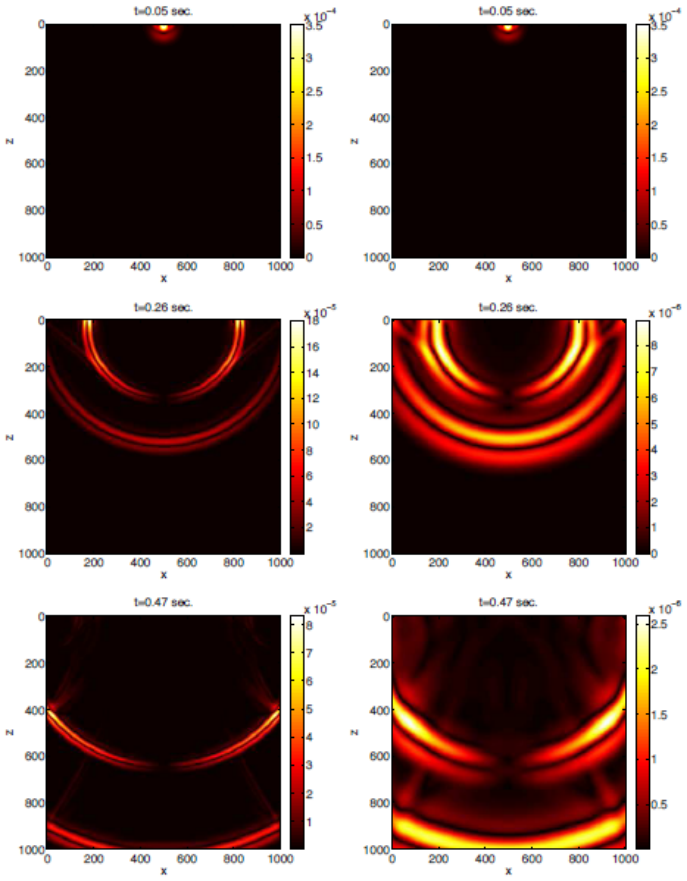

FIG. 1. Elastic vs. Viscoelastic wave propagation.

Time-lapse seismic modeling of CO_2 sequestration at Quest CCS project

Shahin Moradi and Don C. Lawton

ABSTRACT

A time-lapse analysis was carried out to investigate the theoretical detectability of CO_2 for the Shell Quest project. Quest is a Carbon Capture and Storage (CCS) project in Alberta conducted by Shell Canada Energy, Chevron Canada Limited, and Marathon Oil Canada Corporation. The target formation for injection is Basal Cambrian Sandstone (BCS) which is a deep saline aquifer at the approximate depth of 2000 meters below surface. The purpose of this study was to simulate the seismic response of the BCS after injecting 1.2 million tonnes of CO_2 during a one-year period of injection. This was done using Gassmann fluid substitution and seismic forward modeling. A geological model for the baseline scenario was generated based on the data from well SCL- 8-19-59-20W4. For the monitor case, Gassmann fluid substitution modeling was undertaken to model a CO_2 plume within BCS. Numerical stack sections for both scenarios were obtained and subtracted to study the change in the seismic response after injecting CO_2. The difference section shows the location and the spatial distribution of the plume. Based on these results the CO_2 plume could be detected in the seismic data after a year of injection.

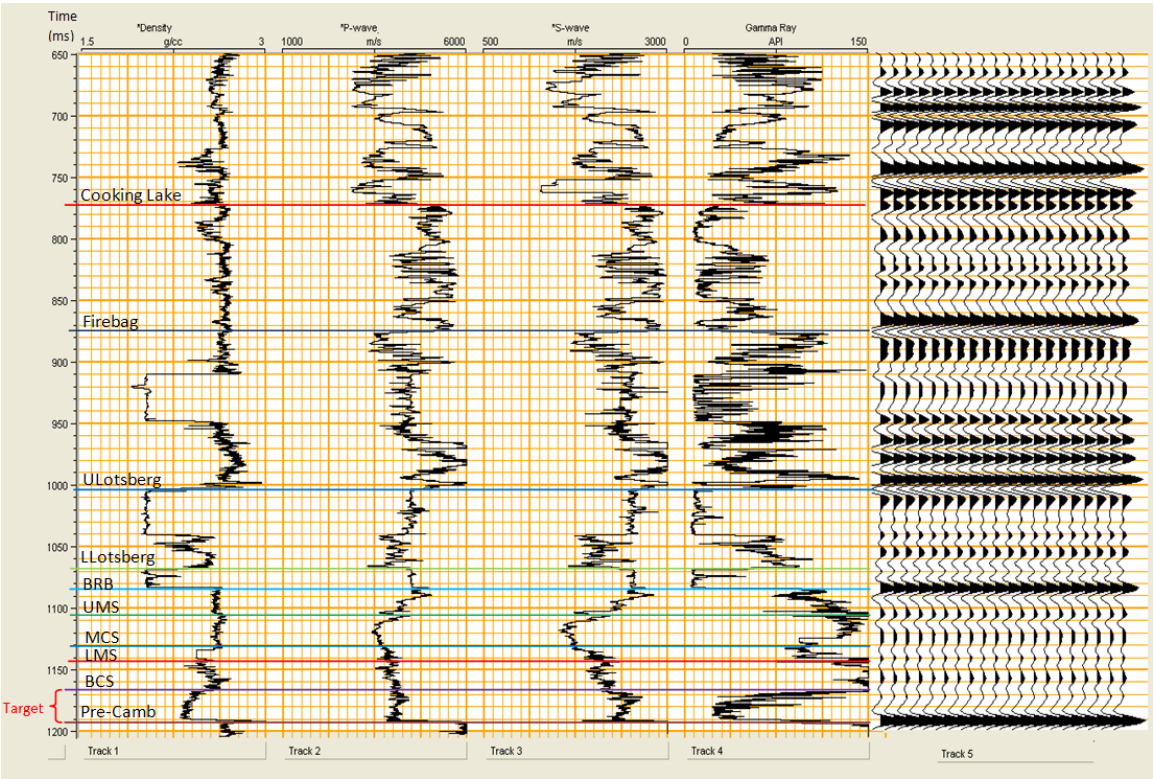

FIG. 1: Well SCL- 8-19-59-20W4 which was used in this study and some of the main horizons. Tracks 1 to 5 show, respectively, the density, P-wave velocity, S-wave velocity, Gamma-ray and synthetic seismograms generated in Hampson-Russell using a 50 Hz zero phase wavelet. The target is Basal Cambrian Sandstone (BCS) which is a deep saline aquifer.

A multicomponent, time-lapse investigation of fractures in a potash mining region

Andrew Nicol and Don C. Lawton

ABSTRACT

Time-lapse seismic analysis is used to monitor changes in the subsurface which occur in between the acquisition of the baseline and monitor surveys. In this study, the analysis of two multicomponent seismic vintages is conducted in order to monitor any fracture-induced changes to the seismic anisotropy in a potash mining region. The Dawson Bay Formation, a fractured carbonate which unconformably overlies the Prairie Evaporite Formation, which contains significant potash ore deposits, is the focus of this study. The two vintages of PP and PS volumes were divided into four sub-volumes consisting of a stack containing a 45 degree aperture of source-receiver ray paths. The azimuthal difference plots created from the PP seismic data show travel-time differences running parallel to the edges of the highest density mine workings. Seismic interpretation and Vp/Vs analysis suggest that random fracturing is present in the subsurface, and is creating a significant low velocity anomaly observed as an increase in travel-time in the PP and PS volumes, while exhibiting a low amplitude effect in both vintages of the PP volumes.

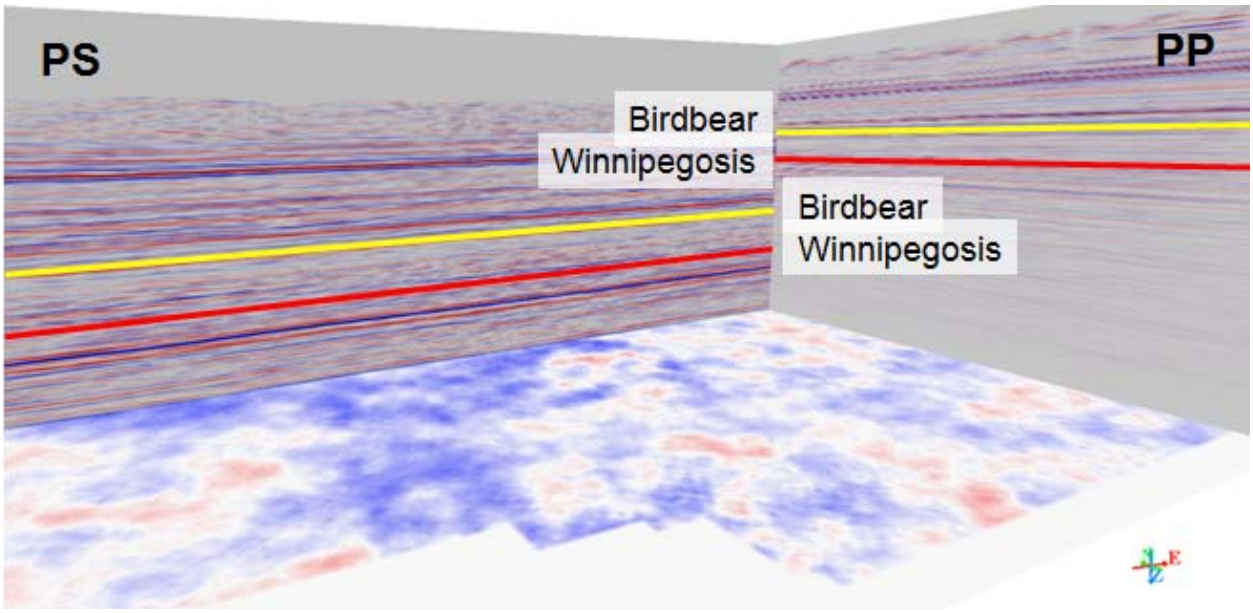

FIG. 1. An inline through the 2004 PP (left) and a crossline through the 2004 PS (right) seismic volumes. The travel-time differences between the interpreted Birdbear Formation (yellow) and Winnipegosis Formation (red) on both the PP and PS seismic volumes are evident here. This along with lower frequency content and increased noise in the PS volume are some of the challenges associated with PP-PS registration.

AVO analysis for a single thin bed using three-layer media equation

Wenyong Pan

ABSTRACT

As effective criteria for hydrocarbon detection, Amplitude Versus Offset (AVO) technology has been widely used in the recent years. Zoeppritz equation, which describes the reflection and transmission of plane wave on a single interface separating two half infinite spaces, is the basis for traditional AVO analysis. This characteristic of Zoeppritz equation makes it unsuitable to analyze the propagation of wave in multi-layered media when the layers are very thin. This study derives the three-layer media equation based on multi-layer media equation by Breshkovsky in elastic regime for discussing the reflection and transmission of plane wave in thin bed. For that the reflection coefficient is a continuous function of incident angle, frequency and thin bed thickness, it is possible to analyze the AVO effects with varying the incident angle, frequency and thin layer thickness. It is concluded that (1) three-layer media equation is more quantitative and precise than Zoeppritz equation to analyze the AVO responses of thin bed; (2) the influence of thin bed thinning on variations of amplitudes is equal to that of dominant frequency decreasing; (3) AVO analysis of P-S wave helps us to eliminate the problem of multi-solutions in fluids prediction; (4) With decreasing Q (quality factor), the AVO curve obtained from three-layer media equation become more smooth and get closer to the curve calculated by Zoeppritz equation.

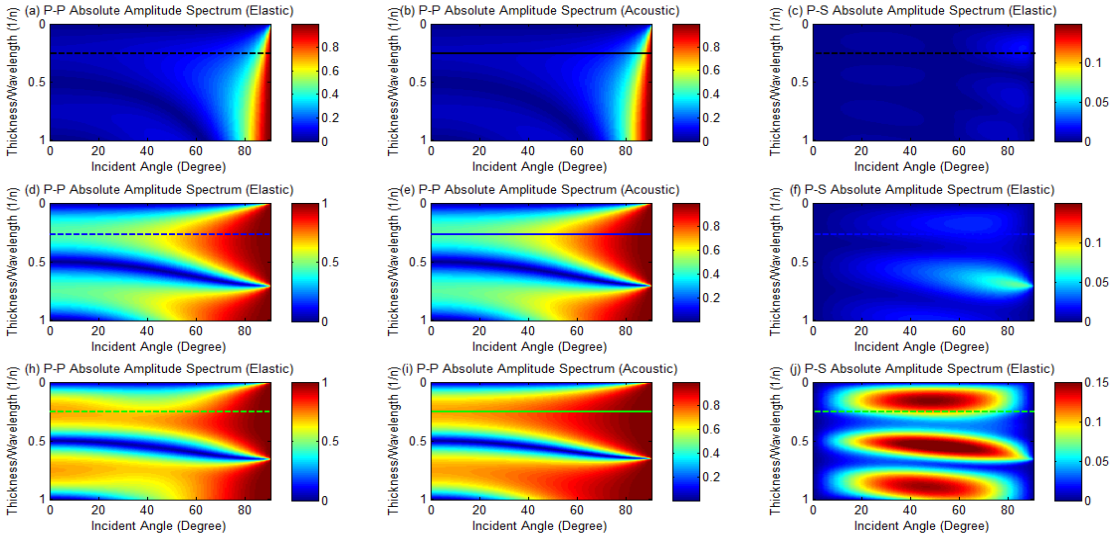

FIG.1. P-P and P-S wave absolute amplitude spectrums with varying incident angle and thickness/wavelength (1/n) at fixed frequency (30Hz) for Model II with water sand ((a), (b), (c)), gas sand ((d), (e), (f)) and coal (h), (i), (j)) in Layer 2 in elastic regime and acoustic regime respectively. The color represents normalized amplitude. This figure helps us analyze the variation of amplitudes with varying incident angles and thickness/wavelength $(1/n)$ more easily.

A brief comparison of the frequency spectra from the Hussar 2011 and Priddis 2012 shoots and the theoretical predictions of the Sharpe Hollow Cavity Model

Christopher C. Petten and Gary F. Margrave

ABSTRACT

We investigate the frequency spectra of the test charges used in the Hussar 2011 and Priddis 2012 experiments. In both experiments the there was a low-frequency roll off and the dominant frequency decreased with increased charge size as predicted by the Sharpe Hollow Cavity Model (SHCM). In the Priddis 2012 experiment a loss in high frequency content with smaller charges was observed which is also predicted by the SHCM however, in the Priddis 2011 tests we did not observe this phenomenon.

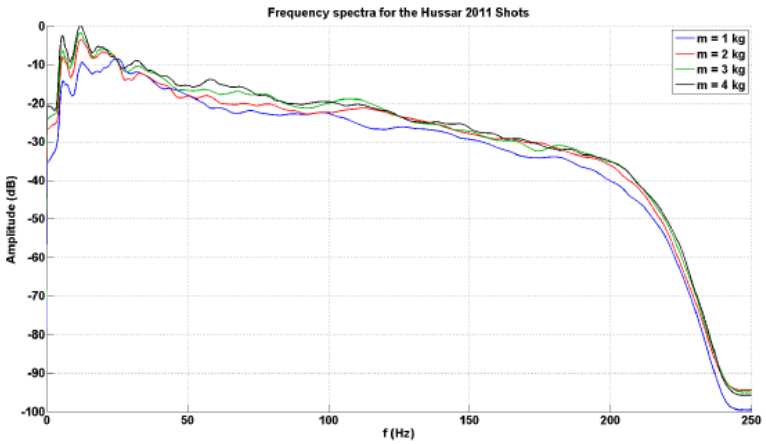

FIG. 1. Frequency spectra resulting from various charge sizes. The dominant frequency decreases with increased charge size however, there appears to be significant variation in the high frequency content regardless of charge size.

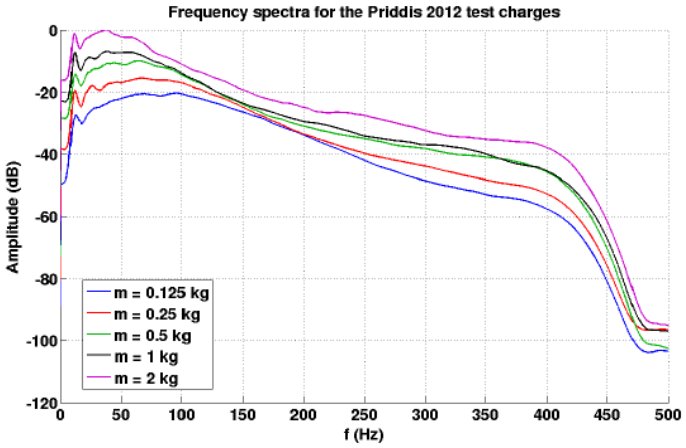

FIG. 2. Frequency spectra for the Priddis 2012 test charges. The dominant frequency appears to decrease with increased charge and there is a loss in high-frequency content with smaller charge sizes as predicted by Sharpe's model.

Using the Sharpe Hollow Cavity model to investigate power and frequency content of explosive pressure sources

Christopher C. Petten and Gary F. Margrave

ABSTRACT

We investigate the nature of waves emitted by an explosive pressure source as predicted by the Sharpe Hollow Cavity Model (SHCM), shown in Figure 1. The SHCM predicts a decrease in dominant frequency with increased charge size, and a decrease in high-frequency content with smaller charges.

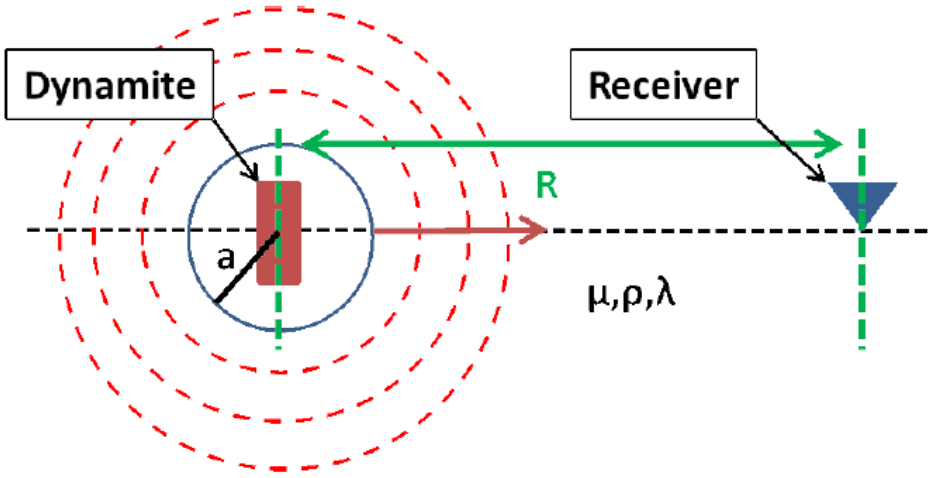

FIG. 1. Graphical representation of the SHCM. The hollow cavity, with radius *a*, is the region in which this model predicts the waves emitted from the source behave in a nonlinear fashion. The waves beyond this point are assumed to be emitted directly from the walls of the cavity and propagation can be predicted with the elastic wave equation.

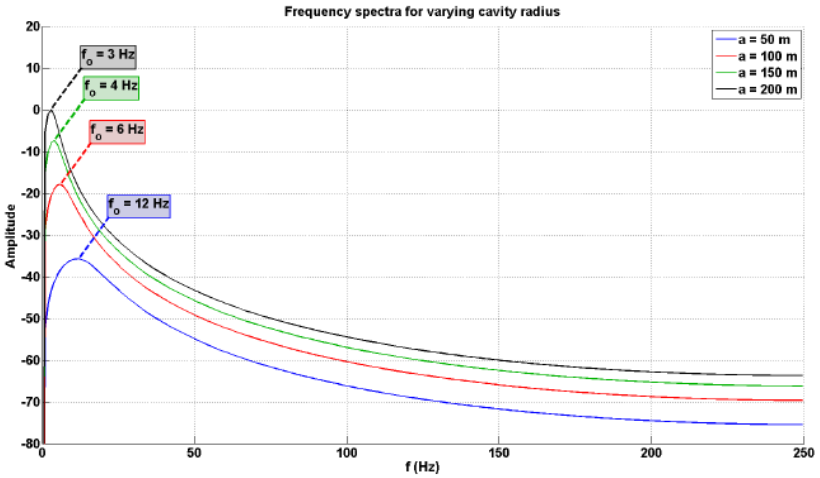

FIG. 2. Theoretical frequency spectra resulting from various cavity radii. The SHCM predicts that the dominant frequency should decrease with increased charge size, however, it also predicts a loss of high frequency content with smaller charges.

Dennis Gabor: The father of seismic attribute analysis

Brian Russell[1]

ABSTRACT

A review of the CREWES reports over the last ten years will reveal the influence of the Gabor transform on the work of Gary Margrave, who has used this transform, along with his colleagues and students, to perform techniques such as seismic deconvolution. However, it is interesting to note that the Gabor transform was only one of three remarkable inventions in Gabor's landmark 1946 paper: "Theory of Communication", the others being time-frequency analysis and the complex signal. In this report, I will first give a brief discussion of time-frequency analysis and the Gabor transform, and then I will focus on Gabor's work on the complex signal and the development of seismic attribute analysis, trying to show the link among all seismic attributes. In this way, I will show that Gabor could be considered to be the "father" of seismic attribute analysis. The report can also be considered as an historical summary of seismic attributes and as an explanation of their inter-relationships, since many seismic interpreters are overwhelmed by the sheer number of currently available attributes.

The figure below is a comparison of maximum curvature attributes computed by both correlation and instantaneous attributes, and shows that each have their own strengths.

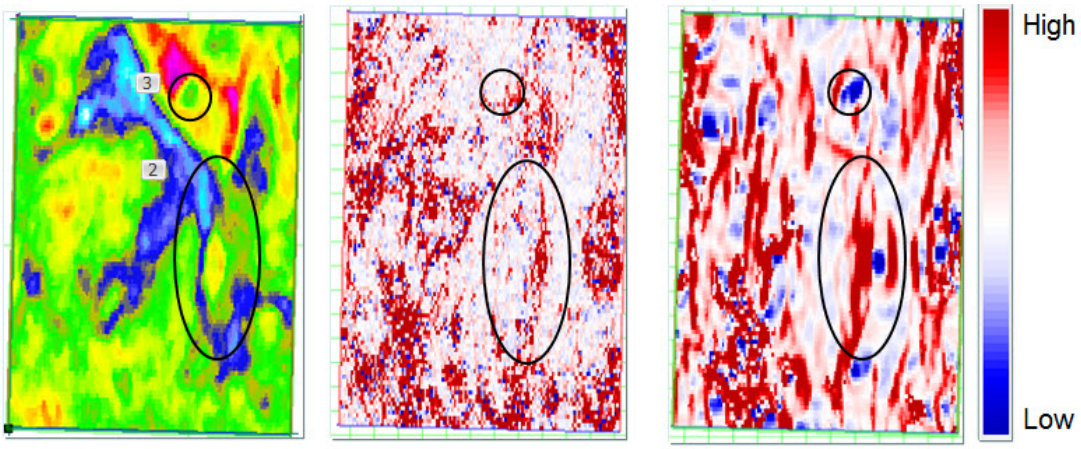

(a) (b) (c)

A display of maximum curvature attributes computed using instantaneous and correlation methods, where the 1000 msec time slice is shown in (a), instantaneous maximum curvature is shown in (b) and correlation maximum curvature is shown in (c). Note that the colour scale on (c) is different than the colour scale used on this plot in Figure 12 b. The ellipses show a lineament feature and the circles show circular feature.

[1]Hampson-Russell, A CGGVeritas Company, Calgary, Alberta, brian.russell@cggveritas.com

Prediction of shear-wave log in Western Canadian Sedimentary Basin (WCSB)

A. Nassir Saeed, Laurence R. Lines and Gary F. Margrave

ABSTRACT

Predictions of shear-wave logs in wells that do not have dipole Sonics are challenging, particularly in heavy oil reservoirs. In this study, we utilized linear-regression, robust locally weighted scattering and smoothing (LOWESS), and several other approaches of iteratively re-weighted linear least- squares inversion (IRLS) techniques to estimate shear-wave logs. The developed computer codes were implemented using well logs from three different types of reservoirs (*conventional oil*, *heavy oil*, and *tight shale oil*) in WCSB. The proposed methods guard against outliers, and have shown improvements in predicting shear-wave sonic logs compared to standard linear relationships (Castagna et. al., 1985).

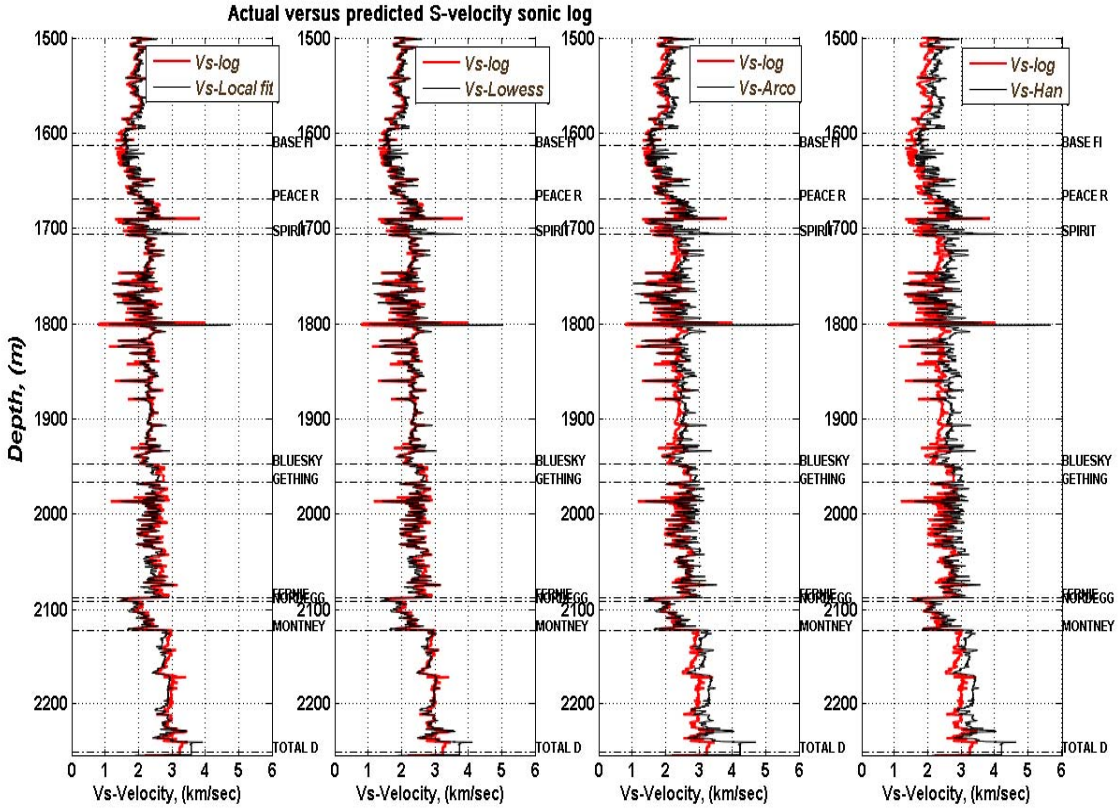

FIG.1. Plots of actual shear-wave (red color) logs versus predicted shear-wave logs using linear regression, LOWESS, Castagna, and Han's universal relationships.

Time-lapse AVO inversion: application to synthetic data

A. Nassir Saeed, Laurence R. Lines and Gary F. Margrave

ABSTRACT

Reservoir characterization workflow for time-lapse studies requires integrating seismic data of different vintages and well log information into a single consistent model to delineate changes of reservoir parameters.

In this report, we implemented three different time-lapse AVO inversion algorithms (*total inversion of the differences*, *inversion of seismic difference only* and *sequential reflectivity-constrained inversion*) using synthetic data that simulate a time-lapse model of a heavy oil reservoir. Elastic physical parameters of the time-lapse model were chosen to represent reservoir conditions at pre-production and post-production periods after reservoir depletion. The time-lapse AVO inversion schemes simultaneously invert baseline and monitor seismic data to estimate the change of model parameters. The proposed algorithms have proved their robustness in terms of computation time as well as stability in presence of noise to ensure smooth changes in estimating reservoir attributes from time-lapse inversion.

Figure (1) left: shows the change of model parameters **Δ(ΔI/I)**, **Δ(ΔJ/J),** and **Δ(Δρ/ρ)** from time-lapse AVO Inversion, using *total inversion of the differences* scheme, before adding low frequency component from well log, while right shows the elastic attributes**,** **Δ(IP)**, **Δ(IS),** and **Δ(ρ)** after adding low frequency. Note that embedded curves in **black dotted** lines in right side represent actual change of elastic parameters estimated from well logs.

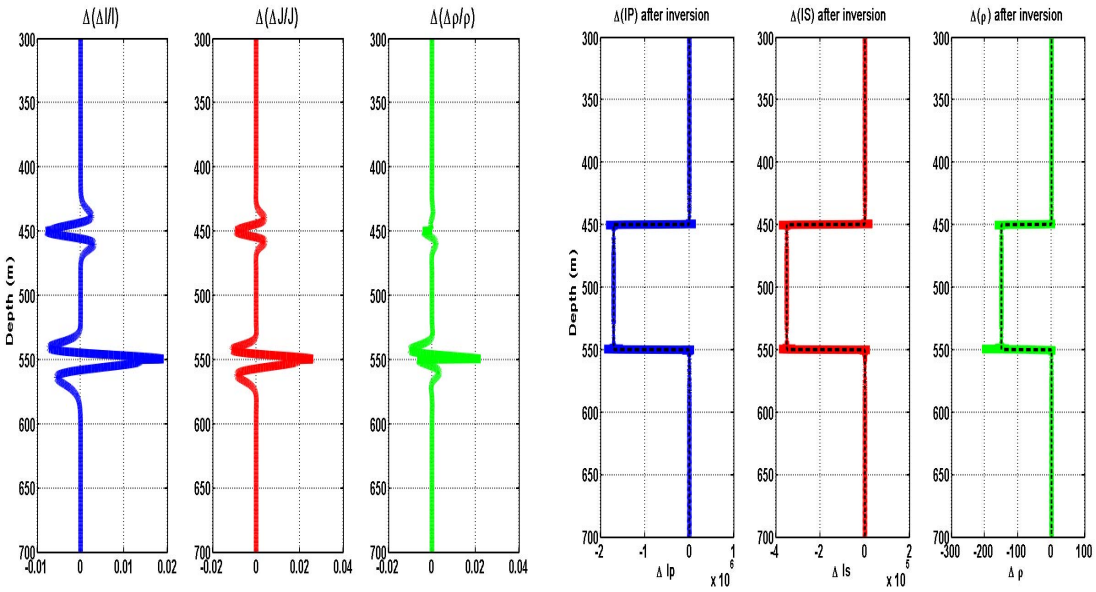

FIG. 1. Left: show **Δ(ΔI/I), Δ(ΔJ/J),** and **Δ(Δρ/ρ)** from time-lapse AVO inversion of base and monitoring data before adding low frequency from well logs. Right: change of elastic parameters **Δ(IP), Δ**(**IS**), and **Δ**(**ρ**) after adding low frequency. Embedded graphs in bold black dotted lines represent actual **Δ**(**IP**), **Δ**(**IS**) and **Δ**(**ρ**) calculated from logs.

Elastic wave 2D modeling of seismic surveys

Joe Wong, Peter M. Manning and David Henley

ABSTRACT

We have developed a 2D finite-difference time-stepping code in MATLAB for simulating seismic surveys in heterogeneous isotropic elastic media. The code, named mFD2D, is designed for easy input of moderately complex velocity structures. Acquisition parameters can be set for a variety of survey types, most notably for reflection and VSP surveys. Output data are common shot gathers that are saved on SEGY files. On a desktop PC with a 3.20 GHz CPU and 4 GB of RAM running 32-bit MATLAB, a synthetic 2D seismic reflection survey with about 100,000 traces can be produced overnight. Common source gathers of vertical and radial component seismograms produced by mFD2D for a variety of velocity models are presented to indicate the potential usefulness of the code for education, for research, and for pre-survey planning of real-world seismic surveys.

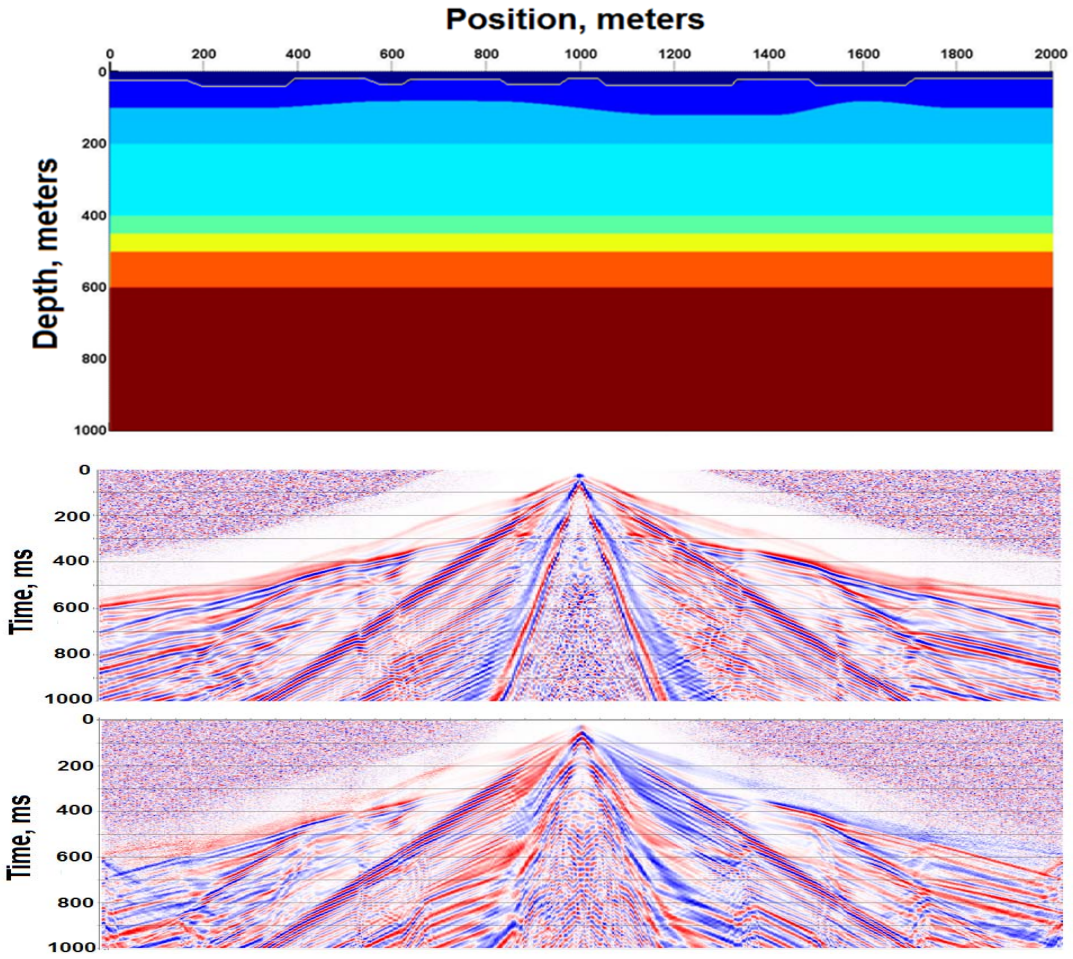

FIG. 1. A 2D model with a low-velocity overburden and a medium-velocity weathered layer, both of variable thickness, and AGC displays of the modeled vertical and horizontal seismograms, showing the complexity due to scattering of Raleigh waves within the low-velocity overburden.

Simultaneous multi-source acquisition using m-sequences

Joe Wong

ABSTRACT

Maximal length sequences, or m-sequences, are mathematical periodic entities with values of -1 and 1. A single m-sequence can be used to construct a set of shifted m-sequences. Each member of this set has a strong autocorrelation peak that closely resembles the delta function. Within a restricted range of lag times, its cross-correlations with other members have a fixed constant much smaller in magnitude. These sequences are known generally as pseudorandom binary sequences (PRBSs), and being weakly correlated to each other, they are suitable for driving multiple seismic vibrators simultaneously with little crosstalk between the3 received signals. Operating multiple vibrators simultaneously in real-world seismic surveys increases acquisition productivity dramatically. This report explains show how signals from multiple vibrators simultaneously driven by shifted m-sequences can be separated into individual seismograms unique to each vibrator with minimal crosstalk.

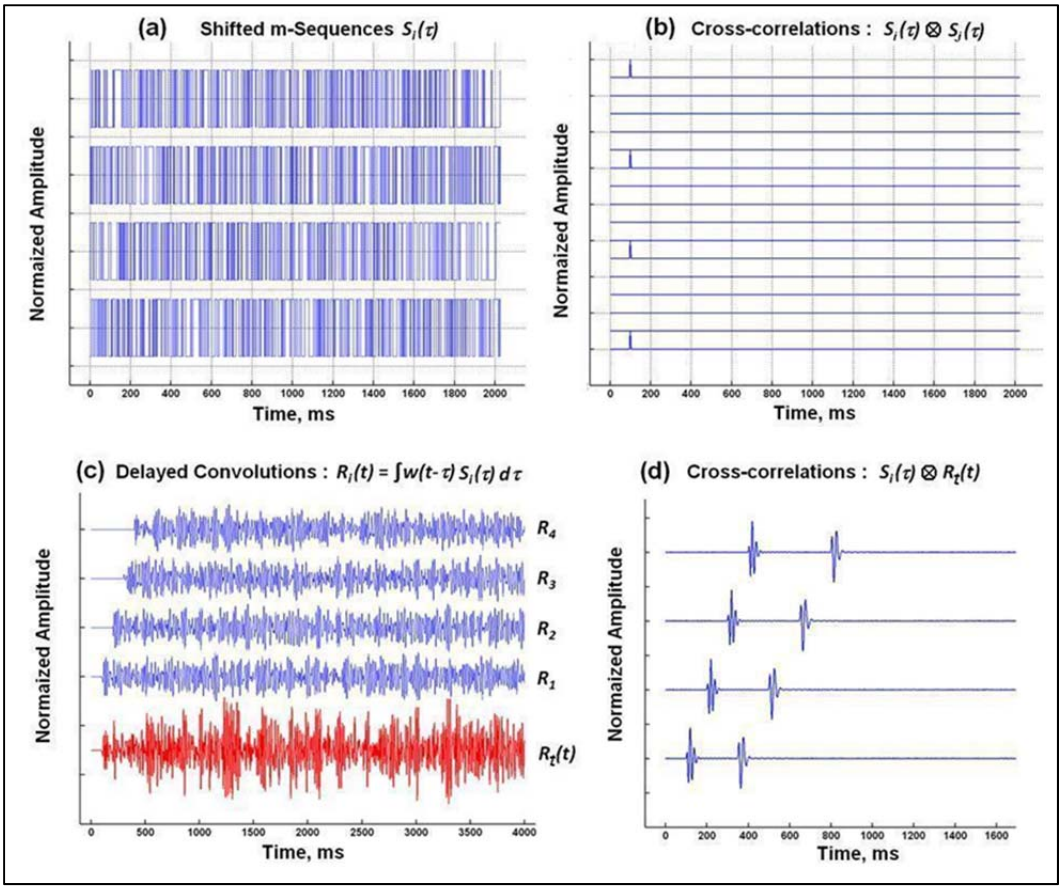

FIG. 1. (a) Four shifted m-sequences $S_i(t)$, I = 1, 2, 3, 4. (b) Correlations $S_i(t) \otimes S_j(t)$, with lags shifted by 100ms, indicating that the set $S_i(t)$ is quasi-orthogonal under correlation. (c) Convolutions $R_i(t)$ of a wavelet $w(t)$ with $S_1(t)$. *The* $R_i(t)$ *are* delayed by arrival times between four sources and a single receiver; $R_t(t)$ in red is the sum of $R_1(t)$ to $R_4(t)$. (d) Cross-correlations of each $S_i(t)$ with $R_t(t)$, recovering the wavelet $w(t)$ delayed by the arrival time.

Spread spectrum techniques for seismic data acquisition

Joe Wong

ABSTRACT

Spread spectrum techniques are widely used in many fields of science and engineering for obtaining accurate estimates of impulse responses of linear systems. They are also used in wireless communications, in data encryption, and in global positioning systems (GPS). The most common spread spectrum techniques use pseudorandom binary sequences (PRBSs) such as maximal length sequences (m-sequences) and the closely related Gold codes. Both are periodic mathematical entities with values of -1 and 1 and autocorrelations that closely approximate the delta function. For m-sequences and Gold codes with the same fundamental length, the ratios between peak values and off-peak values in the autocorrelations are much lower in magnitude for m-sequences. Seismic surveys can be broadly considered as attempts to determine the elastic-wave impulse response of a geological environment. In this context, spread spectrum techniques based on m-sequences and Gold codes can be profitably exploited for seismic data acquisition when the source is a controlled vibrator. This report is an exposition on the salient properties of m-sequences and Gold codes, on software techniques for generating their digital forms, and on the advantages of using them for seismic data acquisition.

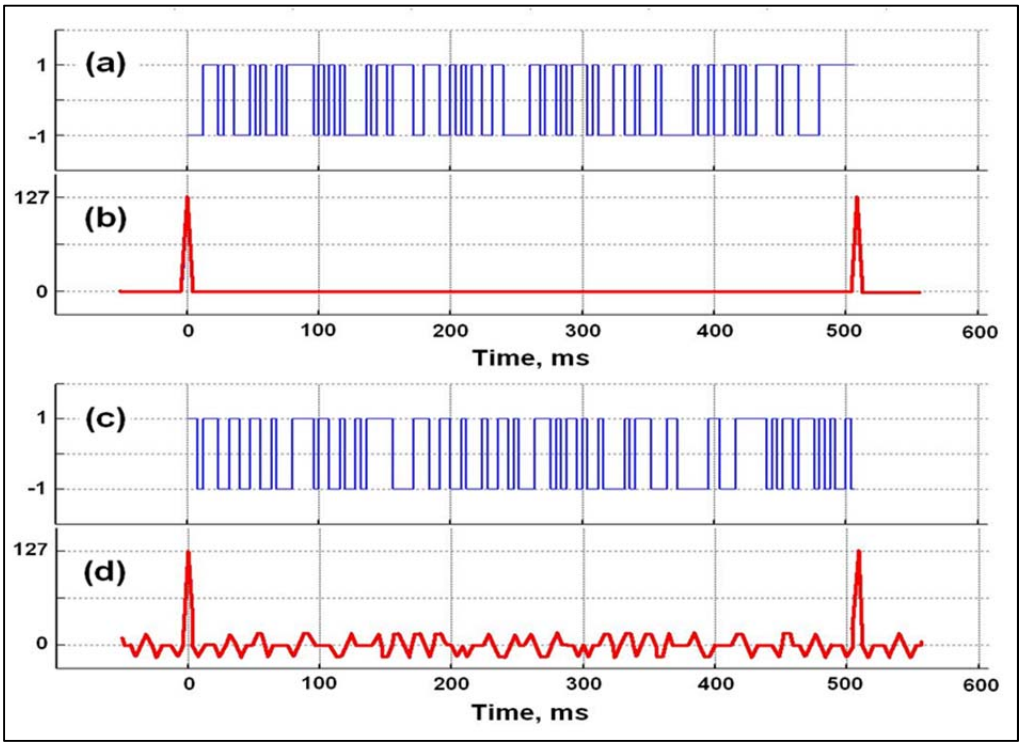

FIG. 1. Examples of digitally-generated pseudorandom binary sequences (PRBSs) with degree m = 7 and fundamental length L = (2m-1) = 127. (a) Maximal-length m-sequence; (b) m-sequence autocorrelation. (c) Gold code; (d) Gold code autocorrelation. The scaled peak values of both autocorrelations are equal to L = 127. The scaled "side lobe" value of the m-sequence autocorrelation is a constant -1. The scaled "side-lobe" values of the Gold code autocorrelation vary between -17, -1, and 15, as predicted by theory.

Multiparameter inverse scattering: preliminary testing results

Glen R. Young, Kris Innanen and Laurence R. Lines

ABSTRACT

The use of inverse scattering methods in the inversion of seismic data has been on the rise in exploration geophysics. With specific computational approaches it is possible to ascertain the material properties of the subsurface using scattered acoustic waves. We seek to determine multiple rock parameters such as density and bulk modulus from reflected seismic signals. A basic approach is used based on straightforward inverse scattering equations. In this case we will examine how multiparameter inverse scattering in a constant 2D background works and what are the results of inverting synthetically generated data.

A simulation was developed for this project in two parts. The forward modeling/migration stage is covered in the 2011 CREWES report by the same authors and the least squares inversion of the data for rock properties is covered in this report. The inversion imagery is examined for accuracy and various models are tested to determine if physically realistic effects are present as would be seen in real seismic data. The conclusion from doing linearized Born inversion is that it is successful in mapping out the 'perturbing' subsurface structure, the results for a two parameter approach seem realistic, a knowledge of the background velocity and also the constant background density would allow for the determination of the absolute values of the rock properties of interfaces at depth.

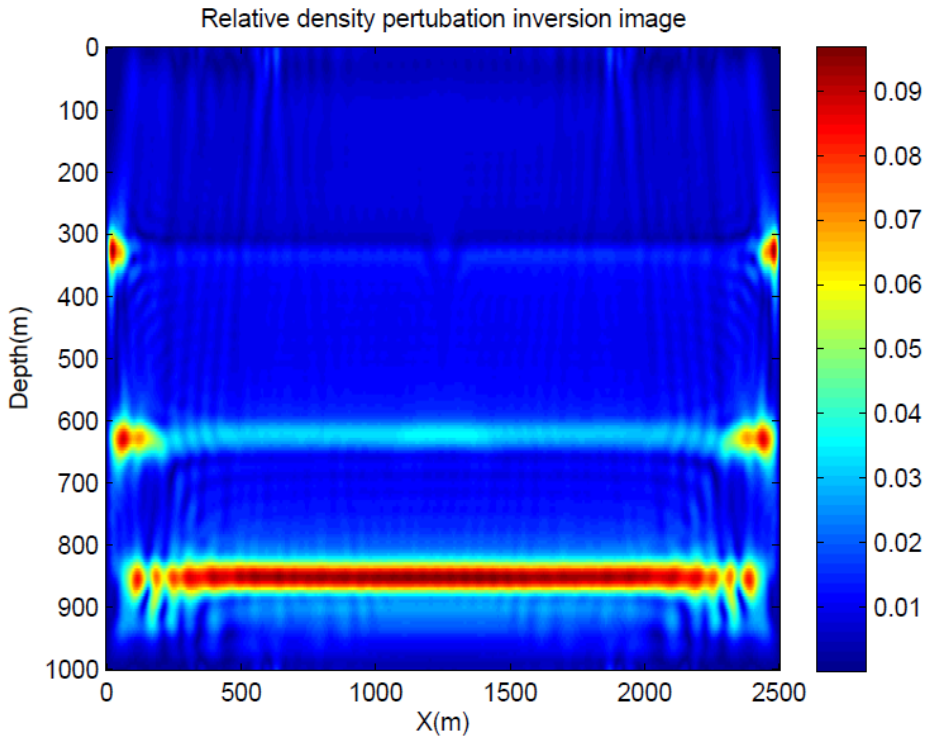

FIG. 1. Inverted density pertubation image for a 4 layer model.

LSPSM/inversion for the pre- and poststack time lapse studies

Abdolnaser Yousefzadeh and John C. Bancroft

ABSTRACT

The ability of separate and joint LSPSM/inversion of time lapse data is shown. Assuming similarity of the acquisition instruments, environmental noise, near surface effects, and processing flows and parameters for both, baseline and monitor surveys, difference in acquisition geometries leaves different artifacts at the migration images. It is shown how separate LSPSM of both, baseline and monitor, datasets can attenuate acquisition footprints and create reliable time lapse images. The reconstructed data from two surveys makes the prestack time lapse studies more feasible. Formulations of the joint inversion of time lapse data to invert for the baseline image and time lapse image by LSCG method are derived.

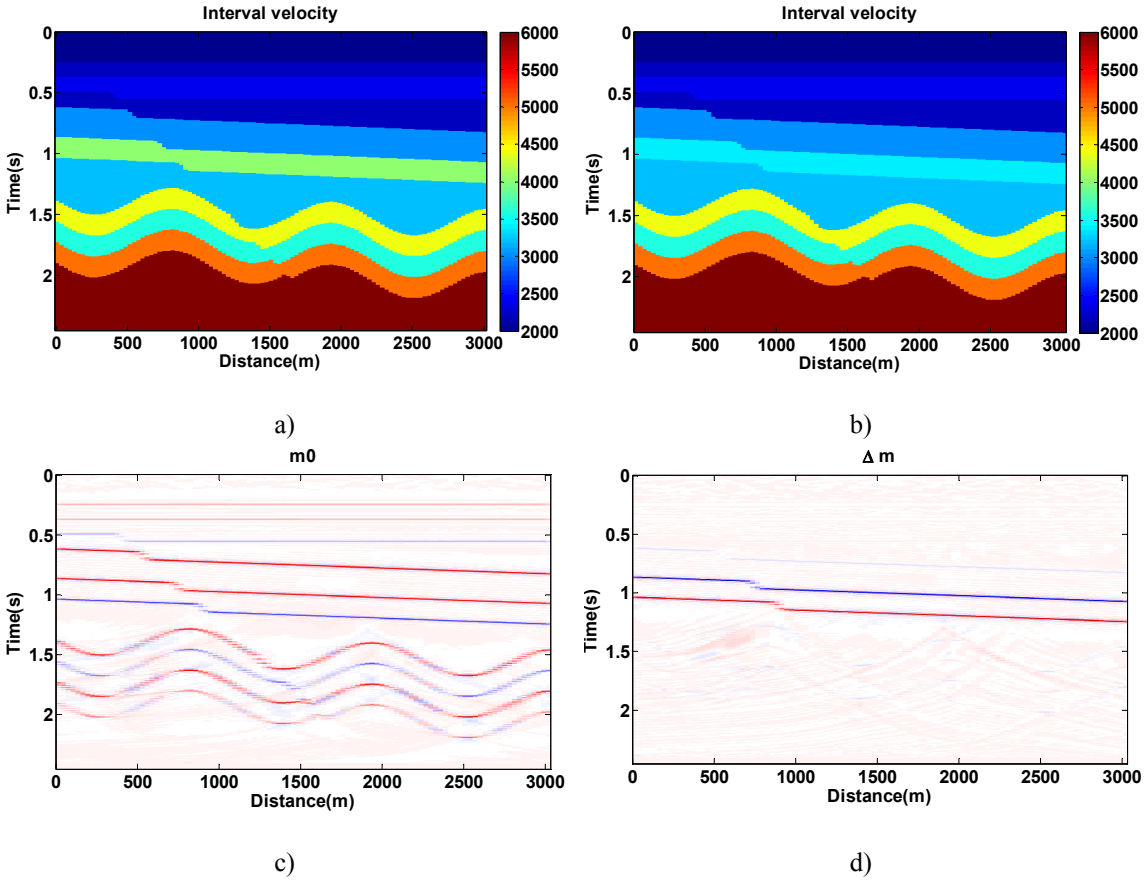

FIG. 1. Joint inversion of time lapse data. a) Velocity model of baseline survey, b) Velocity model at the time of monitor survey, c and d) Reflectivity of monitor survey and the time lapse images obtained by Joint inversion of time lapse data.

Grid scaling 2-D acoustic full waveform inversion with a high frequency impulsive source

Vladimir Zubov, Michael Lamoureux and Gary Margrave

ABSTRACT

Spatial grid multi-scaling with domain decomposition is developed in this study in order to obtain a better convergence rate for the acoustic inverse problem for velocity field with a self-adjoint dispersive operator. The model used in the study is based on the 2D acoustic wave equation boundary problem with Dirichlet boundary conditions approximated with fourth-order spatial finite-difference approximation and factorization schemes on a regular rectangular grid. Combinations of different spatial grid scaling according to impulse source position and its signature are implemented in the present study. The inverse velocity coefficient problem is formulated not in the traditional way of minimizing the residual of the observation data, but as a vector-function root search problem for forward and adjoint wave propagation solutions cross-correlation. This vector-function root search is solved with the same gradient search method which is used for standard residual minimization but many other function optimization approaches are also applicable. The gradient search is implemented in such a way to run cross-correlation function root search as a series of independent (or close to independent) root searches for smaller sub-problems. Manipulations with misfit data time window in iterations of inversion determine the process of convergence to the exact velocity field (Figure 1). The strategy of time window shifting according to distance between point sources and there signatures will be a subject of further study.

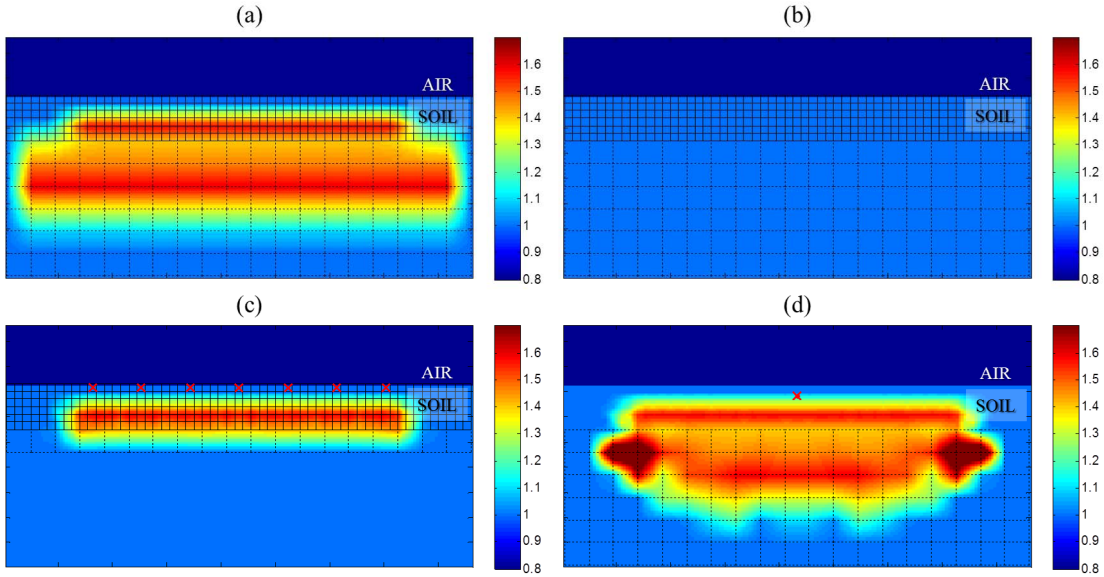

FIG. 1. Velocity fields: in (a) exact velocity field defined on both fine and coarse grids; in (b) initial approximation of velocity field; in (c) approximate velocity after 1000 iterations of gradient search applied to high frequency source inversion; in (d) approximate velocity after 5000 iterations applied to low frequency source inversion; × - point source position.